5-2014

On the Effect of Temperature and Pressure Gradient on the Flow of Non-Homogeneous Fluids

Joseph Anthony Fiordilino
Montclair State University

MONTCLAIR STATE UNIVERSITY

On the Effect of Temperature and Pressure Gradient On the Flow of Non-homogeneous Fluids

by

Joseph Anthony Fiordilino

A Master's Thesis Submitted to the Faculty of

Montclair State University

In Partial Fulfillment of the Requirements

For the Degree of

Master of Mathematics, Pure & Applied Mathematics Concentration

May 9th, 2014

College of Science and Mathematics

Department of Mathematical Sciences

Certified by:

May 9th - 2014

Date

Thesis Committee:

[redacted]

Ashwin Vaidya

[redacted]

Mehrdad Massoudi

[redacted]

Bogdan Nita

On the Effect of Temperature and Pressure Gradient On the Flow of Non-homogeneous Fluids

A THESIS

Submitted in partial fulfillment of the requirements
for the degree of Masters in Mathematics, Pure & Applied
Mathematics Concentration

by

Joseph Anthony Fiordilino

Montclair State University

Montclair, NJ

2014

Acknowledgments

I would like to thank my friends and family, especially my mother, father, and sister, Pasqualina, Epifanio Fiordilino and Rosalia Amodeo, for their love and support throughout the years. I would also like to thank my fiancée, Pamela Guerron, for her love and support and who has been extraordinarily helpful in the preparation for the defense of this thesis. I am grateful to my committee members, Drs. Bogdan Nita, Mehrdad Massoudi, and Ashwin Vaidya, who have given me stellar, and sometimes painful, advice. I am especially grateful to Dr. Ashwin Vaidya for his instruction, guidance, and belief in my ability. He has been instrumental in my current success as a mathematician. Lastly, I am thankful to everyone who has instructed me at one point or another. Thank you all.

Contents

List of Figures

List of Tables

Chapter 1

Introduction

Fluid dynamics is a rich and satiating topic of study. The range of topics that fall under its dominion are vast, encompassing the flow of blood through arteries to the dynamics of the atmosphere. However, it is solely the study of suspensions that will be under consideration here; that is, the rheology of a mixture of two substances, one of which is dispersed in the other (carrier fluid). This class of fluid has applications including industrial, medical, and sustainability, to name a few; in particular, lubrication theory, the rheology of blood, and biomass transport. Let us take a moment to discuss biomass transport and utility, which has been a topic of growing interest in recent years.

It is estimated that biomass constitutes 14% of the world energy use, which makes it the fourth largest energy source [1]. Biomass can be considered as any or a combination of wood residues, agricultural residues (crops, foods, animals), municipal solid waste, and etc. [2], see Figures 1.1 and 1.2. One of the promising approaches to utilizing biomass is the development of coal/waste co-firing technology. For co-firing, biomass has been considered as one of the fuels. Ekmann et al. mention that from a technological point of view, upstream and downstream impacts are important for biomass co-firing to become a viable source of energy; upstream impacts include handling, preparation, and storage, while downstream impacts include pollutant reduction, ash deposition, and corrosion [1].

Traditionally, in fossil fuel combustion processes, coal-water slurry is prepared and in some cases heated prior to testing and use [3]. Its rheological properties are determined using a basic type of viscometer. Coal slurries exhibit non-Newtonian flow characteristics. There are many other applications such as injection moulding or oil-well drilling where there are significant variations in the viscosity of the fluid, caused primarily by shear-rate and temperature [4]. With additional need for fossil fuels, the amount of waste materials and the environmental issues dealing with their disposal also increase.

The major difficulties in modeling and using the co-firing of coal and biomass are: (i) The biomass fuels, especially the switchgrass and wood-residue are neither spheri-

cal nor disk-like in shape; most modeling approaches treat particles either as spherical or as disk-like, with a shape factor to account for other shapes. (ii) Since most of the biomass particles are slender and rod-like, the directionality or anisotropy associated with the axis of the body, i.e., the orientation of the body, becomes an important controlling parameter [5]. (iii) For co-firing applications, the density of the bio-mass fuels is, in certain cases, significantly different from that of coal. These issues, in many ways, determine the efficiency of the mixing process. Most computational fluid dynamics (CFD) codes treat the particles as a homogeneous continuous medium with correlations which depend on the diameter and density of these spherical particles.

The increasing demand and dependency on fuels has brought about a sense of urgency in the long term availability of non-renewable fuel reserves. A possible solution to this ubiquitous crisis is the development and characterization of new types of fuels, which could be environmentally safer and possibly more sustainable. Bio-fuels (a mixture of traditional fossil fuels, such as coal with other waste products such as chipped wood, grass, etc., forming biomass) seem to offer such a viable alternative [6]. Truck-based transport is currently the primary method of supplying feedstock to the biorefinery plants [7]. This type of transport consumes a large amount of fossil fuel in relation to the amount of biomass that is actually transported. However, there are other means of transport including pipeline, barging, and train [2, 7].

The importance of suspensions can be readily seen in the aforementioned application. Let us now move to the purpose of this thesis and briefly discuss the topics of study. We take two approaches to the study of this class of fluid. The first approach is a single regime analysis. The viscosity will be taken as a product of functions of space and temperature and the thermal conductivity of space alone. Consequently, the complete modified Navier-Stokes system of equations must be considered. We are motivated here by the bulk transport of solid material by a carrier fluid to a combustion chamber and/or processing facility, depending on the utility of the biomass being transported. For instance, the effect of the volume fraction and conductive properties of solid material on the flow and temperature of the fluid through a channel.

The second approach is a two regime analysis. The viscosity is taken to be a piecewise function containing a product of functions of pressure gradient, volume fraction, and shear rate. The pressure gradient dependence is based on new experiments conducted recently at the Complex Fluid Laboratory at Montclair State University [8]. The volume fraction and shear rate dependence of the viscosity is well documented in the literature. Unlike the first approach, we do not consider temperature effects, however, the viscosity encompasses more of the underlying physical properties. The motivation for our study is to provide a sound theoretical model to match experimental work. Furthermore, we wish to gain insight into the behavior and micro-structure of the flow.

The objective of subsequent chapters will be to briefly introduce the governing equations of motion and the constituent relations for the Cauchy stress tensor and heat flux vector. Following this will be a review of viscosity and thermal conductivity models discovered and/or used in previous pertinent studies. A chapter will then be

devoted to the setup, solution, and analysis of each of the two approaches.

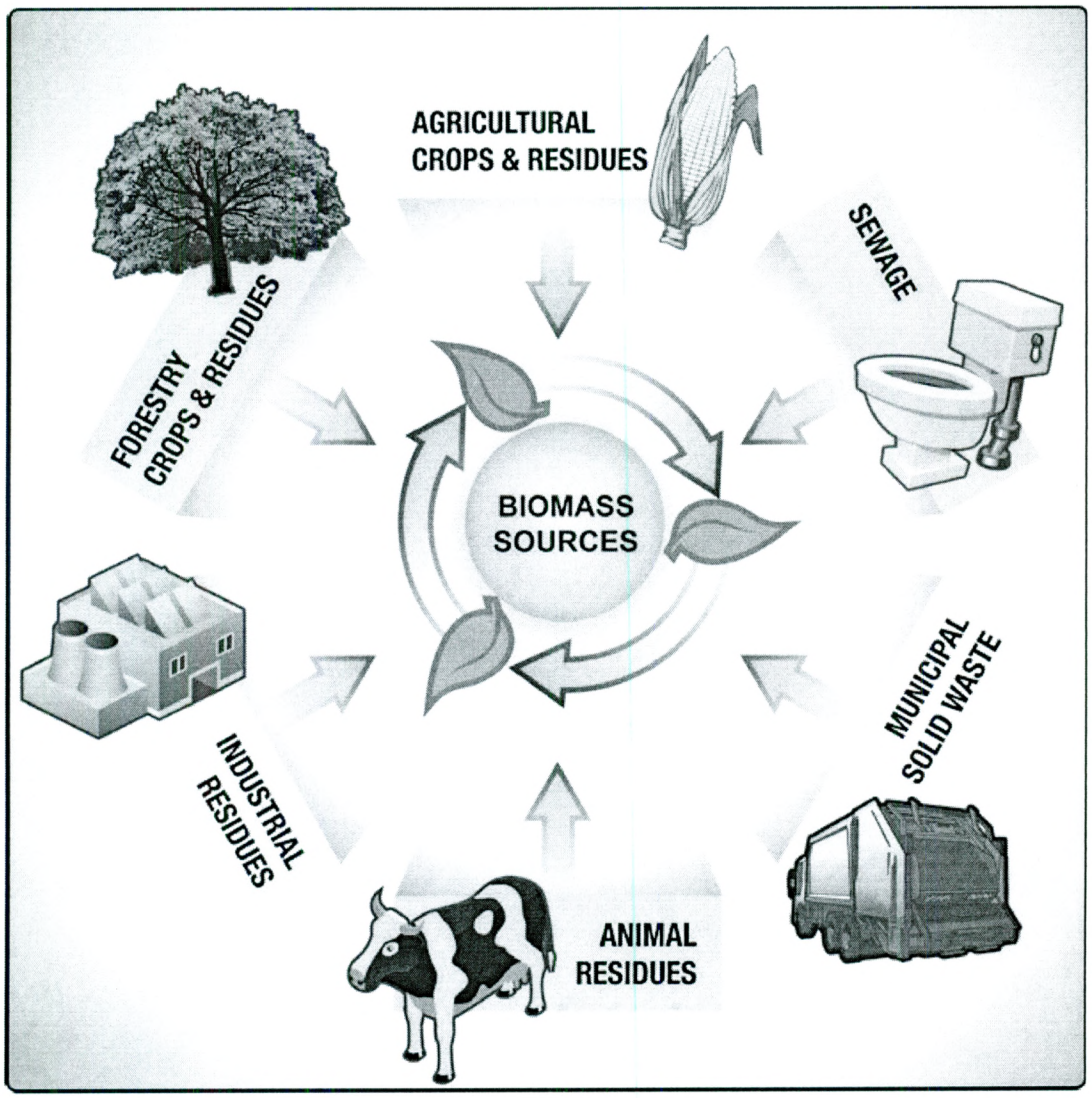

Figure 1.1: An illustration of the many sources of biomass.

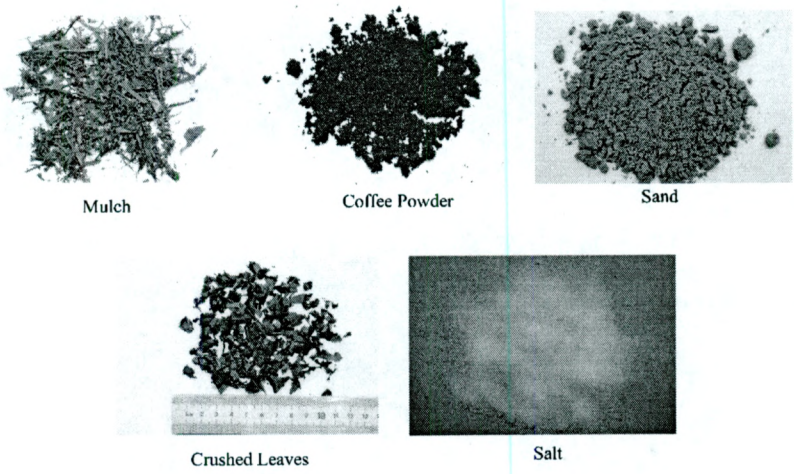

Figure 1.2: The solid particulates used in [8]. Among these, mulch, coffee powder, and crushed leaves are biomass.

Chapter 2

Governing equations

There exists a known mathematical framework for the study of fluid dynamics. The governing equations for all fluid dynamics are the complete Navier-Stokes (N-S) system of equations, which have long been known. There are many notational forms of these equations for the particular physics and mathematical tools involved [9, 10, 11, 12]. Furthermore, the N-S are often formulated assuming constant viscosity, however, this is not always a valid approximation. In fact, if the viscosity is a function of anything other than the shear rate, it is no longer a Newtonian fluid. The governing equations of motion for an incompressible fluid include the conservation of mass, linear momentum, energy equations (N-S), and are given by [12]:

$$\frac{\partial \rho}{\partial t} + \rho \mathrm{div}(\mathbf{u}) = 0, \tag{2.1}$$

$$\rho \frac{\mathrm{d}\mathbf{u}}{\mathrm{dt}} = \mathrm{div}(\mathbf{T}) + \rho \mathbf{b}, \tag{2.2}$$

$$\rho \frac{\mathrm{d}\varepsilon}{\mathrm{dt}} = \mathbf{T} \cdot \mathbf{L} - \mathrm{div}(\mathbf{q}) + \rho r, \tag{2.3}$$

where ρ is the density of the fluid, d/dt is the total time derivative, given by $\frac{\mathrm{d}(.)}{\mathrm{dt}} = \frac{\partial(.)}{\partial t} + [\mathrm{grad}(.)]\,\mathbf{u}$, and $\mathbf{u}$ is the velocity vector. For isochoric motion we have $\mathrm{div}(\mathbf{u}) = \mathbf{0}$. Additionally, $\mathbf{b}$ is the body force vector and $\mathbf{T}$ is the Cauchy stress tensor. Note: In the absence of any chemical and electro-magnetic effects, $\mathbf{b} \equiv \mathbf{g}$, where $\mathbf{g}$ denotes the effect of gravity. The balance of moment of momentum reveals that in the absence of couple stresses, the stress tensor is symmetric.

Lastly, ε is the specific internal energy, $\mathbf{L}$ is the gradient of velocity, $\mathbf{q}$ is the heat flux vector, and r is the radiant heating. Thermodynamical considerations require the application of the second law of thermodynamics or the entropy inequality. The local form of the entropy inequality is given by [13]:

$$\rho\dot{\eta} + \mathrm{div}(\phi) - \rho\mathbf{s} \geq \mathbf{0}, \tag{2.4}$$

where $\eta(\mathbf{x}, t)$ is the specific entropy density, $\varphi(\mathbf{x}, t)$ is the entropy flux, and s is the entropy supply density due to external sources, and the dot denotes the material time derivative. If it is assumed that $\phi = \frac{\mathbf{q}}{\theta}$ and $s = \frac{\mathbf{r}}{\theta}$, where θ is the absolute temperature, then equation (2.4) reduces to the Clausius-Duhem inequality

$$\rho\dot{\eta} + \mathrm{div}\left(\frac{\mathbf{q}}{\theta}\right) - \rho\frac{\mathbf{r}}{\theta} \geq 0.$$

Even though we do not consider the effects of the Clausius-Duhem inequality in our problem, for a complete thermo-mechanical study of a problem, the second law of thermodynamics has to be considered [13, 14, 15, 16].

However, in order to 'close' these equations, we need to provide constitutive relations for $\mathbf{T}$, $\mathbf{q}$, ε and r. In our case, we assume that the radiation effects can be neglected. Furthermore, ε does not need to be modeled due to the nature of the kinematical assumptions for the flow. In the next section, we will provide a brief discussion of the two relevant constitutive relations needed in this problem.

2.1 The stress tensor and heat flux vector

A look at equations (2.2) and (2.3) reveals that in the absence of radiation effects, the two constitutive parameters which need to be modeled are the stress tensor and the heat flux vector. Both the stress tensor and heat flux vector are subject to a variety of different models, especially the stress tensor [17, 18, 19, 20].

The Cauchy stress tensor for an incompressible viscous fluid is given by

$$\mathbf{T} = -\pi\mathbf{1} + 2\mu\mathbf{D}, \tag{2.5}$$

where π is the indeterminate part of the stress due to the constraint of incompressibility, also known as the pressure, μ is the viscosity of the suspension, and $\mathbf{D}$ is the deformation rate tensor defined as

$$\mathbf{D} = \frac{1}{2}(\mathbf{L} + \mathbf{L}^T).$$

The heat flux vector $\mathbf{q}$ is based on Fourier's assumption,

$$\mathbf{q} = -k\mathrm{grad}(\theta). \tag{2.6}$$

2.2 The viscosity relation

The viscosity of a non-homogeneous fluid is highly complicated. In general, it may be a function of a myriad of factors. That is, the viscosity may take the form:

$$\mu = \mu(\mathbf{X}, \phi, \pi, \dot{\gamma}, \theta, ...),$$

where $\mathbf{X}$ is the spatial dependence, ϕ is the volume fraction of solid particles in the suspension, *theta* is the temperature, and $\dot{\gamma}$ is the shear rate, with $\dot{\gamma} = \mathbf{D}$.

A popular approach to study the problem related to modeling a complex inhomogeneous liquid is to treat it as a homogeneous continuous medium whose material properties are averaged. However, our system of interest is composed of a mixture of the carrier fluid and the suspended particles which can be spherical, rod-like or irregular in shape. Furthermore, the stresses involved are highly complicated and varied [21]. Nonetheless, we must begin somewhere. Let us first consider two existing spatially dependent viscosity models.

2.2.1 Spatial dependence

Anand and Rajagopal [23] studied the flow of an inhomogeneous fluid through simple geometries using a quadratic function in space $\mathbf{X}$; they also introduced a parameter ε which can be thought of as a measure of the inhomogeneity of the fluid. They suggested a few equations of the following type:

$$\widehat{\mu}\,(Y) = \widehat{\mu}\,(y) = \mu_0 \left[1 + \varepsilon \left(\frac{6y^2}{h^2} - \frac{1}{2}\right)\right], \tag{2.7}$$

where h is the separation between two plates. Massoudi et al. [24] extended this work considering the feasibility of pipeline transport of biomass after analyzing the flow of such a non-homogeneous fluid; the general viscosity model considered was

$$\mu(y) = \mu_0(1 + \varepsilon f(y)), \tag{2.8}$$

with the three models:

$$f(y) = \begin{cases} 0, \\ (\mu_2 - \mu_1)y + \mu_1, \\ e^{-ky}, \end{cases} \tag{2.9}$$

where μ_1, μ_2, and k are held constant. We now move to discuss volume fraction dependent models for viscosity.

2.2.2 Volume fraction dependence

There is an extraordinary body of literature on modeling the volume fraction dependence of a suspension and their applications. Mahbubul et al. [25] compile and review many of the existing relations for the concentration dependence of the viscosity of a suspension, emphasizing nanofluids. For instance, the Einstein, Brinkman, Batchelor, and Krieger relations are considered. They are, respectively,

$$\mu_r = (1 + 2.5\phi), \tag{2.10}$$

$$\mu_r = (1 - \phi)^{2.5}, \tag{2.11}$$

$$\mu_r = (1 + 2.5\phi + 6.5\phi^2), \tag{2.12}$$

$$\mu_r = (1 - \frac{\phi}{\phi_c})^{-[\eta]\phi_c}, \tag{2.13}$$

where μ_r is the relative viscosity of the suspension, ϕ represents the volume fraction of solid particles in the suspension, ϕ_c is the critical or packing concentration, and $[\eta]$ is the intrinsic viscosity with a typical value of 2.5 for mono diverse hard spheres. Two other popular relations attributed to Arrhenius [26] and Mooney [27] are

$$\mu_r = e^{B\phi}, \tag{2.14}$$

$$\mu_r = \exp\left[\frac{B\phi}{(1 - \frac{\phi}{\phi_c})}\right], \tag{2.15}$$

where B is a fitting parameter set to 2.5 for monodisperse spheres [20]. The pressure dependence of the viscosity can now be considered.

2.2.3 Pressure dependence

The notion of a fluid with a viscosity dependent on the pressure in the system originates with Stokes. In his 1845 paper, he made the remarks [28]:

> Let us now consider in what cases it is allowable to suppose that μ to be independent of pressure. It has been concluded by Du Buat from his experiments on the motion of water in pipes and canals, that the total retardation of the velocity due to friction is not increased by increasing the pressure... I shall therefore suppose that for water, and by analogy for other incompressible fluids, μ is independent of pressure.

Although Stokes dismissed the dependence of pressure in the aforementioned cases, he recognized that the viscosity of a fluid may exhibit pressure dependence, in general.

There has been discussion on this topic ever since [29]. Additionally, there have also been experimental investigations into this relation beginning in the latter half of the 20th century [30, 31, 32, 33, 34, 8]. Quite recently, there has been a revival of interest in this topic, with emphasis on the theoretical aspects [35, 36, 37, 8].

Recently Massoudi et al. [8] performed experimental and theoretical investigations into pipeline flow for low volume fraction suspensions. They modeled the viscosity of the system as

$$\mu = \exp\left(\frac{k_1 \Delta\pi}{L}\right), \tag{2.16}$$

where k_1 is a real constant, $\Delta\pi$ is the pressure difference across the pipe, and L is the length of the pipe. It should be noted that this relation was used to theoretically calculate the volumetric flow rate, which was then compared to the pressure gradient; this theoretical calculation held remarkably well for low pressures ($\pi < 2000$Pa) which is in sharp contrast to the magnitude of pressures studied in previous experimental and theoretical investigation ($\pi \approx 1$MPa), i.e. those that follow below. This model will be discussed in Chapter 4 due to the significant role it plays in our model.

Franta et al. [18] studied a class of incompressible fluids with viscosities dependent on the shear rate and pressure. They addressed the existence of weak solutions in the steady case subject to homogeneous Dirichlet boundary conditions and body forces. The viscosity function took the form of

$$\mu(\pi, |\mathbf{D}|^2) = (A + \gamma_i(\pi) + |\mathbf{D}|^2)^{\frac{r-2}{2}}, i = 1, 2, 3, \tag{2.17}$$

where $A \in (0, 1]$ and $r \in (1, 2)$ are constant, and $\gamma_i(\pi)$ is given by one of three relationships

$$\gamma_1(\pi) = (1 + \alpha^2\pi^2)^{\frac{-q}{2}}, \tag{2.18}$$

$$\gamma_2(\pi) = (1 + e^{\alpha\pi})^{-q}, \tag{2.19}$$

$$\gamma_3(\pi) = \begin{cases} e^{-\alpha q \pi} & \text{if } \pi > 0, \\ 1 & \text{if } \pi \leq 0, \end{cases} \tag{2.20}$$

with α and q positive constants.

Massoudi and Phuoc [37] considered the unsteady flow between two parallel horizontal plates, the top plate moving, with an oscillating pressure gradient. The viscosity of the fluids in consideration took the form:

$$\mu(\pi) = \alpha\pi^\gamma, \tag{2.21}$$

with $\gamma = 1$ constant.

Hron et al. [35] considered three pressure dependent viscosity models for Couette and Poiseuille flow, including relation (2.21):

$$\mu(\pi) = e^{\alpha\pi}, \tag{2.22}$$

$$\mu(\pi) = \mu_0(1 + \alpha\pi), \tag{2.23}$$

where α is a positive constant. It is shown that only particular forms of the viscosity function are allowed for plane Poiseuille flow, which is of interest to us here. Namely, that for relation (2.22), $\gamma = 1$ is the only form which leads to non-trivial flow for an assumed pressure function

$$\pi(x, y) = F(x)G(y). \tag{2.24}$$

Furthermore, for relation (2.23), the only form of the pressure function allowed is

$$\pi(x, y) = R(x) + S(y), \tag{2.25}$$

which leads to trivial flow.

Kalogirou et al. [38] studied the flows of Newtonian liquids with pressure dependent viscosities in the context of plane, round, and annular Poiseuille flow. They used a linear model (2.23) suggested by Renardy. Another successful pressure dependent viscosity model is attributed to Andrade and is given by

$$\mu = A\rho^{\frac{1}{2}} \exp((\pi + \rho^2 r)^{\frac{s}{\theta}}), \tag{2.26}$$

where ρ is the density, π is the pressure, θ is the temperature, and A, r, and s are constants [39].

2.2.4 Shear rate dependence

It is seen that many fluids either shear thin or shear thicken, that is, there is a dependence of the viscosity on the deformation rate tensor $\mathbf{D}$. For instance, ketchup and paint are well-known shear thinning fluids and corn starch in water is well-known for its shear thickening properties. One of the most simple and effective models is the so called power-law model

$$\mu \propto |\mathbf{D}|^{n-2}, \tag{2.27}$$

where n is constant and the quantity $n - 2$ dictates the type of fluid being studied. For $n - 2 < 1$, the fluid shear thins, for $n - 2 > 1$, the fluid shear thickens, and for $n - 2 = 0$, the fluid is Newtonian. The number of models for shear thinning and thickening fluids are legion. See [40] for a review of many such models.

2.2.5 Temperature dependence

The last item under consideration is the temperature θ. It is well known that the viscosity of most fluids decreases with increasing temperature. There are many successful viscosity models which account for temperature effects in a range of applications. For example, the model of Andrade (2.26) and those of Reynold, Vogel, and Gupta and Massoudi, respectively,

$$\mu(\theta) = \mu_0 e^{-M\theta}, \tag{2.28}$$

$$\mu = \mu_0 \exp\left(\frac{a}{b+\theta}\right), \tag{2.29}$$

$$\mu = \mu_0 \left(1 - \frac{\phi}{\phi_{max}}\right)^{-2.5} e^{\gamma(\theta-\theta_0)}, \tag{2.30}$$

where μ_0 is some characteristic viscosity, M is a material parameter, ϕ_{max} is the maximum crystal fraction for which flow can occur, θ_0 is some characteristic temperature, and a,b, and γ are constants [37, 18]. It should be noted that both the Reynolds and Vogel viscosity models have seen positive results pertaining to lubrication applications. Furthermore, the model of Gupta and Massoudi is based on the Einstein-Roscoe relation which has been successful for low volume fractions in magma flows [41].

There is also the model of Kulkarni et al. [42] given by

$$\mu_r = \exp(A(1/\theta) - B), \tag{2.31}$$

which is valid for copper oxide nanoparticles suspended in water for temperatures ranging between 5 and 50 centigrade. A and B are functions of volume percentage. Now that all major relations for viscosity have been discussed, the thermal conductivity relation may now be addressed.

2.3 The thermal conductivity relation

The thermal conductivity k of a material is the property which governs its ability to conduct heat. In general, for anisotropic materials, it is a fourth order tensor, which can also depend on concentration, temperature, etc. In fact, the general forms of the constitutive relations for the heat flux vector $\mathbf{q}$ could also depend on temperature and concentration gradients and include terms often referred to as the Dufour and the Soret effects. There have been many experimental and theoretical studies related to this issue. Kaviany surveys a fairly exhaustive array of thermal conductivity models pertaining to porous media [43].

Regarding suspensions, Duangthongsuck and Wongwises [44] found that for TiO_2-water nanofluids, the thermal conductivity of the nanofluid increased with increasing temperature. They compared several thermal conductivity models, including

$$k = \frac{q}{4\pi(\Delta T)} \ln\left(\frac{t_2}{t_1}\right), \tag{2.32}$$

$$k_r(\phi) = a + b\phi, \tag{2.33}$$

where q is the applied electrical power per unit length of wire, ΔT is the temperature change of the wire between times t_1 and t_2, and a and b are fitting parameters. They found that the first model, and many others, did not agree well with experiment. The second model was proposed and fit well for the parameters a and b for specific temperatures of 15, 25, and 35 centigrade. The first model was also used in the study of Al_2O_3-water nanofluids by Chandrasekar et al. and showed good agreement with experiments [45].

Additionally, there are many other relative models for solid-liquid suspensions, such as that of Maxwell, Hamilton and Crosser, and Timofeeva, respectively,

$$k_r(\phi) = \left[\frac{2k_f + k_p + 2\phi(k_p - k_f)}{2k_f + k_p - \phi(k_p - k_f)}\right], \tag{2.34}$$

$$k_r(\phi) = 1 + 3\phi, \tag{2.35}$$

$$k_r(\phi) = \left[\frac{k_p + (n-1)k_f - (n-1)\phi(k_f - k_p)}{k_p + (n-1)k_f + \phi(k_f - k_p)}\right], \tag{2.36}$$

with

$$n = \frac{3}{\psi},$$

where n is the empirical shape factor, ψ is the sphericity, k_p is the thermal conductivity of the solid particles, and k_f is the thermal conductivity of the base fluid [46, 47, 48].

2.4 General modeling

In the introduction, we proposed two approaches to the study of suspensions. It is the aim of each study to obtain qualitative results, capturing the essence of the proposed system, through analytical and/or numerical techniques. Further explanation will follow in the subsequent subsections. As a first approximation, we study the fluid flow of a suspension between two parallel horizontal plates of infinite length as an idealization of the flow of a suspension in a channel or pipe. For the problem under consideration, we make the following assumptions:

1. the motion is steady and fully developed,

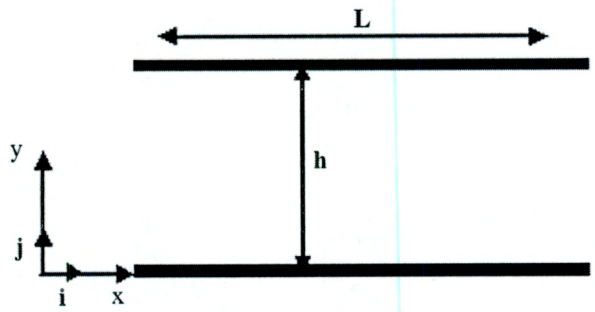

Figure 2.1: The geometry of the system under investigation.

2. chemical and electro-magnetic effects are absent,

3. the constitutive equation for the stress tensor is given by equation (2.5),

4. the internal energy of the system is assumed to be given by

$$\varepsilon = c_v \theta,$$

5. the velocity and temperature fields are 'unidirectional', i.e. they are of the form

$$\mathbf{u}(\mathbf{X}) = U(y)\mathbf{i},$$

$$\theta(\mathbf{X}) = \theta(y).$$

As we've seen, the form of the function for viscosity is generally based on experimental observation, where curve fitting is involved. We take the viscosity function to be an effective viscosity. Let us first consider the first problem, as proposed in the introduction.

Chapter 3

First problem: Heat transfer and flow of an inhomogeneous fluid

Recall that the first approach is a single regime analysis. The viscosity of the suspension is assumed to have spatial and temperature dependency; that is, the viscosity takes on the form:

$$\mu(y, \theta) = f(y)g(\theta), \tag{3.1}$$

where y is the spatial dimension of importance; here, the distance between two plates. Equation (3.5) implies that the viscosity is variable for the non-homogeneous fluid and it also depends on temperature. Although the viscosity of an inhomogeneous fluid is highly complicated and can be a function of volume fraction, temperature, pressure, and etc, we have bypassed these intermediate variables, which are each dependent on position. The amount of solid particulate in that region will also act to modify the thermal conductivity of the surrounding base fluid in analogous fashion to the change of viscosity; that is, the thermal conductivity of such a fluid should follow the same position dependent model as does the viscosity.

Many of the models we have reported earlier are either linear or exponential, however, there is no reason to assume a suspension could not assume a Gaussian distributed viscosity profile, with the majority of the solid particulate clustered about the mean (or even a skewed Gaussian profile). A Gaussian model is justified in that it generalizes the class of suspensions we can consider; a suspension may be a conglomerate of different substances/materials, each with different buoyant tendencies. Furthermore, an exponential model allows us to consider suspensions with monotonically increasing viscosity and is somewhat representative of a skewed Gaussian; such a model is useful for suspensions where there are more light particles than heavy (or the converse). The literature is scarce here, however, Trelles [49] experiences the onset of Gaussian distributed viscosities and thermal conductivities in plasma.

These considerations lead us to,

$$f(y) = \begin{cases} \mu_0 \mu_l e^{2k_1 y/h}, \\ \mu_0 \left[\mu_{ga} e^{-2k_1 \left(\frac{y-\varepsilon}{h}\right)^2} + \mu_{gb} \right]. \end{cases} \tag{3.2}$$

Figures 3.1 (a) and (b) show the behavior of the exponential and Gaussian viscosity models for varying k_1. Furthermore, the temperature dependency is taken to be of the form:

$$g(\theta) = e^{-2k_2\left(\frac{\theta}{\theta_1}-1\right)}, \tag{3.3}$$

where the factor of two in the exponent is introduced for later computational convenience. This particular form is chosen for many reasons. For instance, when $\theta = \theta_1$, the function takes on the reference value $g(\theta_1) = 1$. This corresponds to the base fluid's viscosity μ_0 at $y = 0$ for a floating particle system, for instance. This form also takes into account the effect of increasing temperatures on viscosity. As $\theta \to \theta_2$, the argument in the exponential increases in magnitude which results in a decrease of viscosity.

In relations (3.2) and (3.3), the quantities μ_l, μ_{ga}, and μ_{gb} are arbitrary real quantities. The quantity μ_0 is taken to be the characteristic viscosity of the fluid, k_1 is a non-dimensional parameter related to the concentration and shapes of particles in the inhomogeneous medium, k_2 is a non-dimensional parameter which controls the rate of temperature dependence of the viscosity, ε is taken to be the arithmetic mean in the Gaussian distributed viscosity model and h is the width of the channel.

It should be noted that, for a fluid with viscosity μ_0, the introduction of a quantity of solid particles will increase the viscosity of the fluid, which is now a suspension. Increasing the amount of solid particles will result in an increase in the effective viscosity of the fluid. Therefore, it is reasonable to assume k_1 should be related to the volume fraction of 'light' solid particles in the suspension; k_1 will effectively increase the viscosity at all points within the channel except for y = 0. The height dependence of $f(y)$ allows for the modeling of different distributions of a suspension. k_1 is taken to be positive in our model; however, a decreasing exponential function can be used to model a suspension with 'heavy' particles or even sedimentation. Lastly, the parameter k_2 is taken to be positive and is taken to be independent of the volume fraction of solid particles within the suspension. Note: If $g(\theta) = 1$, temperature has no effect on the viscosity and the two viscosity models revert to an exponential and a Gaussian function of height y alone.

The thermal conductivity is taken to be of the form

$$k(y) = \begin{cases} k_0 e^{-k_3 y/h}, \\ k_0 \left(k_b - k_a e^{-k_3 \left(\frac{y-\varepsilon}{h}\right)^2} \right), \end{cases} \tag{3.4}$$

where k_0 is a constant reference thermal conductivity, k_3 is taken to be a positive non-dimensional parameter and is related to the volume fraction of solid particles within the suspension. It is proportional to k_1, with k_a and k_b positive constants for the Gaussian model of thermal conductivity. It is to be noted that, for example, coal has a lower conductivity than water and therefore such a model would make physical sense, in that case. This model can be readily extended to suspensions where the solid particles have a larger thermal conductivity than the base fluid. Let us move to set up the system to be solved.

3.1 Governing equations

In Chapter 2.4, the main assumptions were laid out. With these assumptions, the conservation of mass is automatically satisfied and the balance of linear momentum in the x-direction reduces to:

$$\frac{d\pi}{dx} = \frac{d}{dy}\left(\mu \frac{dU}{dy}\right). \tag{3.5}$$

The no-slip boundary conditions at the two plates are imposed such that:

$$U(y = 0) = U(y = h) = 0.$$

Furthermore, the energy equation reduces to:

$$0 = \mu\left(\frac{dU}{dy}\right)^2 + \left(\frac{dk}{dy}\right)\left(\frac{d\theta}{dy}\right) + k\frac{d^2\theta}{dy^2}. \tag{3.6}$$

where the first term represents the dissipation of the kinetic energy into internal energy by the viscosity, which results in an increase in temperature. The second and third terms represent the transfer of internal energy through molecular effects (diffusion and particle collision). These terms play a vital role in certain systems. For instance, when the boundaries are heated, it is the conductive term that introduces heat into the system.

The boundary conditions are

$$\theta(y = 0) = \theta_1,$$
$$\theta(y = h) = \theta_2,$$

where θ_1 and $\theta 2$ are the temperatures at the bottom and top plate, respectively. It is assumed that $\theta_2 > \theta_1$.

Let us now non-dimensionalize the equations (3.5) and (3.6) by using the following dimensionless forms:

$$\begin{aligned}
\overline{U} &= \frac{U}{U_0}, \\
\overline{\mu} &= \frac{\mu}{\mu_0}, \\
\overline{y} &= \frac{y}{h}, \\
\overline{\theta} &= \frac{(\theta - \theta_1)}{(\theta_2 - \theta_1)}, \\
\Delta\theta &= \theta_2 - \theta_1, \\
\overline{k} &= \frac{k}{k_0}.
\end{aligned}$$

where U_0 is the average velocity of the fluid flow, μ_0 is the viscosity of the base fluid at the bottom plate, h is the distance between the two plates, $\Delta\theta$ is the temperature difference between the two plates, and k_0 is the thermal conductivity of the base fluid at the bottom plate. With these, equation (2.10) becomes:

$$-c = \frac{d\overline{\mu}}{d\overline{y}}\frac{d\overline{U}}{d\overline{y}} + \overline{\mu}\frac{d^2\overline{U}}{d\overline{y}^2}$$

where c is related to the pressure drop $\Delta\pi$ across the length of the channel, and the Reynolds number (Re) and given by $Re\frac{d\Delta\pi}{U_0 L}$. Note: the Reynolds number does not explicitly appear due to the assumption $d\pi/dx \sim \Delta\pi/L$. The boundary conditions for the momentum equation are:

$$\overline{U}(0) = \overline{U}(1) = 0.$$

The dimensionless form of the energy equation (2.12) becomes:

$$0 = \gamma\left[\overline{k}\frac{d^2\overline{\theta}}{d\overline{y}^2} + \frac{d\overline{k}}{d\overline{y}}\frac{d\overline{\theta}}{d\overline{y}}\right] + \overline{\mu}\left(\frac{d\overline{U}}{d\overline{y}}\right)^2,$$

where γ is a non-dimensional quantity defined as

$$\gamma = \frac{k_0\Delta\theta}{\mu_0 U_0^2},$$

where k_0 is the thermal conductivity of the base medium and $\Delta\theta$ is the temperature difference across the channel. We note that γ can be viewed as a parameter which relates heat production due to both thermal (conduction) $k_0\Delta\theta$ and viscous

(dissipation) $\mu_0 U_0^2$ effects, a sort of competition between the two. Finally, the non-dimensional forms of the boundary conditions for the energy equation are:

$$\overline{\theta}(0) = 0,$$
$$\overline{\theta}(1) = 1.$$

The bar notation is now dropped, recognizing that all quantities are non-dimensional from this point on. The governing equations for this system are:

$$-c = \frac{d\mu}{dy}\frac{dU}{dy} + \mu\frac{d^2U}{dy^2}, \tag{3.7}$$

$$0 = \gamma\left[k\frac{d^2\theta}{dy^2} + \frac{dk}{dy}\frac{d\theta}{dy}\right] + \mu\left(\frac{dU}{dy}\right)^2, \tag{3.8}$$

subject to

$$U(0) = U(1) = 0, \tag{3.9}$$

$$\theta(0) = 0, \theta(1) = 1. \tag{3.10}$$

In the next section, a numerical (parametric) study for different values of the relevant dimensionless numbers and transport properties, i.e. viscosity and thermal conductivity, is performed.

3.2 Results

In this section, we describe the results of our computations for the various cases described below. In Case 1, the system (3.7) and (3.9) is solved, where the system is taken to be isothermal; a simple analytical solution is possible to obtain, at least in the case of the exponential viscosity model. In Case 2, temperature effects are taken into account; that is, the system (3.7) - (3.10) is solved.

Case 1: Variable viscosity with constant temperature. The solution to the system (3.7) and (3.9), when temperature is a constant permits a closed form for the velocity $U(y)$. The exponential viscosity case is more tractable and is shown below. In particular, the velocity $U(y)$ and flow rate Q are given by:

$$U(y) = \frac{ce^{-2k_1 y}}{2k_1\left(e^{2k_1}-1\right)}\left(1-e^{2k_1 y}-y\left(1+e^{2k_1}\right)\right), \tag{3.11}$$

$$Q = \frac{c\left(\coth\left(k_1\right) - 1\right)\left(\cosh\left(2k_1\right) - 2(k_1)^2 - 1\right)}{(2k_1)^3}. \tag{3.12}$$

The analytical solutions for the Gaussian model remain complex and cannot be presented in a simple enough analytical form. The results are computed numerically and shown in Figures 3.2 and 3.3. In addition to the velocity, we also compute the flow rate since this provides meaningful insight into the physics of the problem and a way to discuss the feasibility of pipeline transport of suspensions (biomass). A detailed analysis of the variations in the flow rate is presented towards the end of this section. The Figures 3.2 and 3.3 show the steady velocity profile and its dependence upon the parameters k_1 and c.

The overall profile in the aforementioned figures remain skewed parabolic in the exponential case and parabolic in the Gaussian case. In the former, the velocity achieves its maximum away from the centerline of the channel while in the latter case, the maximum speed of the flow is along the centerline, determined by the nature of the viscosity function and hence the 'distribution of the suspended particles'. The effect of k_1 in the exponential viscosity case is to contract the profile and increasing values of k_1 results in a lowering of the position of the maximum speed. The overall speed of the flow becomes slower with increasing k_1; the value of this parameter effectively increases viscosity due to increased particle concentration, see the introduction to this chapter for more details. Note that with regard to the parameter c increasing values cause the velocity to increase since c is related to the pressure gradient of the flow.

Case 2: Variable viscosity and temperature. When thermal effects are included, the velocity profiles change considerably. The solutions for the system (3.7) - (3.10) were found numerically and are plotted below in Figures 3.4 - 3.8, for select values of the parameters k_1, k_2, k_3, γ and c. The figures below specifically show the velocity and temperature profiles for the exponential and Gaussian viscosity models. In the former case, the combined effect of spatial and temperature variation of viscosity renders the velocity profile less skewed away from the centerline of the channel than in Figure 3. As seen earlier, increasing k_1 decreases the speed while k_2 has the effect of stretching the profile, i.e. increasing the speed of the flow. The parameter k_3 has a relatively negligible effect upon the flow profile, as seen in Figure 3.6. The temperature distribution is seen to be nonlinear in both viscosity models and unaffected by any variations in k_1 and k_2 but is effected by k_3. Note that in the case where $k_3 = 0$, the temperature assumes a linear profile, which is anticipated for non-varying thermal conductivity. The prominent difference between the two models remains the shape of the velocity curve; in particular the presence of an almost uniform-flow region in the Gaussian case. In all the cases analyzed, the temperature profile for the exponential viscosity model shows a concave down profile while the Gaussian model reveals the presence of an inflection point. The most noteworthy plot is Figure 3.8 which shows the variation of velocity and temperature for different values of γ. The

effect of changing γ results in no prominent change in the flow speed, but surprisingly gives rise to a 'hot spot' in the top half of the channel. This phenomenon is present in both viscosity models and is pronounced in the case of smaller values of γ approaching zero. This phenomenon was also observed by Gupta and Massoudi [4] who attributed it to the effects of viscous dissipation.

In Tables 3.1 and 3.2, we summarize the results by looking at the effects of fluid properties on the numerical simulations for various parametric sweeps. We identify the location ξ of the maximum velocity U_{max} achieved in the channel. The variation of the parameters k_1, k_2, and k_3 has a net effect of changing the maximum and minimum viscosity in the channel. This in turn determines the magnitude of the velocity. As k_1 is increased, the ratio between the maximum velocity and the base case decreases. However, this ratio does not vary much with variation in k_2, k_3 or γ but does show a noticeable change with parameter c. The primary difference between the tables seems to be the position of the maximum. The flow speed shows a changing maximum and is strongly dependent upon the various parameters employed in this study. However, in Table 3.2, the values of ξ remains fairly uniform, showing a slight shift from the centerline due to thermal effects.

Finally, we also computed the flow rates for the cases analyzed in this section. The flow rate in our study is given in the non-dimensional form as

$$Q = \int_0^1 U(y)\, dy \tag{3.13}$$

The flow rate was computed numerically using the trapezoidal method with maximum step-size $\Delta y_{max} = 0.000005$. Figures 3.9 - 3.11 present the variations of the flow rate Q versus the rest of the parameters in our study. In all of the figures the profile for both models is essentially similar. Note that despite the exponential model's larger maximum velocity for each case, the Gaussian model exhibits a larger flow rate. Figure 3.9 (a) shows that the flow rate decreases rapidly with increasing k_1 while the remaining parameters are fixed and non-zero. In fact, we note that increasing concentration of particles by varying k_1 between 0 and 2.5 results in a nearly a 90% drop in the flow rate. However, k_2 has the effect of increasing the flow rate as seen in Figure 3.9 (b). Figure 3.10 (a) exhibits a relatively small flow rate dependence on k_3; in fact the Gaussian model nearly remains unchanged over the range of k_3 explored. Therefore, we infer that the introduction of thermal effects can help increase the flow rate by decreasing the effective viscosity of the system, however, variability of the thermal conductivity does not affect the flow rate very much. Figures 3.10 (b) and 3.11 validate the results from the previous subsection that flow rate strongly depends upon c but is minimally affected by γ.

3.3 Notes on Convergence of Numerical Solutions

The high nonlinear coupling in the system made it difficult to obtain precise solutions, even with sophisticated numerical techniques. The system of equations (3.7) - (3.10) are solved using MATLAB's 'bvp4c' package, which utilizes a three-stage Lobatto IIIa scheme, a variation of the Runge-Kutta method. The step-size Δy was chosen to be 0.00005 and the relative tolerance was set to 10^{-9}. Solutions were verified by seeking zeros of equations (3.7) and (3.9). It was found that the parameters k_1, k_2, k_3, c, and γ play an important role on the stability of the numerical solutions.

The most important of these parameters was c. The range of values tested range between 1 and 30. It was found that as $c \to 1$, solutions became increasingly stable. Futhermore, with $c \approx 1$, stability was exceptional for all choices of the other parameters. However, for c exceeding 20 and approaching 30, the numerical stability deteriorates; to reach stable solutions, the parameters k_1 and k_3 must take on increasingly larger values; that is, for $c \to \infty$ we require $k_1, k_2 \to \infty$.

The two parameters, k_1 and k_3, interacted with one another to each other's benefit, with increasing k_1 values acting to stabilize the solutions. However, $k_1 \approx 1$, deviations in solutions were noticed; k_1 proved to be the second most influential parameter in dictating the stability of the solutions. k_2 became problematic for small values of k_1, γ, and c; the larger the value, the greater the deviation from zero (noticeably so at the top of the channel). Lastly, γ also played a role in the numerical stability. In particular, for $\gamma \to 0$ and $k_2 \geq 2$, oscillations in the numerical solutions occur (alluded to above in the case of $c > 20$ and $k_1 \to 1$).

Let's take a moment to analyze the convergence figures, Figures 3.12 (a) and (b). As we decrease the step-size Δy, the magnitude of the relative errors decrease, in general. Furthermore, for the exponential case, the magnitude of the relative error between these values decreases as the relative tolerance decreases in solving the problem. This is not true for the Gaussian case, which exhibits nearly no change in accuracy with change in the relative tolerance. Regardless, the difference between solutions with relative tolerances of 10^{-9} and 10^{-12} is negligible; that is, the extra demand on the computation is unnecessary. These trends can be seen in Figure 8.

The values of all parameters in our study were chosen such that the errors were minimized while encompassing a broad enough range to give a suitable enough idea of trends in the solutions, while simultaneously minimizing the values of parameters k_1, k_2, and k_3.

3.4 Notes on applications

There are powerful implications in real applications of the results obtained here. Kumar et al. [52] discusses biomass transport with simultaneous saccharification of corn stover. It is estimated that a temperature of 65 degrees Celsius is needed for

the process over a 36 hour period. This could be achieved, for instance, by uniformly heating the pipeline. Although the reduction in processing time would be significantly reduced, the cost associated with heating is undoubtedly significant; the proposal of a method to mitigate this cost by any feasible means would be welcome.

In our study, we show that the ability to modify the thermal conductivity of an inhomogeneous fluid allows us to potentially control the temperature distribution within a pipe; for instance, corn stover has a tendency to float and so we may mix solid particulate into a suspension with the same tendency, but with a higher thermal conductivity. In principle, this could yield a rapid increase in temperature at the bottom of the channel to near top channel temperatures. This would maximize the percentage of the channel, and therefore the corn stover, which experiences near top channel temperatures. In other words, the pipeline can be heated non-uniformly and cheaper. The specific details can be fleshed out by those with intimate knowledge of the cost of such industrial processes; however, we have supplied the recipe, so to speak. Although biomass transport is used as motivation for the development of the model, the study is intended to be more general.

Another interesting consequence is that we could potentially optimize the flow rate output such that the maximum amount of solid particulate is transfered per unit time per capital spent. This can be done by recognizing that the parameter c is related to the pressure drop across the channel. An optimization model could be coupled to the system pairing our parameters with monetary considerations, such as the cost of maintaining the pressure drop across a pipe. From our analysis, the parameters c and k_1, related to the volume fraction of solid in the suspension, should have the most impact on the feasibility of pipeline transport of biomass, for instance.

3.4.1 Concluding remarks

A model for the transport of a fluid with suspended particles in it is discussed. The effect of temperature and heat transfer upon the flow is analyzed rendering the general problem highly nonlinear. Analytical and numerical solutions to the governing equations are obtained and the flow rate of the system is obtained. The important dimensionless numbers are c (related to the pressure drop and the Reynolds number) and γ (related to the viscous dissipation).

Two models were proposed: an exponentially increasing model and a Gaussian model for the viscosity and thermal conductivity of the suspension. The parameters k_1 and k_3 are related to the volume fraction of suspended particles in the base fluid and k_2 decides the impact of temperature on the viscosity. The effect of k_1 in the exponential viscosity case is to contract the profile and increasing values of k_1 results in a lowering of the position of the maximum speed. The overall speed of the flow becomes slower with increasing k_1; the value of this parameter has the effect of essentially increasing viscosity due to increased particle concentration. The parameter k_3 has a relatively negligible effect upon the flow profile. However, it has a powerful effect upon the

temperature distribution. The temperature distribution is seen to be nonlinear in both viscosity models and unaffected by any variations in k_1, k_2 but is effected by k_3. Note that in the case where $k_3 = 0$, the temperature assumes a linear profile, which is anticipated for non-varying thermal conductivity. It was also found that the parameters k_1, k_2, k_3, c, and γ play an important role on the stability of the numerical solutions. The most important of these was c.

k_1	k_2	k_3	γ	c	$U_{\max}$	ξ	$\frac{\mu_{\max}}{\mu_{\min}}$	$\frac{U_{\max}}{U_b}$	$\frac{k_{\max}}{k_{\min}}$
0.00	1.00	1.00	100.00	10.00	1.4121	0.522	1.3138	0.9842	2.7183
1.00	1.00	1.00	100.00	10.00	0.5305	0.361	5.6243	0.3697	2.7183
2.50	1.00	1.00	100.00	10.00	0.1499	0.201	112.9680	0.1045	2.7183
1.00	0.00	1.00	100.00	10.00	0.4752	0.343	7.3891	0.3312	2.7183
1.00	1.00	1.00	100.00	10.00	0.5305	0.361	5.6243	0.3697	2.7183
1.00	2.50	1.00	100.00	10.00	0.6287	0.39	3.7350	0.4382	2.7183
1.00	1.00	0.00	100.00	10.00	0.5399	0.362	5.6243	0.3763	1.0000
1.00	1.00	1.00	100.00	10.00	0.5305	0.361	5.6243	0.3697	2.7183
1.00	1.00	2.50	100.00	10.00	0.5184	0.358	5.6243	0.3613	12.1825
1.00	1.00	1.00	1.00	10.00	0.5763	0.37	5.6243	0.4016	2.7183
1.00	1.00	1.00	100.00	10.00	0.5305	0.361	5.6243	0.3697	2.7183
1.00	1.00	1.00	1000.00	10.00	0.5301	0.361	5.6243	0.3695	2.7183
1.00	1.00	1.00	100.00	1.00	0.0530	0.361	5.6243	0.0369	2.7183
1.00	1.00	1.00	100.00	10.00	0.5305	0.361	5.6243	0.3697	2.7183
1.00	1.00	1.00	100.00	20.00	1.0634	0.36	5.6243	0.7412	2.7183

Table 3.1: Summary of flow properties for the exponential models of viscosity and thermal conductivity. $U_b = 1.4121$ corresponding to the case for $k_1 = 0$.

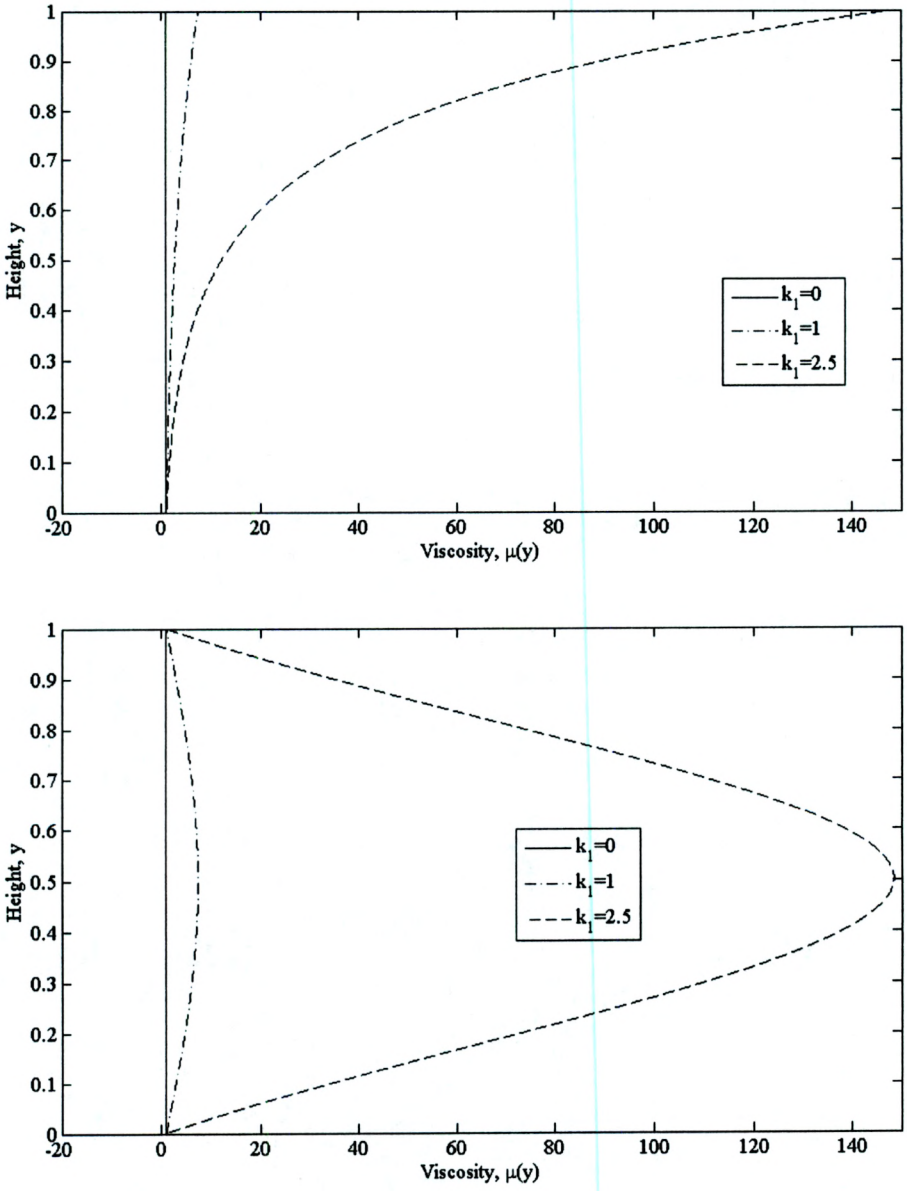

Figure 3.1: (a) The exponential viscosity model, (b) The Gaussian viscosity model for varying k_1, $\mu_l = 1$, $\mu_{ga} = (e^{2k_1} - 1)/(1 - e^{-\frac{k_1}{2}}$) and $\mu_{gb} = e^{2k_1} - \mu_{ga}$

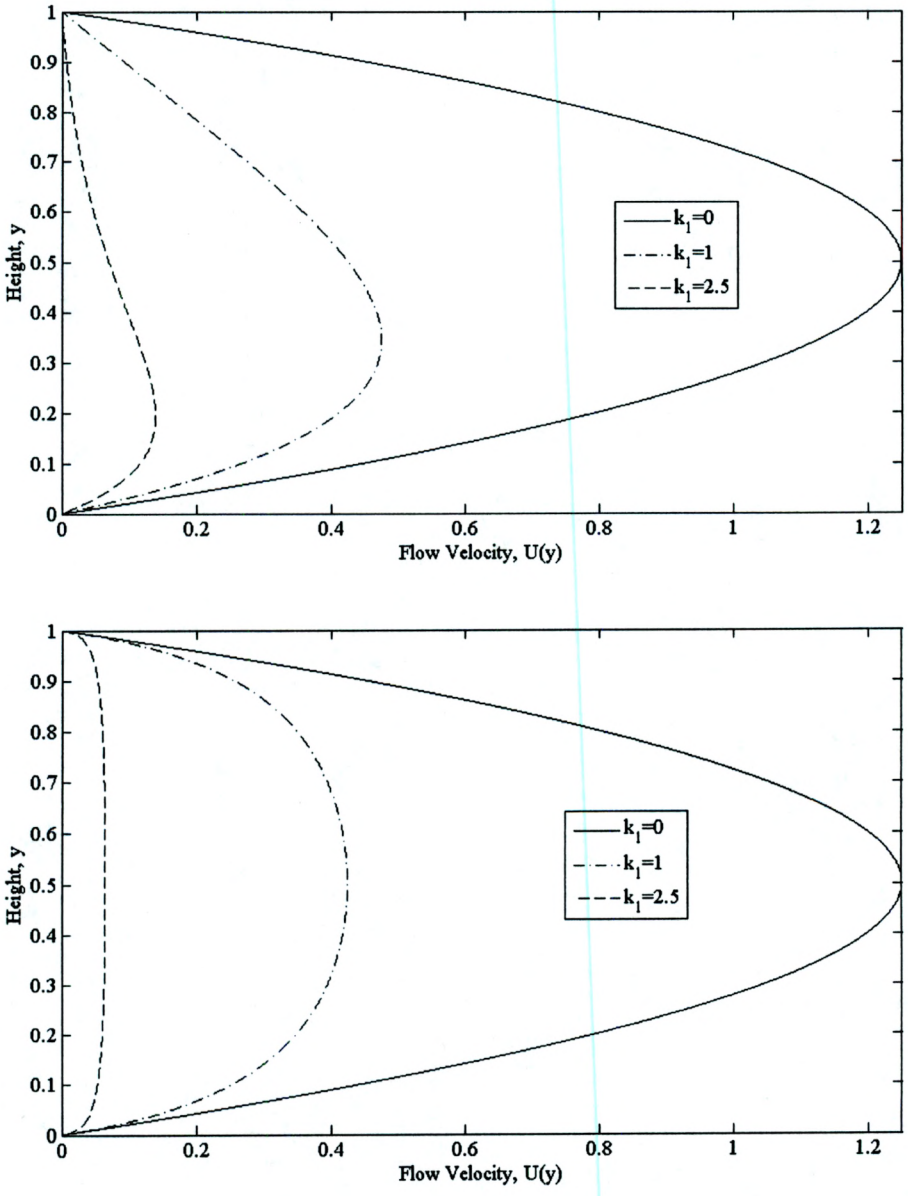

Figure 3.2: Velocity profiles for (a) exponential and (b) Gaussian viscosity models with varying k_1 and $c = 10$

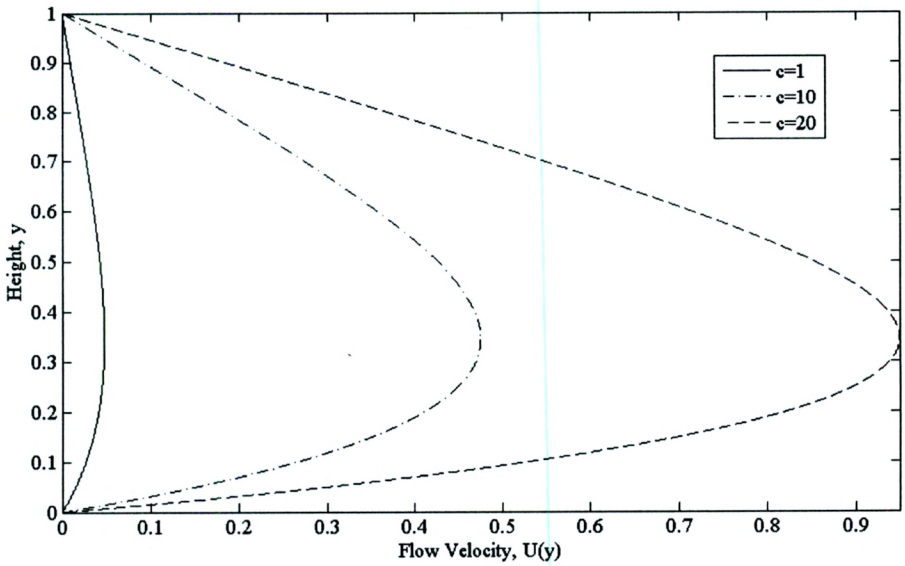

Figure 3.3: Velocity profiles for (a) exponential and (b) Gaussian viscosity models with varying c and $k_1 = 1$

k_1	k_2	k_3	γ	c	$U_{\max}$	ξ	$\frac{\mu_{\max}}{\mu_{\min}}$	$\frac{U_{\max}}{U_b}$	$\frac{k_{\max}}{k_{\min}}$
0.00	1.00	1.00	100.00	10.00	1.4348	0.524	1.3138	1.0000	2.7183
1.00	1.00	1.00	100.00	10.00	0.4848	0.537	8.5395	0.3379	2.7183
2.50	1.00	1.00	100.00	10.00	0.0735	0.55	171.0562	0.0512	2.7183
1.00	0.00	1.00	100.00	10.00	0.4238	0.499	7.3891	0.2954	2.7183
1.00	1.00	1.00	100.00	10.00	0.4848	0.537	8.5395	0.3379	2.7183
1.00	2.50	1.00	100.00	10.00	0.5887	0.592	10.9270	0.4103	2.7183
1.00	1.00	0.00	100.00	10.00	0.4851	0.534	8.5016	0.3381	1.0000
1.00	1.00	1.00	100.00	10.00	0.4848	0.537	8.5395	0.3379	2.7183
1.00	1.00	2.50	100.00	10.00	0.4843	0.54	8.7061	0.3375	12.1825
1.00	1.00	1.00	1.00	10.00	0.4983	0.536	8.5440	0.3473	2.7183
1.00	1.00	1.00	100.00	10.00	0.4848	0.537	8.5395	0.3379	2.7183
1.00	1.00	1.00	1000.00	10.00	0.4847	0.537	8.5259	0.3378	2.7183
1.00	1.00	1.00	100.00	1.00	0.0485	0.537	8.0849	0.0338	2.7183
1.00	1.00	1.00	100.00	10.00	0.4848	0.537	8.5395	0.3379	2.7183
1.00	1.00	1.00	100.00	20.00	0.9704	0.537	8.5436	0.6763	2.7183

Table 3.2: Summary of flow properties for the Gaussian models of viscosity and thermal conductivity. $U_b = 1.4348$ corresponding to the case for $k_1 = 0$.

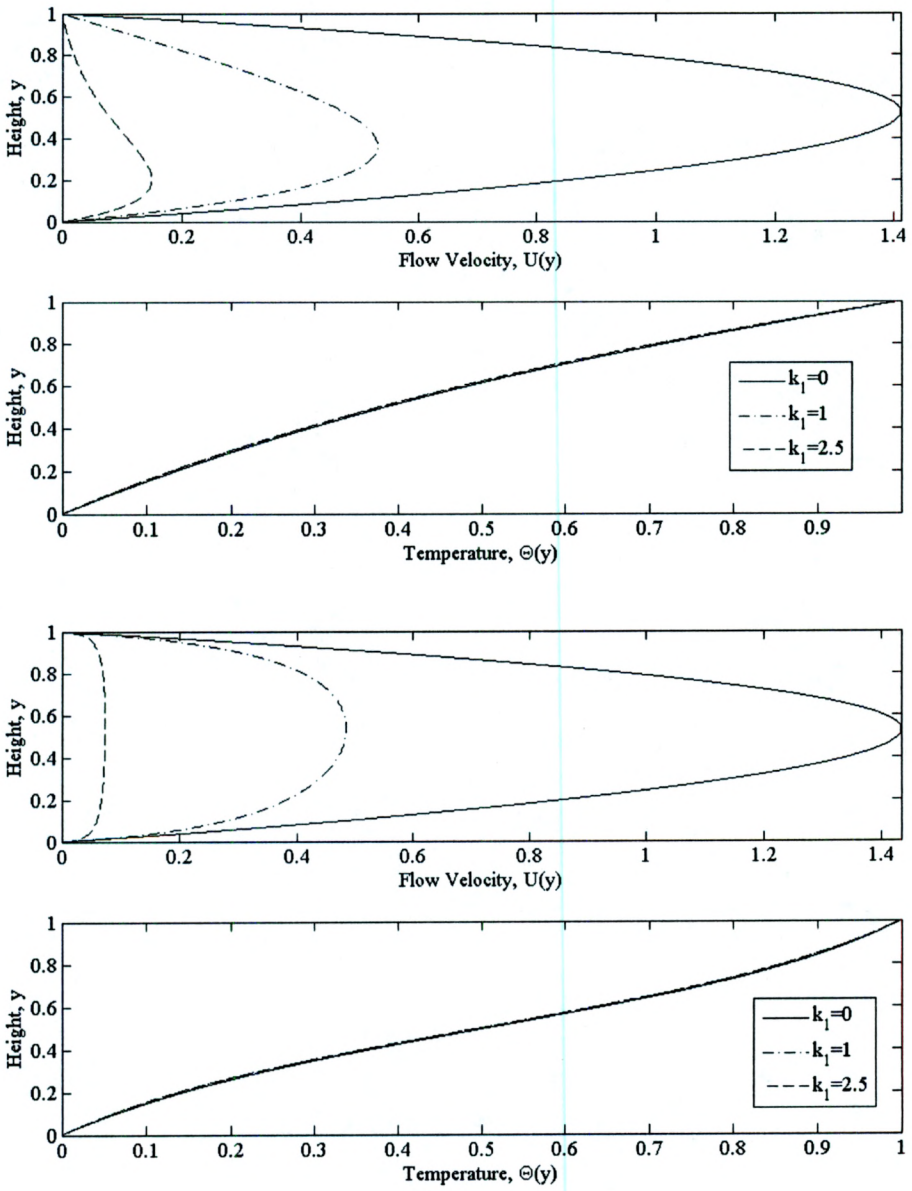

Figure 3.4: (a) Velocity and temperature profiles for exponential viscosity model with k_1 varying for $k_2 = k_3 = 1$, $\gamma = 100$, and $c = 10$ (b) Gaussian viscosity model with k_1 varying for $k_2 = k_3 = 1$, $\gamma = 100$, and $c = 10$.

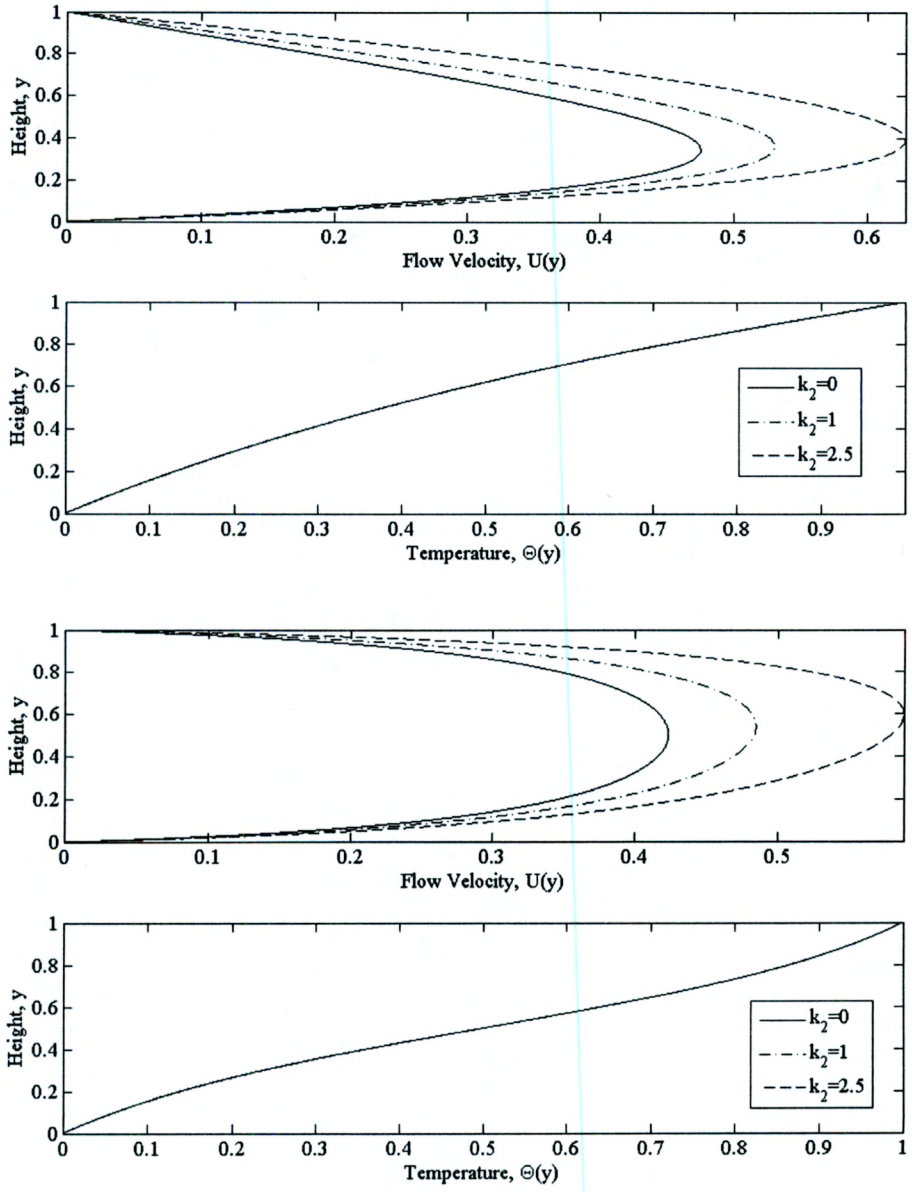

Figure 3.5: (a) Velocity and temperature profiles for exponential viscosity model with k_2 varying for $k_1 = k_3 = 1$, $\gamma = 100$, and $c = 10$ (b) Gaussian viscosity model with k_2 varying for $k_1 = k_3 = 1$, $\gamma = 100$, and $c = 10$.

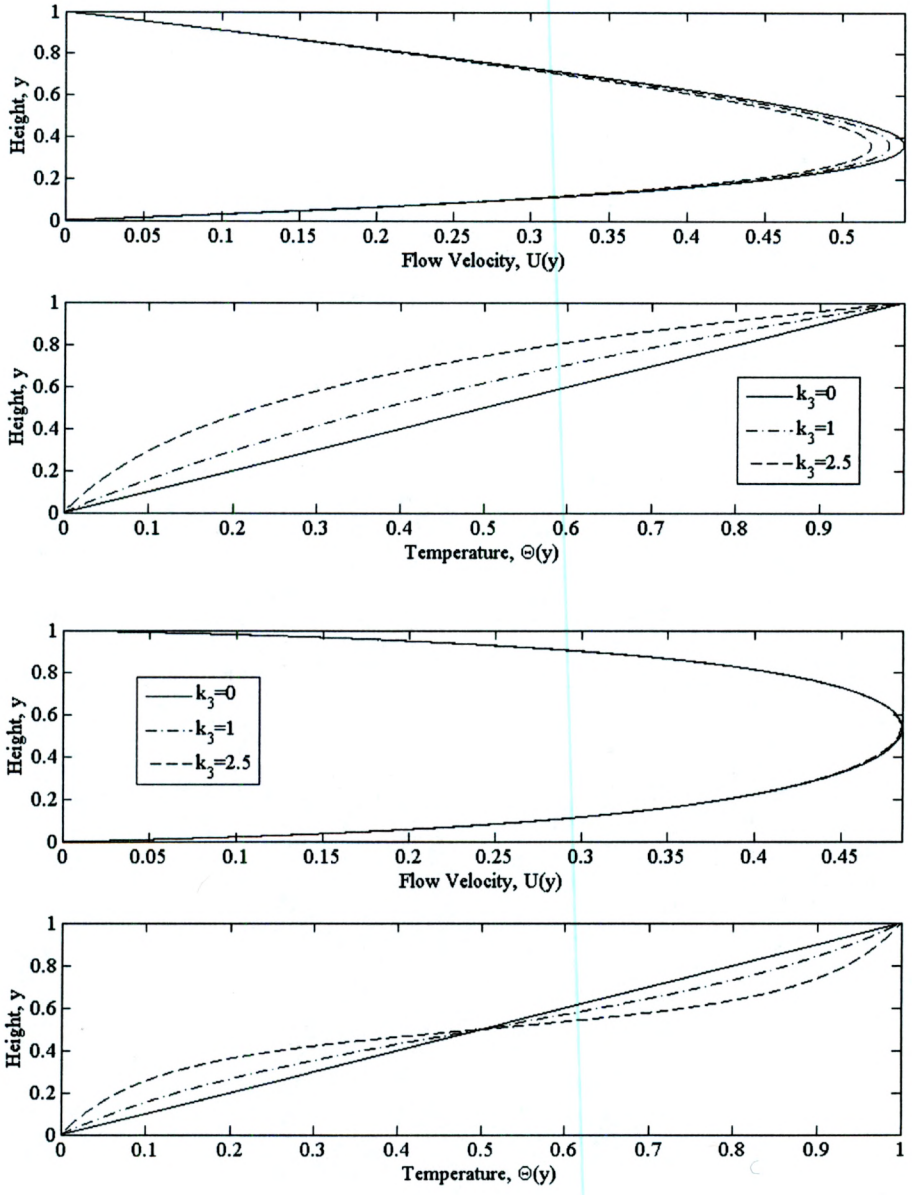

Figure 3.6: (a) Velocity and temperature profiles for exponential viscosity model with k_3 varying for $k_1 = k_2 = 1$, $\gamma = 100$, and $c = 10$ (b) Gaussian viscosity model with k_3 varying for $k_1 = k_2 = 1$, $\gamma = 100$, and $c = 10$.

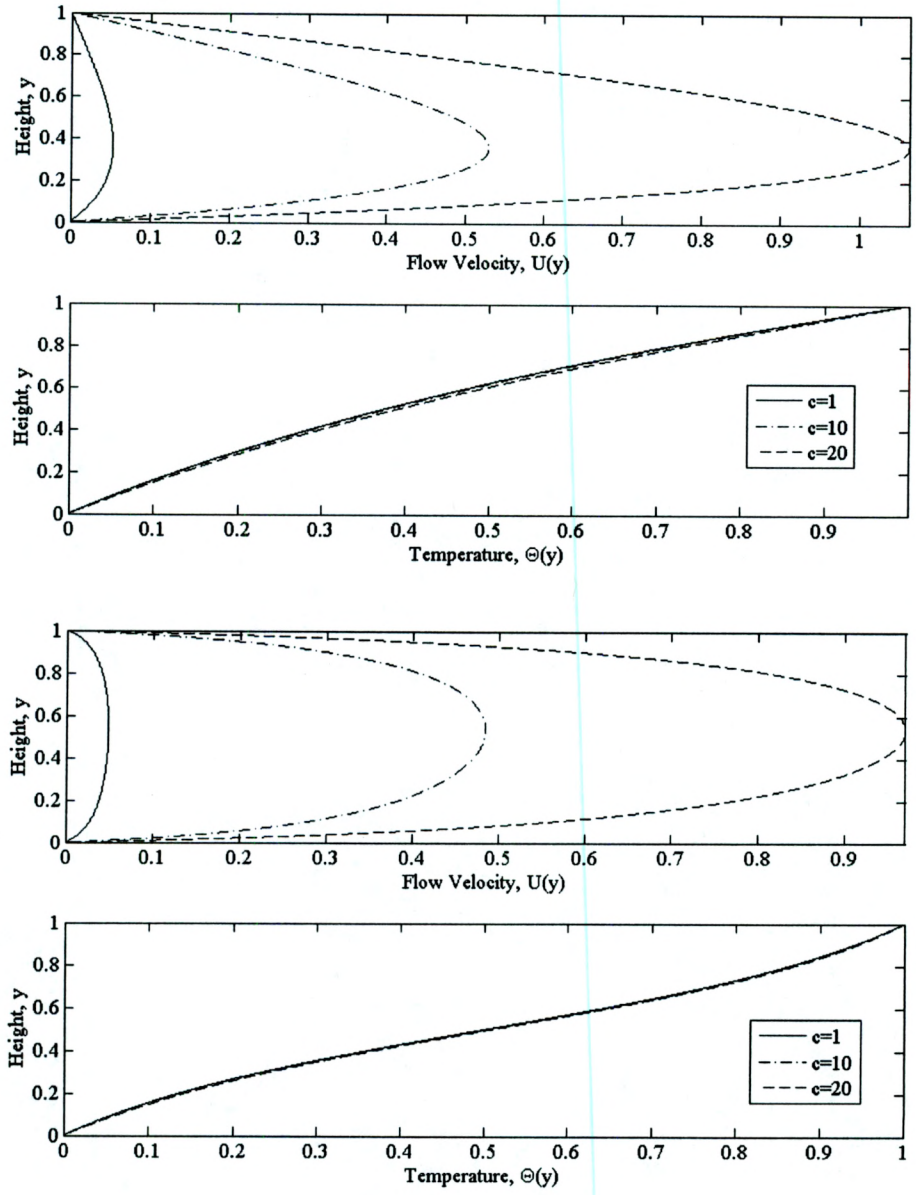

Figure 3.7: (a) Velocity and temperature profiles for exponential viscosity model with c varying for $k_1 = k_2 = k_3 = 1$, and $\gamma = 100$ (b) Gaussian viscosity model with c varying for $k_1 = k_2 = k_3 = 1$, and $\gamma = 100$.

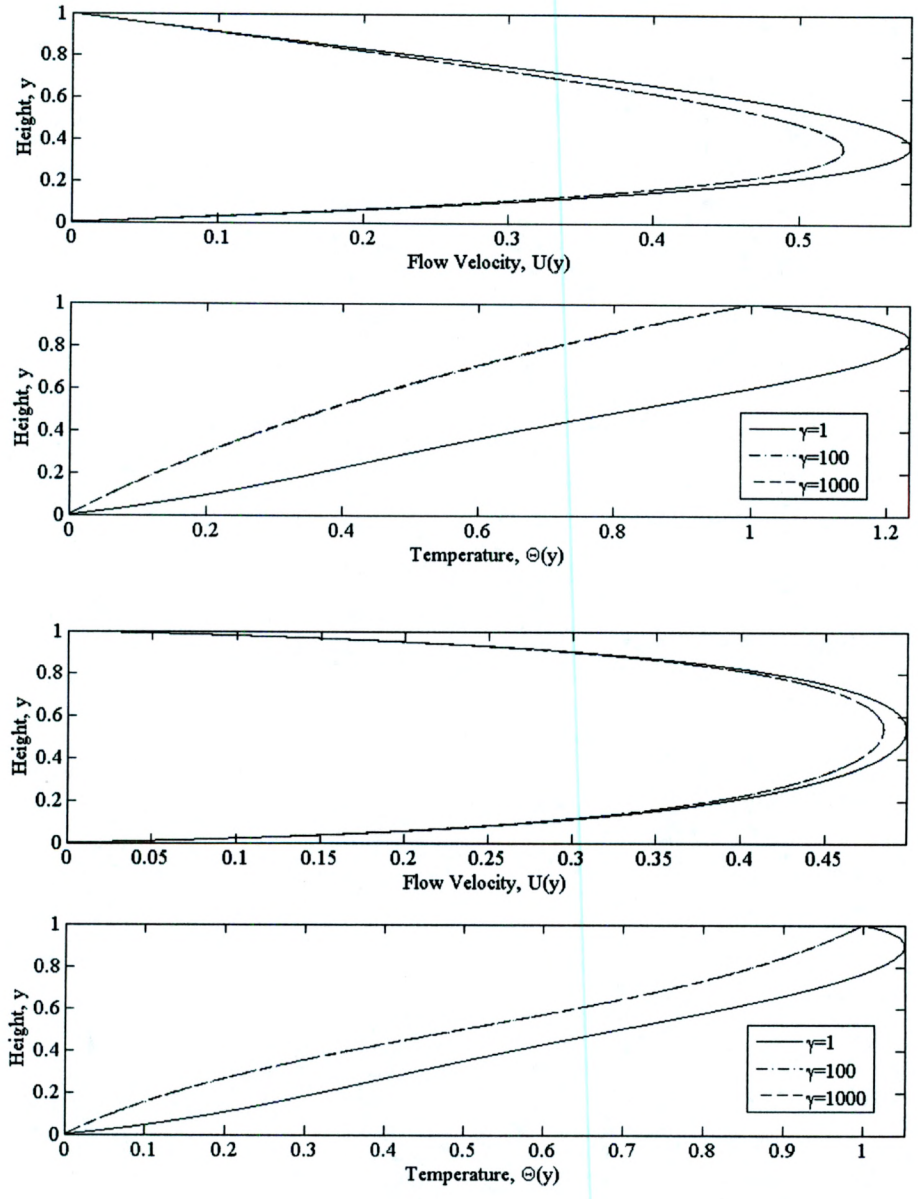

Figure 3.8: (a) Velocity and temperature profiles for exponential viscosity model with γ varying for $k_1 = k_2 = k_3 = 1$, and $c = 10$ (b) Gaussian viscosity model with γ varying for $k_1 = k_2 = k_3 = 1$, and $c = 10$.

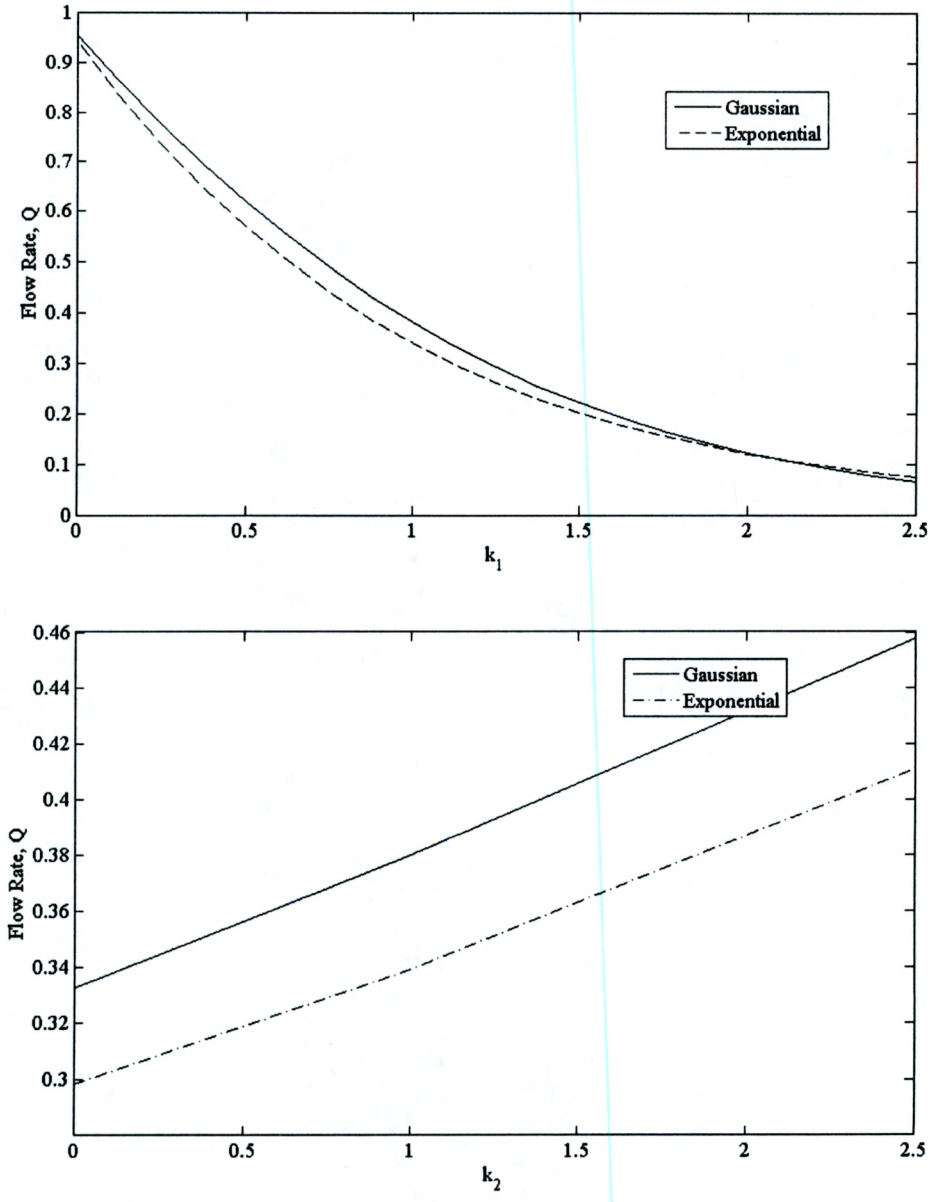

Figure 3.9: (a) Flow rate comparison between the exponential and Gaussian models with k_1 varying for $k_2 = k_3 = 1$, $\gamma = 100$, and $c = 10$ (b) with k_2 varying for $k_1 = k_3 = 1$, $\gamma = 100$, and $c = 10$.

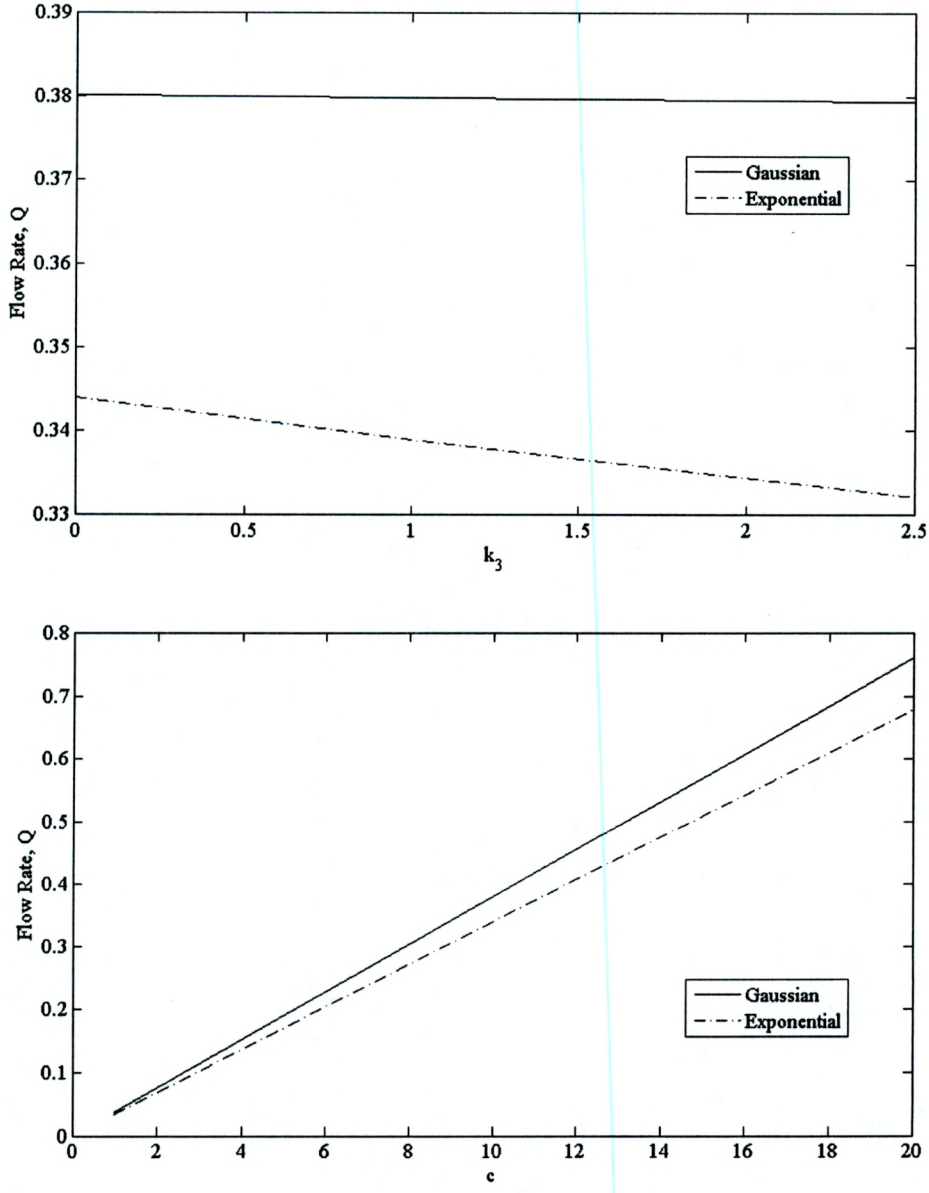

Figure 3.10: (a) Flow rate comparison between the exponential and Gaussian models with k_3 varying for $k_1 = k_2 = 1$, $\gamma = 100$, and $c = 10$ (b) with c varying for $k_1 = k_2 = k_3 = 1$, and $\gamma = 100$.

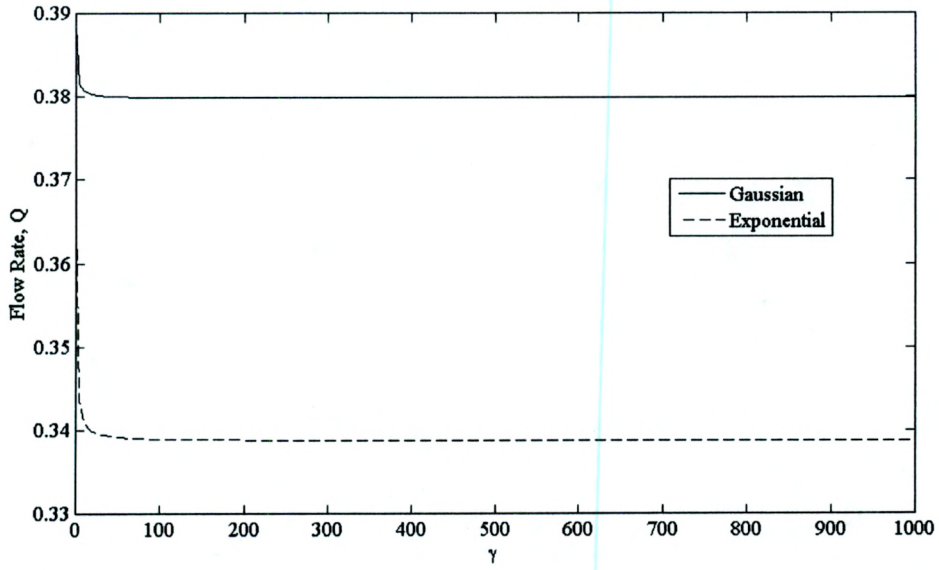

Figure 3.11: Flow rate comparison between the exponential and Gaussian models with γ varying for $k_1 = k_2 = k_3 = 1$, and $c = 10$.

Parameter	Value	Unit
U_0	0.00020040	m/s
μ_0	0.001002	$Pa \cdot s$
h	1	m
L	5000	m
ρ	1000	kg/m^3
θ_1	293.15	K
$\Delta\theta$	40	K
k_0	0.6	$W/m \cdot K$
Δy	0.00005	-
$RelTol$	10^{-9}	-

Table 3.3: Summary of parameter values for the numerical study in this chapter. Parameters which are swept are not listed here.

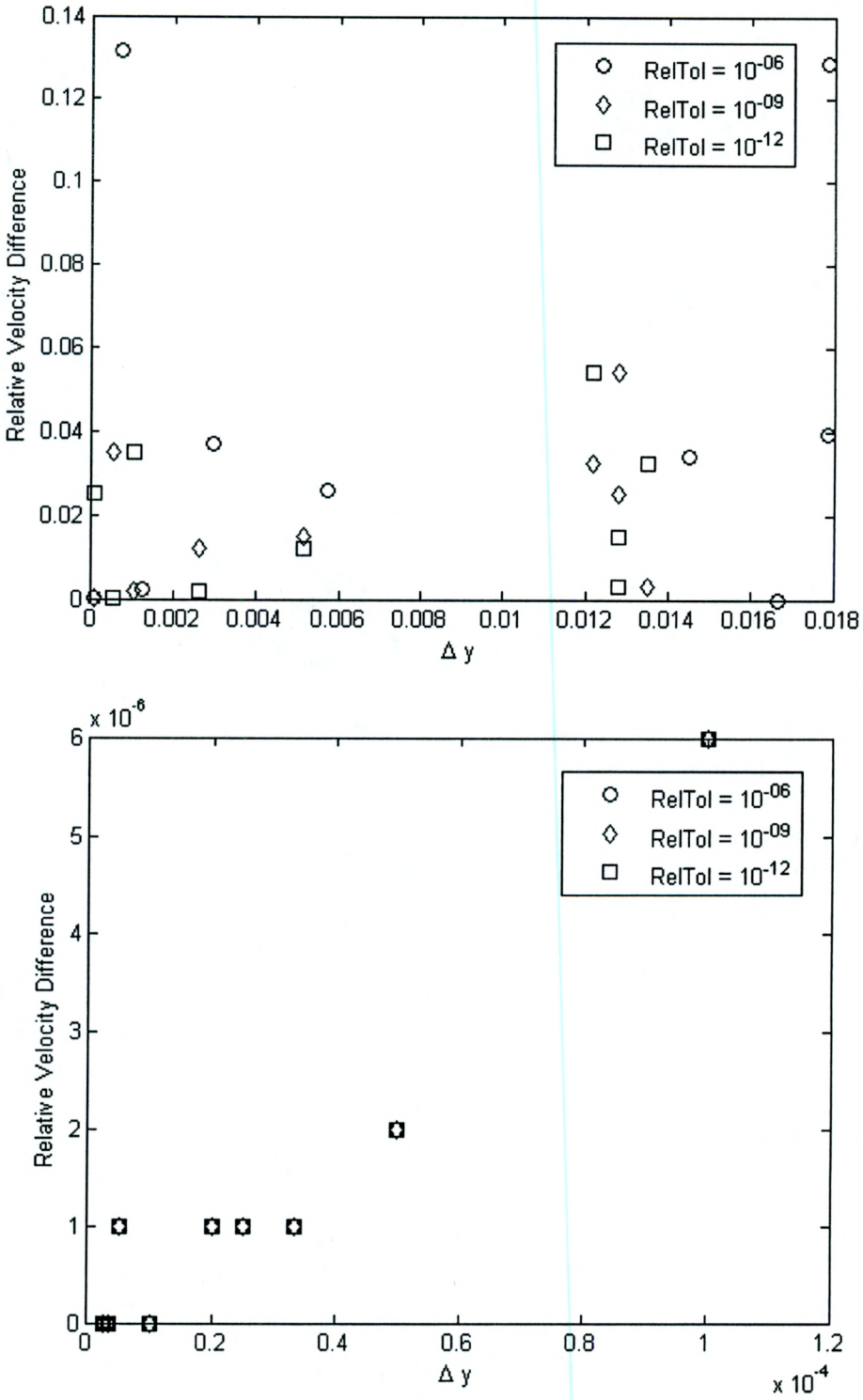

Figure 3.12: Relative velocity differences vs. step-size for the (a) exponential model and (b) Gaussian model .

Chapter 4

Second problem: Two regime pressure gradient dependent flow of an inhomogeneous fluid

The effect of pressure on the viscosity of fluids has been well documented in the high pressure regime experimentally, but the low pressure regime has not been studied systematically. The recent experimental study by Massoudi et al. [8] is a crucial motivating factor in the implementation of this dependency in our model. This study was performed at the Complex Fluids Laboratory at Montclair State University. Experiments were performed using salt water, crushed leaves, mulch, sand and coffee powder in water. A mixture was poured into an initial holding tank and then transfered to a second tank. This transfer was moderated by a valve, which served to maintain the pressure head in conjunction with a second valve. The mixture was then allowed to flow through a pipe and collected into a third tank, see Figure 4.25.

The volume fractions of each of the inhomogeneous mixtures were varied between 2% and 6%. Additionally, the pressure head was varied between 240 and 1250 Pa. The volumetric flow rate and percentage of solid particles transfered were recorded, which are pertinent to our study. The authors compared the results for an inhomogeneous fluid to that of salt water, a homogeneous fluid (mixture).

The volumetric flow rate measurements were curve fit to,

$$Q = \alpha_0 \frac{\Delta\pi}{L} \exp\left(\frac{-k_1 \Delta\pi}{L}\right), \tag{4.1}$$

where k_1 is the same real constant seen in relation (2.16), α_0 is related to the volume fraction of solid particles in the flow, $\Delta\pi$ is the pressure difference across the pipe, and L is the length of the channel. This relationship was derived using a physically reasonable exponential pressure dependent viscosity model (2.16) under the same conditions we will impose on our system. This model is different from all other previously posed models mentioned in the literature review in that it depends on the

pressure gradient, rather than the point-wise pressure; this is an important difference. The relationship (4.1) fits remarkably well to the experimental data and therefore is a valid predictor of this phenomena.

Three figures have been reproduced here from [8]. In Figures 4.1 and 4.2, we see the volumetric flow rate plotted versus the pressure gradient across the channel. Water and salt water show linear behavior over the range of pressure gradients imposed on the system; this holds for salt concentrations up to 35% in their experiments. A sand mixture shows the same behavior for 2% and 4% volume fraction of sand in water. Coffee powder, mulch, and leaves in water at 2, 4, and 6% volume fractions show an exponentially decaying profile with an initial linear growth period. It is these profiles that are particularly interesting.

The table found in Figure 4.3 lists the percentage of solid material transfered for a given pressure head. Furthermore, these percentages are gathered for different volume fractions of each solid material. From the table, we see that as the pressure head increases, the percentage of solid material transfered increases. This trend is seen across the board. As we increase the pressure gradient, the amount of solid particles entering the fluid flow increases; that is, volume fraction ϕ is dependent on Δpi.

Although the pressure gradient is an important factor, it should not be the only factor effecting the viscosity of an inhomogeneous fluid; among other parameters, there should at least be dependence on the volume fraction of solid particles in the suspension, which has been shown to be important in numerous studies. This dependence has been the primary target of suspension rheology in its varied aspects. For volume fractions less than 5%, the Einstein model (2.10) is both accurate and simple. Furthermore, we may also consider both shear thinning and shear thickening fluids. Such a dependence is of great importance because it allows for the consideration of a far greater scope of suspensions; in effect, this dependence acts to generalize the study further, although adding a significant degree of complexity.[1]

We assume that the viscosity of the suspension can be adequately accounted for by a product of functions of volume fraction, shear rate, and pressure gradient; that is,

$$\mu(\pi, \text{grad}(\pi), \phi, \dot{\gamma}, ...) \equiv f(\text{grad}(\pi))g(\phi)h(\dot{\gamma}). \tag{4.2}$$

We contend that theoretical consideration based on sound physical principles should be able to further validate the pressure gradient dependence of the viscosity in this regime. Furthermore, a two regime flow is considered; that is, the fluid is broken into a developing regime and fully developed regime. In the former, the fluid is thought to have some volume fraction distribution throughout the height of the channel. As the pressure gradient across the channel increases, more solid particles are propelled into

[1]Note: there is a pertinent phenomenon called 'hydroclustering' which occurs when a colloidal suspension experiences relatively large stresses (shearing rates). The colloidal particles form 'clusters' which increase the viscosity of the suspension; this is a shear-dependent viscosity. See, for instance, Wagner and Brady [50] for further discussion.

the flow from either a sedimented or floating state. The increase of solid particles entering the flow causes the viscosity to increase; that is, the viscosity is dependent on the pressure gradient across the channel. This continues until the suspension is saturated with virtually all of the solid material. At this point, the fluid is considered to behave as a homogeneous fluid independent of pressure effects; that is, although the fluid is inhomogeneous, the bulk qualities of the fluid are homogeneous-like. Such behavior is seen in other contexts, such as fluidized beds [51].

4.1 Governing equations

Let us now define each of the functions. The viscosity μ of the suspension is given by relation (4.2) with

$$f(\text{grad}(\pi)) = \begin{cases} \mu_0 e^{\alpha|\text{grad}(\pi)|} & \text{if } \Delta\pi < \Delta\pi_c, \\ \mu_1 & \text{if } \Delta\pi \geq \Delta\pi_c, \end{cases} \tag{4.3}$$

$$g(\phi) = (1 + 2.5\phi), \tag{4.4}$$

$$h(\dot{\gamma}) = |\mathbf{D}|^{n-2}, \tag{4.5}$$

where $g(\phi)$ and $h(\dot{\gamma})$ are given by the Einstein and power-law models, respectively. Also, μ_0 and μ_1 are some characteristic viscosities, $\Delta\pi_c$ is a critical pressure which depends on the material properties of the system and α is a constant.

Regarding $f(\text{grad}(\pi))$, which is a generalization of the model of [8] and an extension of Stokes' idea of pressure dependent viscosity, this model was chosen over the many other explicit pressure dependent models for several reasons. For instance, the exponential pressure dependent model (2.22) leads to a trivial plane Poiseuille flow under steady and unidirectional conditions [35].

Furthermore, in the context of a two-dimensional system, when the steady laminar flow of a fluid between two parallel plates (or within a pipe) has become established, the fluid profile $U(x, y)$ is independent of x and therefore takes the form $U(y)$; that is, the flow profile does not change as we move downstream (unidirectional). We may view such a fluid as a series of layers, where each layer (or parcel) of fluid is constrained to it's own horizontal plane. Since the fluid's flow profile is established, the properties of the fluid will not change on each layer, however, they may change between layers (i.e. perpendicular). For this reason, a viscosity function dependent on both x and y is not valid, which would be the result of the choice of an explicit pressure dependent model. This physical notion is identified and discussed in a more general context pertaining to stratified fluid flow by Anand and Rajagopal [23].

Lastly, our model directly lends itself to existing low pressure regime experiments mentioned above, where the pressure differences are known, but not the point wise pressure; this matter will become apparent after we implement the model. It is for

the above aforementioned reasons that our choice of model excludes explicit pressure dependence although such models have seen success for homogeneous fluids in the high pressure regime.

We will seek solutions, velocity, to the system (2.1) and (2.2) under the assumptions of steady and unidirectional flow between two horizontal parallel plates of infinite length. Furthermore, the no-slip boundary conditions are applied at the two plates. Volume fraction conservation across any cross-section of the channel is imposed, as well as a non-negativity condition on the volume fraction relation. The flow rate will be calculated and compared to the pressure difference across the length of the plates. The results will be compared to known experimental work in the low pressure regime. Further analysis will be undertaken to determine any other unique qualities of this system, including the volume fraction distribution of solid particles in the suspension.

As in the previous chapter, we use the assumptions in Chapter 2.4. The conservation of mass is automatically satisfied and the balance of linear momentum reduces to:

$$\frac{\partial \pi}{\partial x} = \frac{d}{dy}\left(\mu(\text{grad}(\pi), \phi, \dot{\gamma})\frac{dU}{dy}\right), \tag{4.6}$$

$$\frac{\partial \pi}{\partial y} = -\rho_e g, \tag{4.7}$$

where ρ_e is the effective density of the fluid and g is the gravitational constant. The no-slip boundary conditions at the two plates is given by,

$$U(y = 0) = U(y = h) = 0. \tag{4.8}$$

The volume fraction of solid particles in the suspension must remain constant and positive, therefore,

$$\int_0^h \phi(y)dy = \phi_0, \tag{4.9}$$

$$\phi(y) \geq 0, \tag{4.10}$$

where ϕ_0 is the total volume fraction of solid within the suspension and $\phi_0 > 0$.

Before we move to non-dimensionalize and then solve the system (4.6) and (4.7), we consider the pressure function $\pi(x, y)$. The pressure function $\pi(x, y)$ can assume two general forms, the sum or product of functions solely dependent on x and y. If we replace π in equations (4.6) and (4.7) with $\pi(x, y) = F(x)G(y)$, the result is

$$\frac{dF}{dx} = A(y), \tag{4.11}$$

$$\frac{dG}{dy} = B(x), \tag{4.12}$$

with

$$A(y) = \frac{1}{G(y)}\left[\frac{d}{dy}\left(\mu(\text{grad}(\pi), \phi, \dot{\gamma})\frac{dU}{dy}\right)\right],$$

$$B(x) = \frac{-\rho_e g}{F(x)}.$$

The second condition implies that $F(x)$ is a constant function and so the pressure is independent of x; that is, there is no driving force for the fluid along the direction parallel to the channel. Since we are interested in pressure driven flows, a pressure function consisting of products of functions of x and y is inappropriate.

If we replace π in equations (4.6) and (4.7) with $\pi(x, y) = R(x) + S(y)$, the result is

$$\frac{dR}{dx} = \frac{d}{dy}\left(\mu(\text{grad}(\pi), \phi, \dot{\gamma})\frac{dU}{dy}\right), \tag{4.13}$$

$$\frac{dS}{dy} = -\rho_e g. \tag{4.14}$$

We can rewrite equation (4.13) in a more illuminating form using our model for the viscosity as

$$\frac{dR}{dx}e^{-\alpha\sqrt{\frac{dR}{dx}^2 + \frac{dS}{dy}^2}} = \frac{d}{dy}\left(\mu(\phi, \dot{\gamma})\frac{dU}{dy}\right), \tag{4.15}$$

where $\frac{dS}{dy} = -\rho_e g$ is constant. In this form, the first condition implies one of three possibilities; either $R(x)$ is constant and we have no driving force, it is a complex transcendental function, when $S'(y) = 0$ it results in a Lambert W function, or linear in x. The second condition implies that $S(y)$ is linear in y. The dependence of the pressure on the height y of the channel is now in immediate need of discussion.

Under the assumption of incompressible flow, we have arrived at the equation (4.14), which leads to a linear relationship in y of $S(y)$. We are now left with two choices: either we move to solve the system using the generalized functions $R(x)$ and $S(y)$ or we choose to draw physical connections, specifying the nature of these functions before proceeding. The nature of these functions is important to the physics of the problem and therefore we move to discuss the latter.

We notice that, from the equation (4.14), the term $S(y)$ is related to the effective density ρ_e, which is constant under the assumption of incompressible flow. The density, however, is known to be dependent on position, temperature, volume fraction and etc. under different contexts; that is, ρ should be compressible. Although we recognize the compressibility of the density, we ignore such effects and treat the suspension as incompressible. In the case of compressibility, the density would be a

function of height y^2; however, in principle, the density could be a function of the volume fraction and possibly its derivatives. Note: If $\rho \propto \phi$, the pressure gradient will depend on the y coordinate. This leads to a contradiction in our assumption of unidirectionality of the velocity field.

From the above observation, we propose that $S(y)$ behaves either like ϕ or $\frac{d\phi}{dy}$; that is, the pressure is related to either the local volume fraction of solid material in the flow or spatial rate of change. Note: for either choice, the independence of $f(\text{grad}(\pi))$ on the spatial coordinates is guaranteed.

The natural physical meaning of the function $R(x)$ is the driving force of the fluid flow and therefore it is related to the pressure drop $\Delta\pi$ across the length of the channel. This is taken to be linear in x, opposed to a complex transcendental function.[3] This dependence is shared under similar flow conditions by homogeneous Newtonian fluids [10, 11].

The last item to consider before non-dimensionalizing the system is the effective density ρ_e. Although we presented an argument for the dependence of $S(y)$ on the volume fraction through a height dependent density, it is treated as a constant in this study. We define the effective density by $\rho_e = \rho_{base}\,(1 - \phi_0) + \rho_{solid}\phi_0$; for discussion on choices for the density of suspensions, see [53].

We non-dimensionalize the system using the following dimensionless forms,

$$\overline{U} = \frac{U}{U_0},$$
$$\overline{\mu} = \frac{\mu}{\mu_0},$$
$$\overline{y} = \frac{y}{h},$$
$$\overline{x} = \frac{x}{L},$$
$$\overline{\pi} = \frac{\pi}{\Delta\pi}.$$

[2]For a compressible fluid, the conservation of momentum is given by,

$$\frac{\partial\rho}{\partial t} + \text{div}(\rho\mathbf{u}) = 0.$$

For steady unidirectional flow, the above equation reduces to,

$$\frac{\partial\rho}{\partial x}U(y) = 0,$$

which implies that ρ is a function of height y alone.

[3]In the latter case, the viscosity μ would become a function of both x and y. It was argued earlier, based on the physical assumption of unidirectional flow, that such a function could not occur. Also, in the interest of simplicity, a linear model would be a more appropriate choice.

where U_0 is the average velocity of the fluid flow, μ_0 is the viscosity of the base fluid at the bottom plate, h is the distance between the two plates, L is the length of each plate, and $\Delta\pi$ is the pressure drop across the length of the plates. The system (4.7) and (4.8) becomes,

$$c\frac{\partial\bar{\pi}}{\partial\bar{x}} = \frac{d}{d\bar{y}}\left(\bar{\mu}(\text{grad}\bar{\pi}, \phi, \bar{\dot{\gamma}})\frac{d\bar{U}}{d\bar{y}}\right), \tag{4.16}$$

$$\frac{\partial\bar{\pi}}{\partial\bar{y}} = -\frac{\rho_e g h}{\Delta\pi}, \tag{4.17}$$

with c defined as

$$c = \frac{\Delta\pi h^n}{U_0^{n-1}\mu_0 L}.$$

The three conditions (4.9) - (4.11) become,

$$\overline{U}(0) = \overline{U}(1) = 0, \tag{4.18}$$

$$\int_0^1 \phi(\overline{y})d\overline{y} = \phi_0, \tag{4.19}$$

$$\phi(\overline{y}) \geq 0. \tag{4.20}$$

Note: It is interesting to see that c is dependent on n and so for any pressure differential $\Delta\pi$ along the channel, the value of c may vary depending on the type of fluid being studied.

We will now drop the bar notation for convenience, noting that further discussion of the solution quantities and independent variables are non-dimensional.

Case 1 We relate $S(y)$ to the volume fraction $\phi(y)$ through the relation

$$S(y) = \epsilon\phi(y).$$

This leads to the pressure function,

$$\pi(x, \phi(y)) = \frac{\Delta\pi x}{L} + \epsilon\phi, \tag{4.21}$$

where $\Delta\pi$ is the pressure difference across the channel, L is the channel length, and ϵ constant. The equation (4.17) simplifies under this relation to,

$$\frac{d\phi}{dy} = -\frac{\rho_e g h}{\epsilon}. \tag{4.22}$$

Integrating with respect to y, setting $\phi(y=0)=0$ and using condition (4.19) leaves us with a closed form solution for the volume fraction:

$$\phi(y) = 2\phi_0 y, \tag{4.23}$$

with $\epsilon = -\frac{\rho_e g h}{2\phi_0}$. The parameter ϵ is uniquely determined here by the condition at the boundary $\phi(y=0)=0$. Note: the volume fraction is set to zero at the bottom of the channel to simulate a floating particle suspension; that is, a suspension where the buoyant tendency of the solid material is skewed towards the bottom. This can be easily changed to simulate an initially fully sedimented system. See the previous chapter for more discussion on this item.

Notably, $\phi(y)$ is linear in y and independent of the pressure gradient. In fact, once the total volume fraction ϕ_0 of solid particles in the flow is specified, the volume fraction profile remains unchanged. Although such a distribution may be possible, it does not capture the physics of the problem under consideration. Solid particles should be entering the fluid flow from the boundaries with increasing pressure gradient. This effect is thought to be the mechanism that 'invokes' a pressure gradient dependence on the viscosity at low pressures. For this reason, we do not pursue such a model further.

Case 2 We relate $S(y)$ to the volume fraction gradient $\mathrm{grad}(\phi)$ through the relation

$$S(y) = \beta \mathrm{grad}(\phi).$$

This leads to the pressure function,

$$\pi(x, \phi(y)) = \frac{\Delta\pi x}{L} + \beta \mathrm{grad}(\phi), \tag{4.24}$$

where $\Delta\pi$ is the pressure difference across the channel, L is the channel length, and β constant. The quantity $\mathrm{grad}(\phi)$ represents the local effect of differences in volume fraction on the pressure. The equation (4.17) may be simplified using the pressure relation (4.24). We arrive at,

$$\frac{d^2\phi}{dy^2} = -\frac{\rho_e g h^2}{\beta}.$$

Integrating twice with respect to y, setting $\phi(y=0)=0$ and using condition (4.19) leaves us with a closed form solution for the volume fraction:

$$\phi(y) = (2\phi_0 + \frac{\rho_e g h^2}{3\beta})y - \frac{\rho_e g h^2}{2\beta} y^2. \tag{4.25}$$

The identity of the parameter β is still unknown to us at this point. However, it should depend both on the pressure gradient $\Delta\pi$ across the channel and some critical pressure $\Delta\pi_c$ where the critical pressure marks the transition to pressure gradient independent fluid flow. In other words, as $\Delta\pi \to \Delta\pi_c$, volume fraction contributions to the pressure should stabilize, $\beta \to \beta_1$, due to the suspension becoming more homogeneous-like; the fluid will not be homogeneous in space, however, the bulk properties will become independent of the pressure gradient. We may represent this by

$$\beta \equiv \beta_0|\Delta\pi - \Delta\pi_c| + \beta_1,$$

with β_0 positive. Since $\phi(y)$ is parabolic and $\phi(y) \geq 0$, we require $\phi(y = 1) \geq 0$, thus

$$\phi(y = 1) = (2\phi_0 + \frac{\rho_e g h^2}{3\beta}) - \frac{\rho_e g h^2}{2\beta} \geq 0.$$

Solving for β,

$$\beta \geq \frac{\rho_e g h^2}{12\phi_0}.$$

Note that the quantity $\beta_0|\Delta\pi - \Delta\pi_c|$ will always be greater than or equal to zero. Since the nature of β is unknown to us, we make the simple choice of $\beta_0 = \frac{1}{2}$ and $\beta_1 = \frac{\rho_e g h^2}{12\phi_0}$, which guarantees the above condition is met. It should be noted that β has the effect of modifying the strength of the volume fraction gradient on the pressure. Experimental work towards the determination of the nature and numerical value of this parameter would be novel. Furthermore, it is interesting to note that, for the problem under consideration, $\beta/\Delta\pi \approx 1$ and $\epsilon/\Delta\pi \approx 10$.

Now that we have dealt with equation (4.17) completely, we move our attention to equation (4.16). First, we note that the shear rate dependence transforms under the assumption of unidirectional flow,

$$|\mathbf{D}|^{n-2} = \left|\frac{dU}{dy}\right|^{n-2}.$$

Combining this result with the pressure relation (4.24), equation (4.16) becomes,

$$ce^{-\alpha\sqrt{(\frac{\Delta\pi}{L})^2+(-\rho_e g h^2)^2}} = \frac{d}{dy}\left[(1 + 2.5\phi)\left|\frac{dU}{dy}\right|^{n-2}\frac{dU}{dy}\right]. \tag{4.26}$$

The pressure dependent component $f(\text{grad}(\pi))$ of the viscosity function is independent of both spatial coordinates; however, it is dependent on the pressure drop $\Delta\pi$ across the channel, as alluded to in the opening of this section. Together with our relationship for the volume fraction (4.25) and the no-slip boundary condition (4.18), we may now solve for the flow velocity $U(y)$.

4.2 Results

In this section, we describe the results of our numerical experiments described below. The system (4.16) and (4.18) is solved, where the viscosity is taken to be piecewise pressure gradient dependent. No exact analytical solutions could be found due to the nonlinearity introduced by the viscosity. Discussion will be broken down into two regimes. The pressure gradient dependent regime will be discussed, followed by discussion of the pressure gradient independent regime.

It is worthwhile to discuss the parameter α which has the effect of shifting the maximum. Furthermore, as α increases, the maximum shifts towards the lower pressure regime. This is intuitive if we look at the flow rate relation (4.1); the exponential term will dominate earlier for larger α and the linear term will dominate for smaller α. The value chosen for computation is $\frac{18}{|\Delta\pi_c|}$, which is approximately $(2\pi)^{-1}$ times the value fitted for experiment.

Mathematically, the effect of the critical pressure $\Delta\pi_c$ on the flow rate vs. pressure differential profile is to modify the 'peaks'. As the critical pressure increases, the peaks become sharper and more pronounced. The opposite effects holds for decreasing values of the critical pressure. This value should be a property of the given fluid. For instance, this value is approximately 8500 Pa for coffee powder suspended in water at 2% volume fraction, when approximating a linear relationship between pressure drop and percentage of solid particulate transfered. The value chosen for two-dimensional computation is $\Delta\pi_c = -1350$ Pa, which is approximately $(2\pi)^{-1}$ times the three-dimensional approximate analog, similar to α;

Regime 1: Pressure gradient dependent viscosity The complex nonlinearity of the viscosity, which is a product of the functions $\phi(y)$ and $\left|\frac{dU}{dy}\right|^{n-2}$, does not permit analytical solutions. Solutions to the system (4.16) and (4.18) were found numerically, as in the previous study. The channel velocity, concentration, pressure, and flow rate were computed. Each of these quantities offers a different perspective of the system. The flow rate is of particular interest and is calculated using the relation (3.13). In [8], the volumetric flow rate was compared to the pressure differential in their experimental work; each of these quantities was measurable, compared to the velocity, pressure, and concentration profiles. Consequently, we can perform a similar comparison to see if our results match experiment.

The velocity $U(y)$ was computed after fixing the parameters n and ϕ_0; the system was then solved for $\Delta\pi = \frac{\Delta\pi_c}{4}, \frac{3\Delta\pi_c}{8}, \frac{\Delta\pi_c}{2}$, which were chosen arbitrarily for a parametric sweep. In Figures 4.4 - 4.6, we see that as $\Delta\pi$ increases, the velocity contracts dramatically. Also, the total volume fraction of solid particles in the suspension ϕ_0, acts to contract the velocity as well, although, significantly less than $\Delta\pi$. Another interesting feature is that for $n = 1.8$, the velocity profile is rounded and reaches a maximum below the center line. For $n = 2.0$, the velocity profile narrows and reaches a maximum along the center line. Lastly, for $n = 2.2$, the velocity profile narrows

more greatly and reaches a maximum above the center line.

The volume fraction $\phi(y)$ was computed for the same values of n and ϕ_0, however, the parametric sweep is over $\Delta\pi = \frac{\Delta\pi_c}{4}, \frac{\Delta\pi_c}{2}, \frac{3\Delta\pi_c}{4}$. It is found that for any n, the volume fraction profile will reach higher (maximum) values near the center line as $\Delta\pi$ increases. Consequently, due to the fixed amount of solid particles in the fluid, the amount of solid particles along the top half of the channel will decrease. So, as the pressure drop along the channel increases, more and more solid particles are 'dragged' into the flow, as expected. This effect causes the suspension velocity to contract and, as we will see, the flow rate to diminish. Lastly, the effect is more greatly marked as ϕ_0 is increased. These effects can be seen in Figures 4.7 - 4.9.

The flow rate Q is computed after fixing n and ϕ_0 and sweeping through values of $\Delta\pi = \frac{k\Delta\pi_c}{20}$ for $k = 0, 1, 2, ..., 20$, which were chosen for a parametric sweep. In Figures 4.10 (a), 4.11 (a), and 4.12 (a), we immediately see a marked resemblance to the experimental results found in [8]. It should be noted that some deviation is expected due to experiment being three-dimensional and this study being two-dimensional. Regardless, the profile is qualitatively captured. Additionally, we see that the maximum is reached around $\Delta\pi = -180$ for $n = 1.8$ and $\Delta\pi = -300$ for both $n = 2.0$ and 2.2. Another interesting feature is that for $n = 1.8$, the flow rate decreases more rapidly after reaching its maximum than for the cases of $n = 2.0$ and $n = 2.2$, with the latter being the least rapid. If we compare Figures 4.2 (a) and (b) to the abovementioned figures, the exponential decay of the flow rate profiles show stronger resemblance to one another in the shear thickening fluid regime ($n > 2$); that is, the introduction of solid material to a base homogeneous fluid acts to create a shear thickening solid-liquid suspension. Additionally, as ϕ_0 is increased, the profile contracts, with the effect being strongest for shear-thinning fluids.

In Figures 4.13 - 4.15, we see contour plots of the pressure within the channel. The pressure was computed by fixing n, ϕ_0, and $\Delta\pi$. There are no noticeable differences between differing values of n. Overall, we see larger values for the pressure as we both rise in the channel and travel along the length. Noticeably, the effect due to the volume fraction gradient is initially stronger than that of the pressure differential along the channel. Furthermore, as $\Delta\pi$ increases, the relative strength of the pressure differential to the volume fraction gradient increases. This is readily seen through the increasing slope.

Regime 2: Pressure gradient independent viscosity The velocity $U(y)$ was computed after fixing the parameters n and ϕ_0; the system (4.16) and (4.18) was then solved for $\Delta\pi = \frac{5\Delta\pi_c}{4}, \frac{3\Delta\pi_c}{2}, \frac{7\Delta\pi_c}{4}$. In Figures 4.16 - 4.18, we see that as $\Delta\pi$ increases, the velocity increases quite dramatically. Also, the effect of ϕ_0 is to contract the velocity as it does in the pressure gradient dependent regime. We see the same trends due to the parameter n as well.

The volume fraction $\phi(y)$ was computed in the same way the velocity was. It is found that for any n, the volume fraction profile will reach higher values near

the center line as ϕ_0 increases. There is little to no effect on the volume fraction profile with varying n and $\Delta\pi$, as should be the case; the volume fraction profile has established itself into a stable configuration that is a symmetric parabolic profile with $\phi(y = 0) = \phi(y = h) = 0$; that is, the top floating solid particles have all entered the 'interior' of the suspension. See Figure 4.19.

The flow rate Q is computed after fixing n and ϕ_0 and sweeping through values of $\Delta\pi = \frac{(20+k)\Delta\pi_c}{20}$ for $k = 0, 1, 2, ..., 20$. In Figures 4.10 (b), 4.11 (b), and 4.12 (b), we see a linear profile analogous to that seen in Chapter 3, that holds for each n. Note that for both $n = 1.8$ and 2.2, the profiles have slight curvature to them; the former exhibits downwards curvature and the latter exhibits upwards curvature. Furthermore, as in the pressure gradient dependent regime, the effect of increases in ϕ_0 is to contract the flow rate profile, and vice-versa.

In Figures 4.20 - 4.22, we see contour plots of the pressure within the channel. The pressure was computed in the same way as in the previously discussed regime. Again, there are no noticeable differences between differing values of n. We see the same overall trends throughout the domain. Note that as $\Delta\pi$ increases, the relative strength of the pressure differential to the volume fraction gradient increases, continuing from the previous regime. The pressure drop along the channel becomes much stronger than the effect due to the gradient of volume fraction across the channel.

4.3 Notes on Convergence of Numerical Solutions

As in the previous study, the system is highly nonlinear. The system of equations (4.16) and (4.18) are solved using MATLAB's 'bvp5c' package, which implements a four-stage Lobatto IIIa scheme. The system was solved for varying step-size and relative tolerance. Two extreme values of n were chosen, $n = 1.8$ and 2.2, and the pressure differential was set to $\frac{\Delta\pi_c}{7.5} = -200$ and -2362.5 for the pressure gradient dependent and independent regimes, respectively. The relative tolerance was then set to one of three values, 10^{-6}, 10^{-9}, and 10^{-12}. The initial guess for step-sizes were then set to $\frac{1}{j}$ for j = 2, 5, 10, 20, 100, 200, 500, 1000, 10000, 20000, 30000, 40000, 50000, 100000, and 200000. The solution for each regime was computed at half the distance between the plates; that is, $U(y = h/2)$. The difference between the solutions for subsequent step-sizes was evaluated for each relative tolerance value. This gives us the relative difference between solutions from which we may readily find error percentages.

It is found that for any n, there is strong correlation between the varying relative tolerance values. However, the correlation is especially strong for 10^{-9} and 10^{-12}. Note that the differences are of magnitude 10^{-7} or smaller. In Figures 4.23 - 4.24, we see a general downward trend across the board which indicates convergence. However, for the pressure gradient dependent regime for $n = 2.2$, we see some oscillation. This indicates that the solution has not yet converged for the given range of step-sizes; however, the scale is 10^{-7}, which is quite tiny.

In general, when $n > 2$, the system is more sensitive to the step-size Δy. Although, for all cases, the solutions converge to particular values as the step-size decreases, there are issues with some solutions. There is a threshold step-size such that the solution is met throughout the channel for each particular value of n with $\Delta\pi$ and a fixed relative tolerance. This threshold step-size is larger for $n \leq 2$ and smaller for $n > 2$. If we exceed this threshold, the solutions show noticeable deviations at one or more locations within the solution domain. This phenomenon does not appear in the linear regime until step-sizes become incredibly tiny ($\Delta y = 5\text{x}10^{-6}$). With this in mind, the step-size was chosen such that the threshold would be met for all cases. This is done by setting our initial value for the step-size to $\Delta y = 0.002$ and the relative tolerance was set to 10^{-9}. Although the solution has not yet fully converged at this value of Δy, as we see oscillations in the differences, the relative differences are less than 0.5% in the pressure gradient dependent regime. The vastly increased time required to compute a solution is not warranted for a qualitative study.

4.4 Concluding remarks

A model for the transport of a fluid with suspended particles in it is discussed. The effects of pressure, volume fraction and shear rate upon the flow is analyzed. The velocity, flow rate, volume fraction, and pressure are computed and analyzed in different contexts. It is found that the flow rate versus pressure differential relationship qualitatively matches experiments performed on inhomogeneous fluids in the low pressure regime. It is seen that experimental results match the behavior of a shear thickening fluid than the alternatives.

Additionally, we see a linear relationship between the two until approximately $\Delta\pi = -300$. Once this value is reached, an exponentially decaying profile is seen. Once the critical pressure is reached, we see a linear relationship once again. We could even consider the first regime to have a linear and exponential sub-regime. Note that the slope of lines in the first sub-regime and in the second regime indicate the effective viscosity of the fluid. The linear relationship in the first sub-regime has a greater slope than in second regime which is intuitive since all of the solid particles have entered the flow in regime two, increasing the viscosity above that initially experienced. Figure 4.26 illustrates these remarks.

Furthermore, the micro-structure of the flow is investigated by analyzing the effect of the pressure differential on the volume fraction. It is found that as the pressure drop across the channel increases, an increase in solid material entering the flow is seen. This trend holds until all the solid material has entered the flow and reaches a stable configuration. The fluid thereafter behaves as a homogeneous fluid independent of the pressure gradient. This is seen through the linear relationship between the flow rate and pressure differential; the bulk properties behave in analogous fashion to a homogeneous fluid.

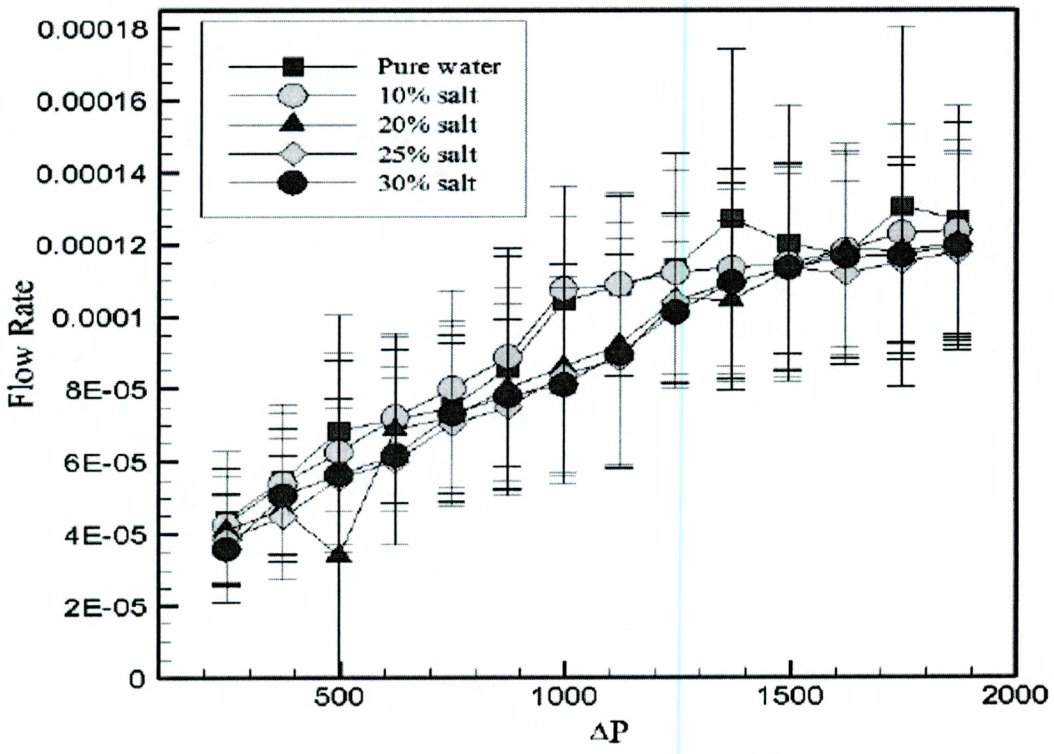

Figure 4.1: The volumetric flow rate versus pressure differential plots for salt water mixtures found in [8].

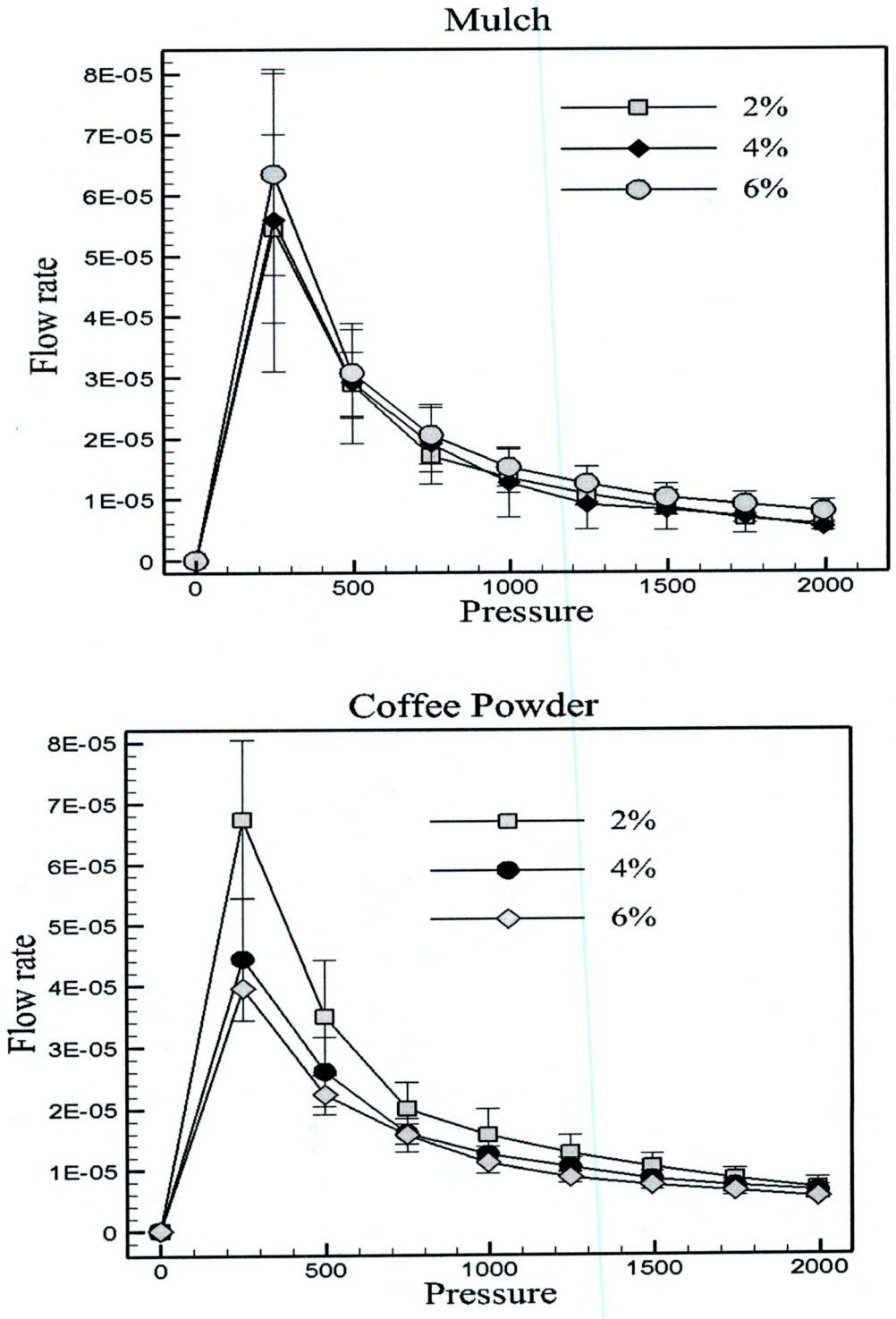

Figure 4.2: Volumetric flow rate versus pressure differential plots for suspensions with (a) mulch and (b) coffee.

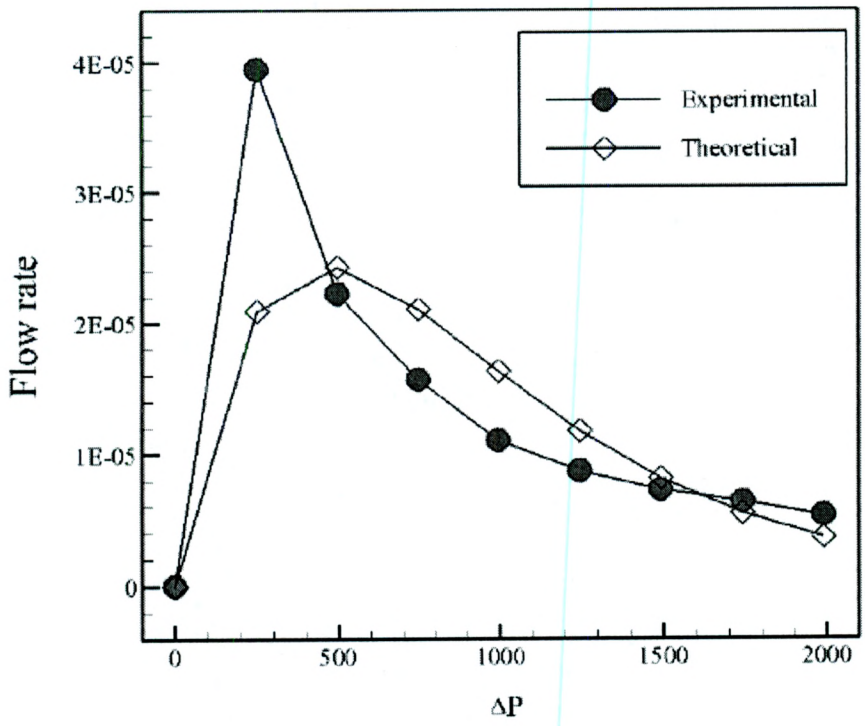

Particulate \ Pressure(Pa)	249.2	498.3	747.5	996.7	1245.9
2% Coffee Powder	8.6%	9.6%	13%	15.2%	19.6%
4% Coffee Powder	10.3%	11.3%	13.1%	14.5%	15.1%
6% Coffee Powder	10.3%	11.4%	13.5%	13.5%	15.3%
2% Mulch	13%	21%	31%	37%	35.2%
4% Mulch	22%	29%	42%	43.6%	46%
6% Mulch	26%	27%	31%	41.2%	56%
2% Crushed Leaves	30%	13%	31.6%	37.4%	38%
4% Crushed Leaves	30%	15.5%	20.5%	30.5%	-
6% Crushed Leaves	26.7%	14.3%	14.5%	22%	16.7%
2% Sand	2%	4%	1%	0.2%	5%
4% Sand[3]	3.6%	0.3%	0.14%	0.71%	2.9%

Figure 4.3: (a)Volumetric flow rate versus pressure differential where the model 4.1 is best fit to the experimental data for the case of 6 % volume fraction of coffee powder in water; the correlation is 0.8 (b) Table with values for percentage of solid material transfered for any given pressure head.

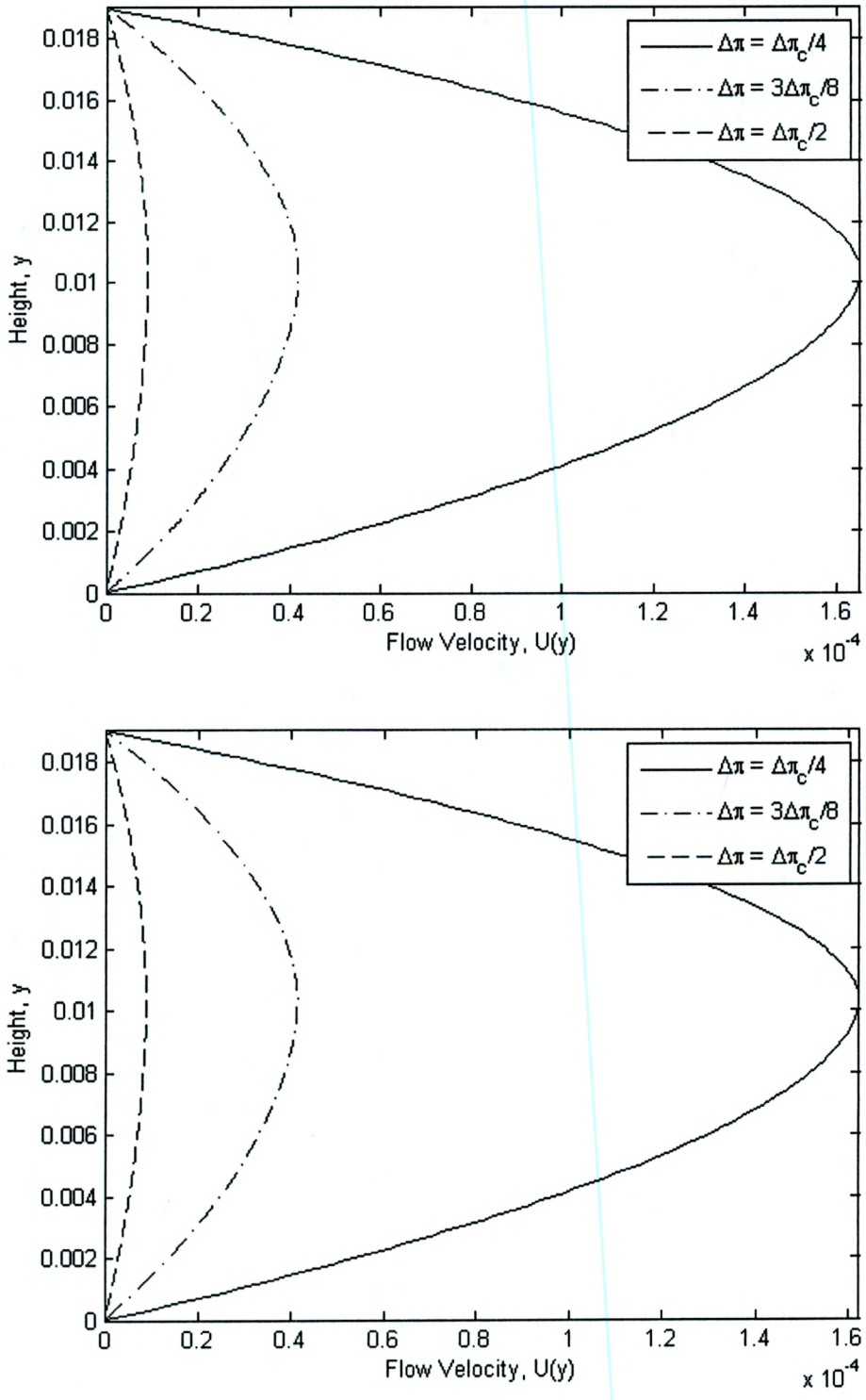

Figure 4.4: Velocity profiles for $n = 2.2$ and (a) $\phi_0 = 0.01$, (b) $\phi_0 = 0.02$.

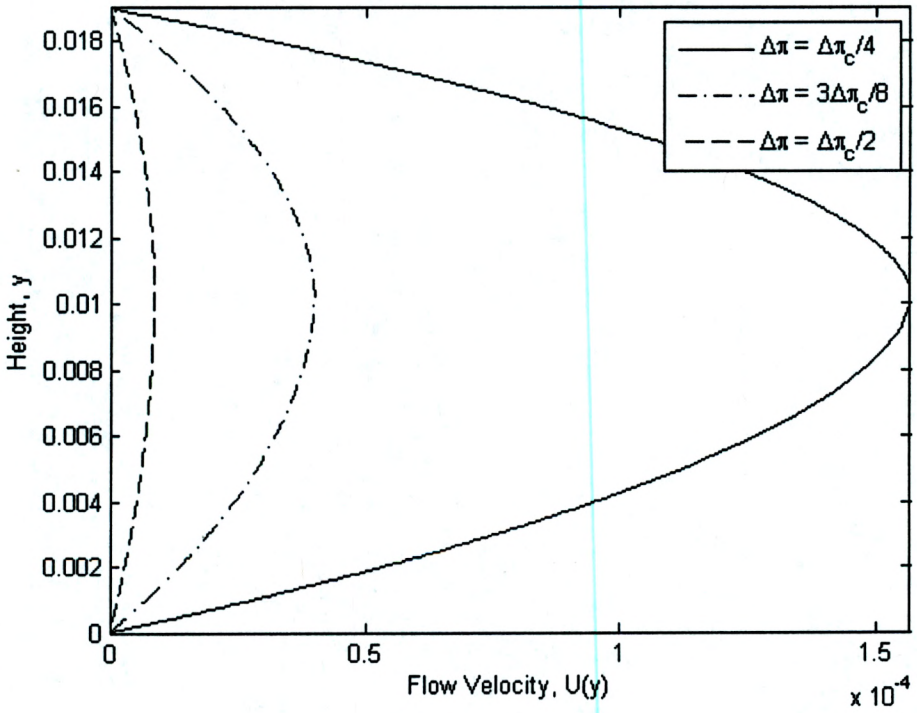

Figure 4.5: Velocity profile for $n = 2.2$ and $\phi_0 = 0.04$.

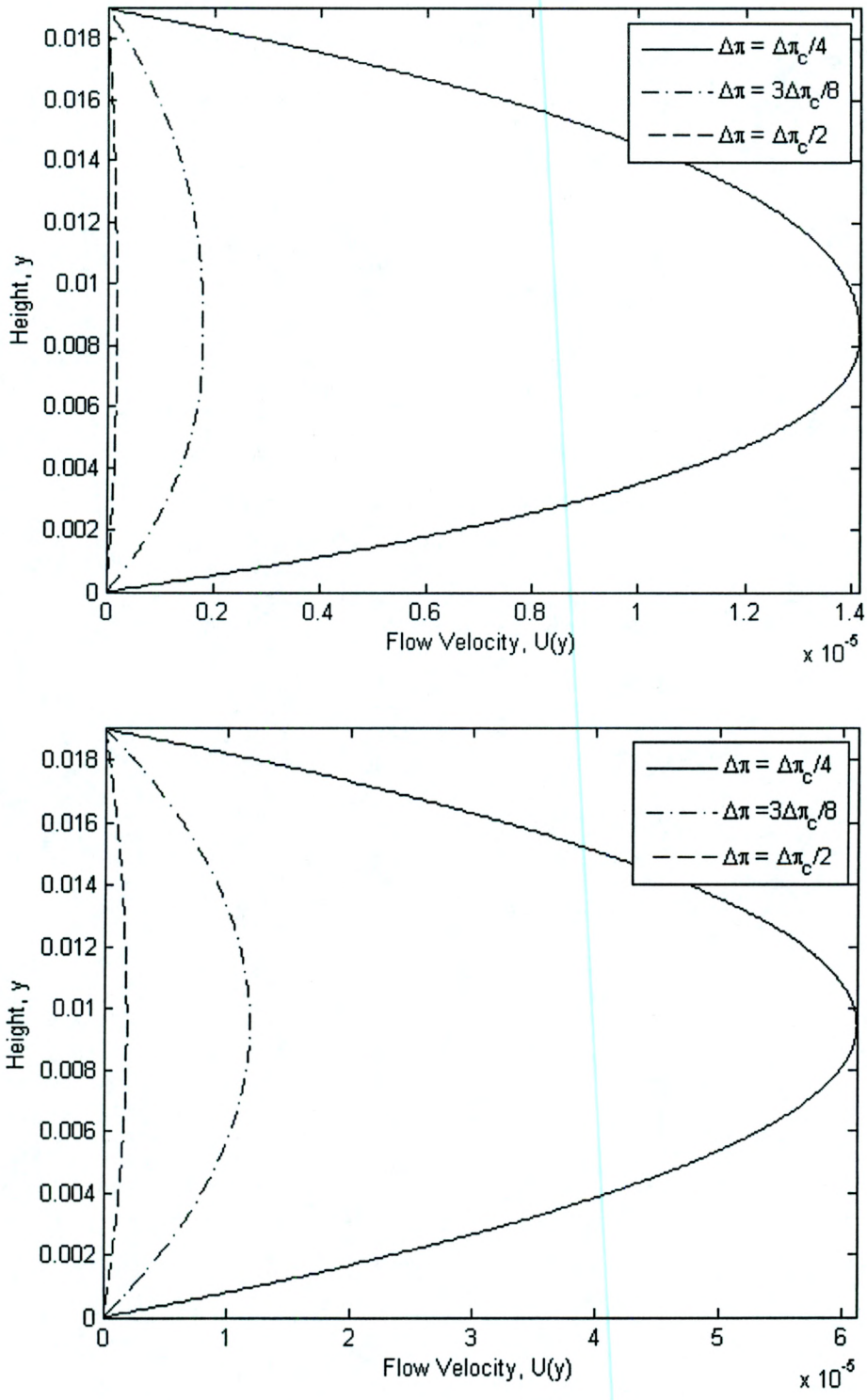

Figure 4.6: Velocity profiles for $\phi_0 = 0.02$ and (a) $n = 1.8$, (b) $n = 2.0$.

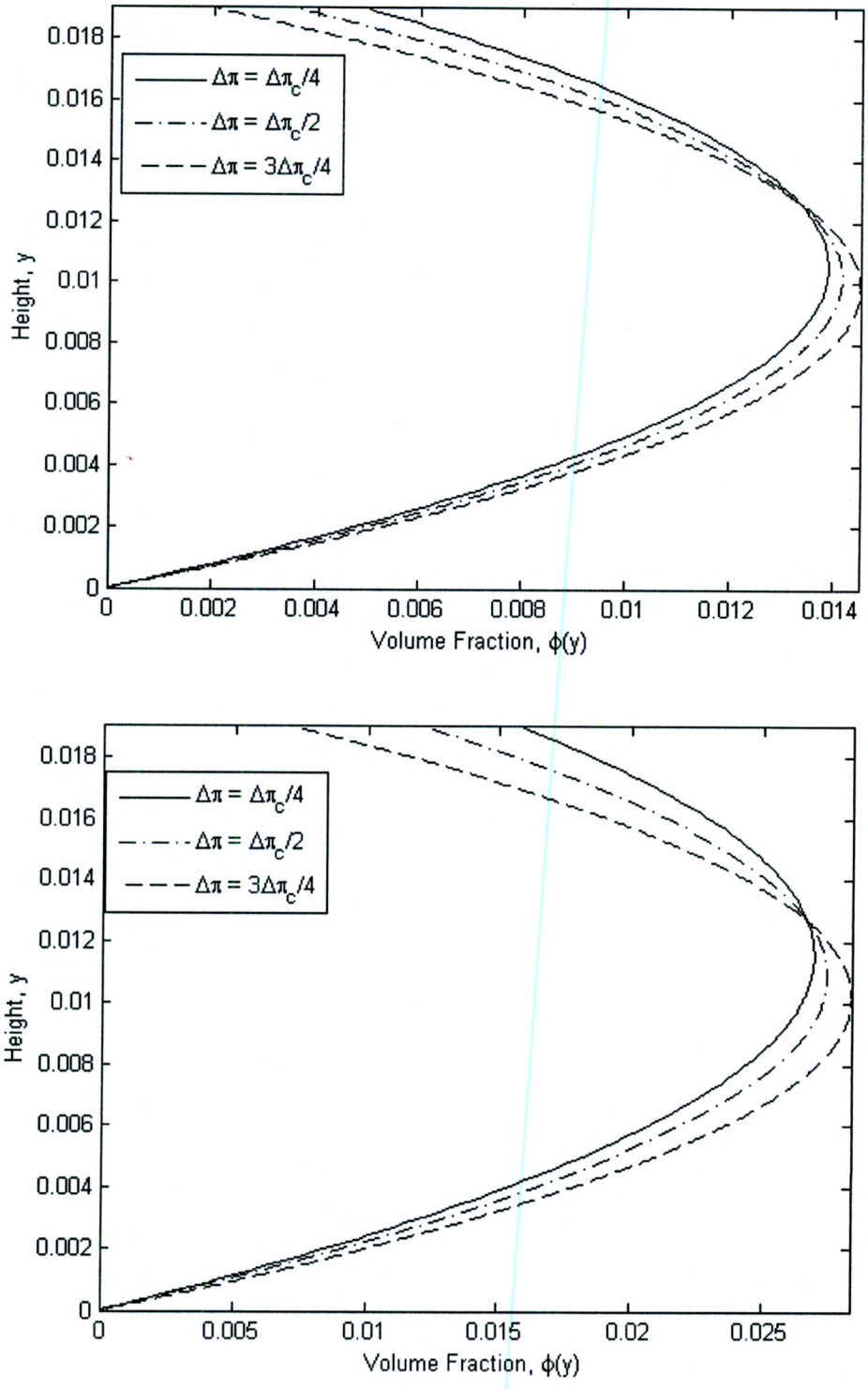

Figure 4.7: Concentration profiles for $n = 2.2$ and (a) $\phi_0 = 0.01$, (b) $\phi_0 = 0.02$.

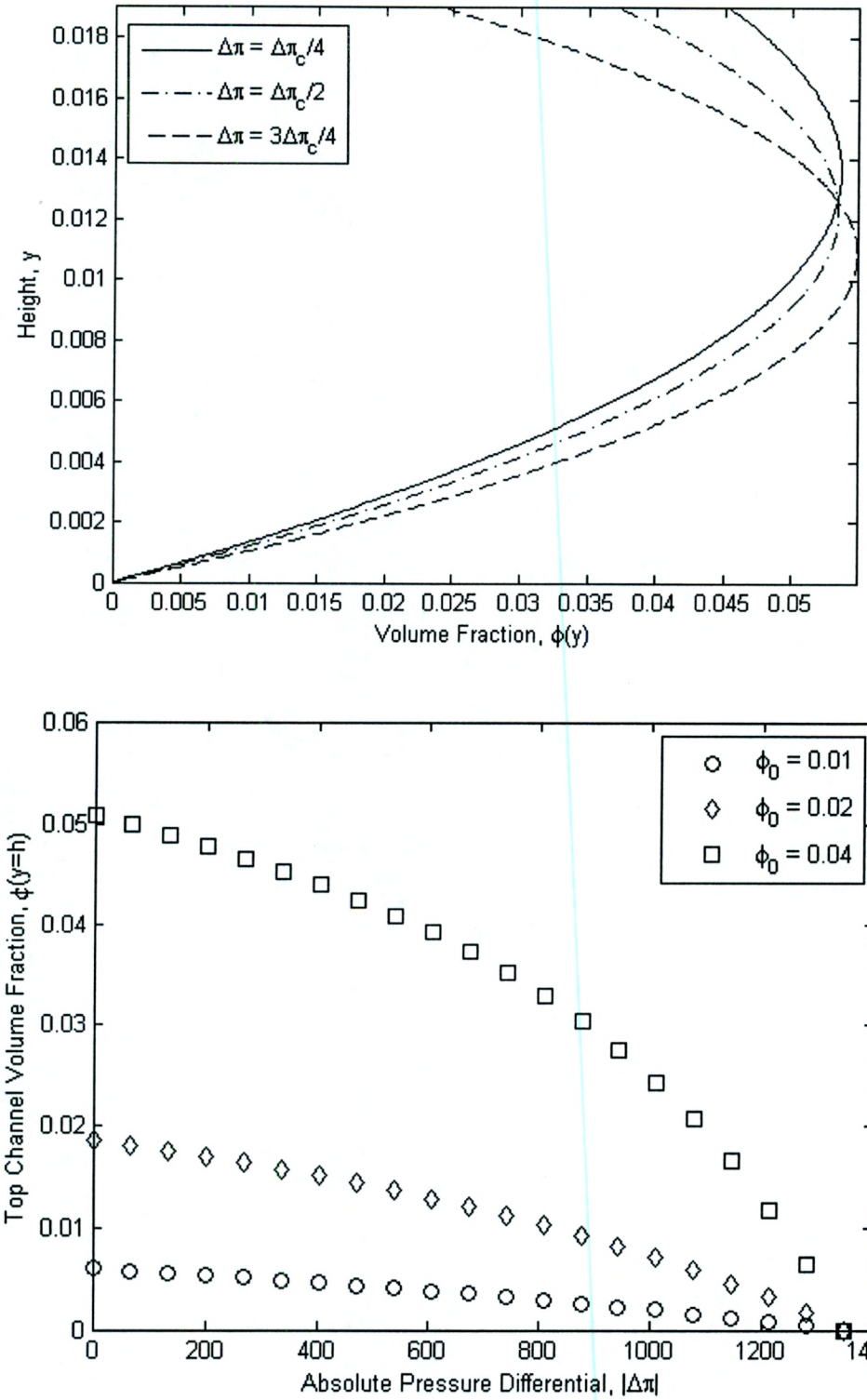

Figure 4.8: (a) Concentration profile for $n = 2.2$ and $\phi_0 = 0.04$ (b) Top channel volume fraction $\phi(y = 1)$ is plotted versus Δpi for $\Delta\pi = \frac{k\Delta\pi_c}{20}$ for $k = 0, 1, 2, ..., 20$.

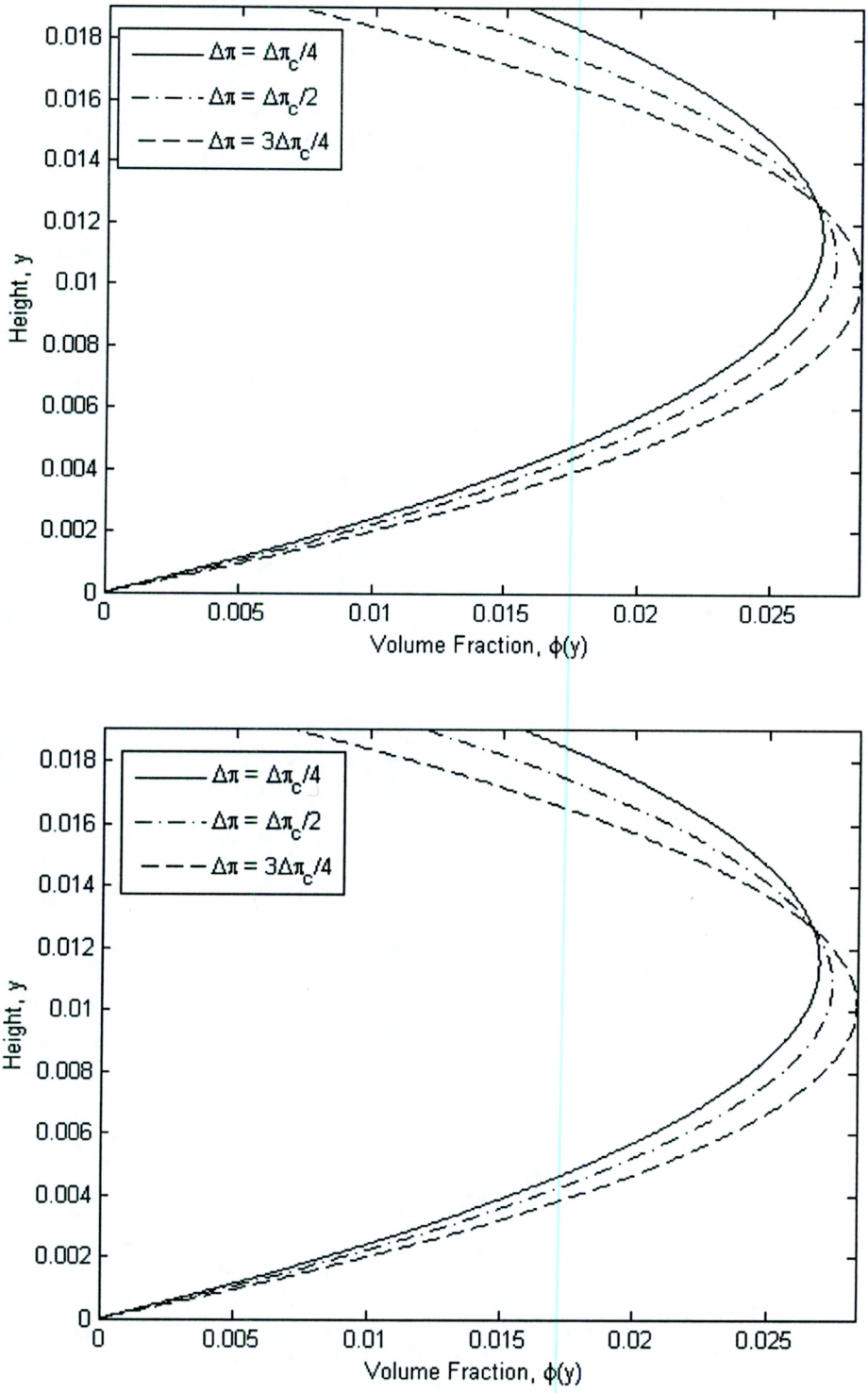

Figure 4.9: Concentration profiles for $\phi_0 = 0.02$ and (a) $n = 1.8$, (b) $n = 2.0$.

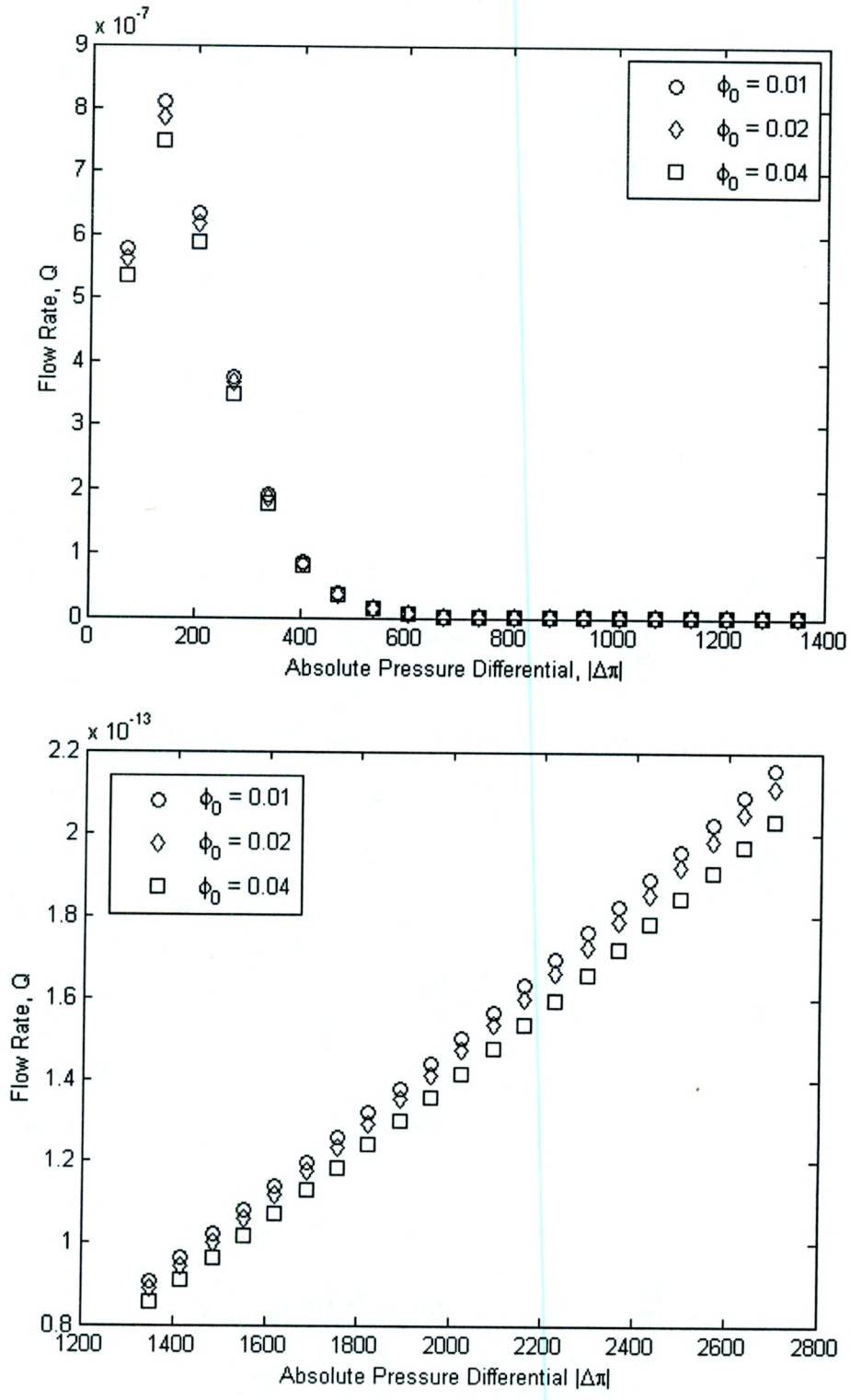

Figure 4.10: Flow rate profiles for $n = 1.8$ and (a) $\Delta\pi = \frac{k\Delta\pi_c}{20}$ for $k = 0, 1, 2, ..., 20$, (b) for $\Delta\pi = \frac{(k+20)\Delta\pi_c}{20}$ for $k = 0, 1, 2, ..., 20$.

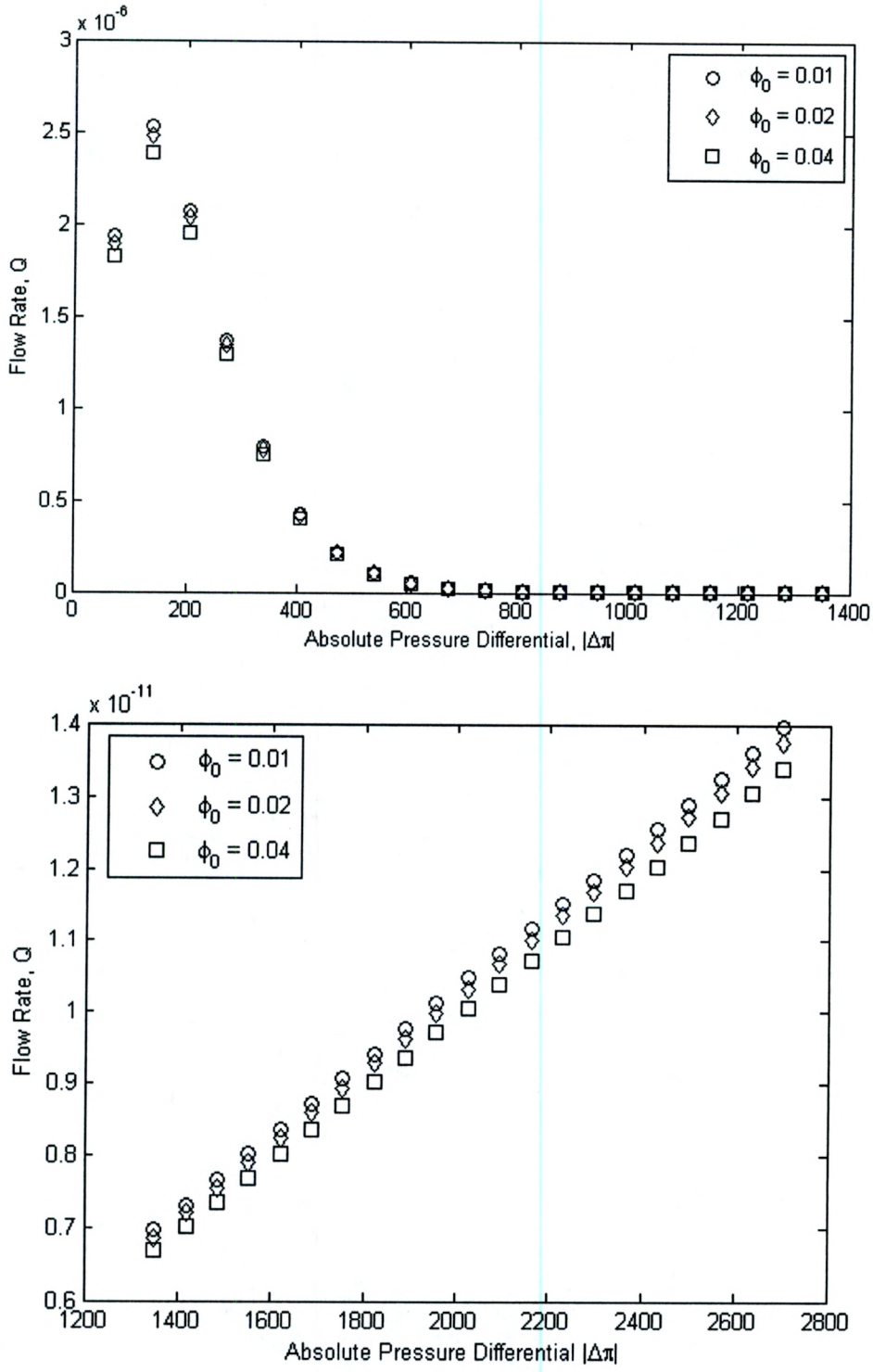

Figure 4.11: Flow rate profiles for $n = 2.0$ and (a) $\Delta\pi = \frac{k\Delta\pi_c}{20}$ for $k = 0, 1, 2, ..., 20$, (b) for $\Delta\pi = \frac{(k+20)\Delta\pi_c}{20}$ for $k = 0, 1, 2, ..., 20$.

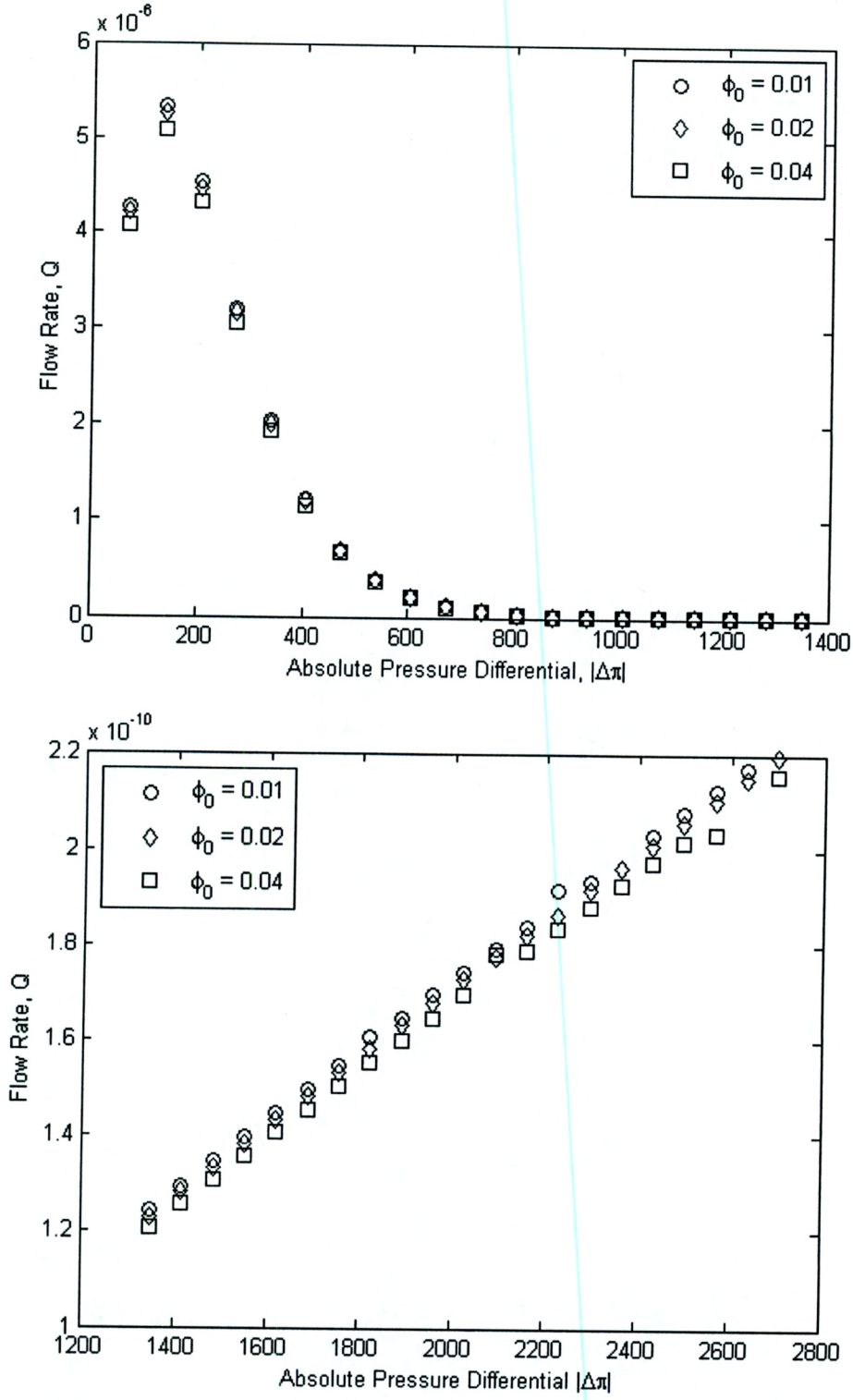

Figure 4.12: Flow rate profiles for $n = 2.2$ and (a) $\Delta\pi = \frac{k\Delta\pi_c}{20}$ for $k = 0, 1, 2, ..., 20$, (b) for $\Delta\pi = \frac{(k+20)\Delta\pi_c}{20}$ for $k = 0, 1, 2, ..., 20$.

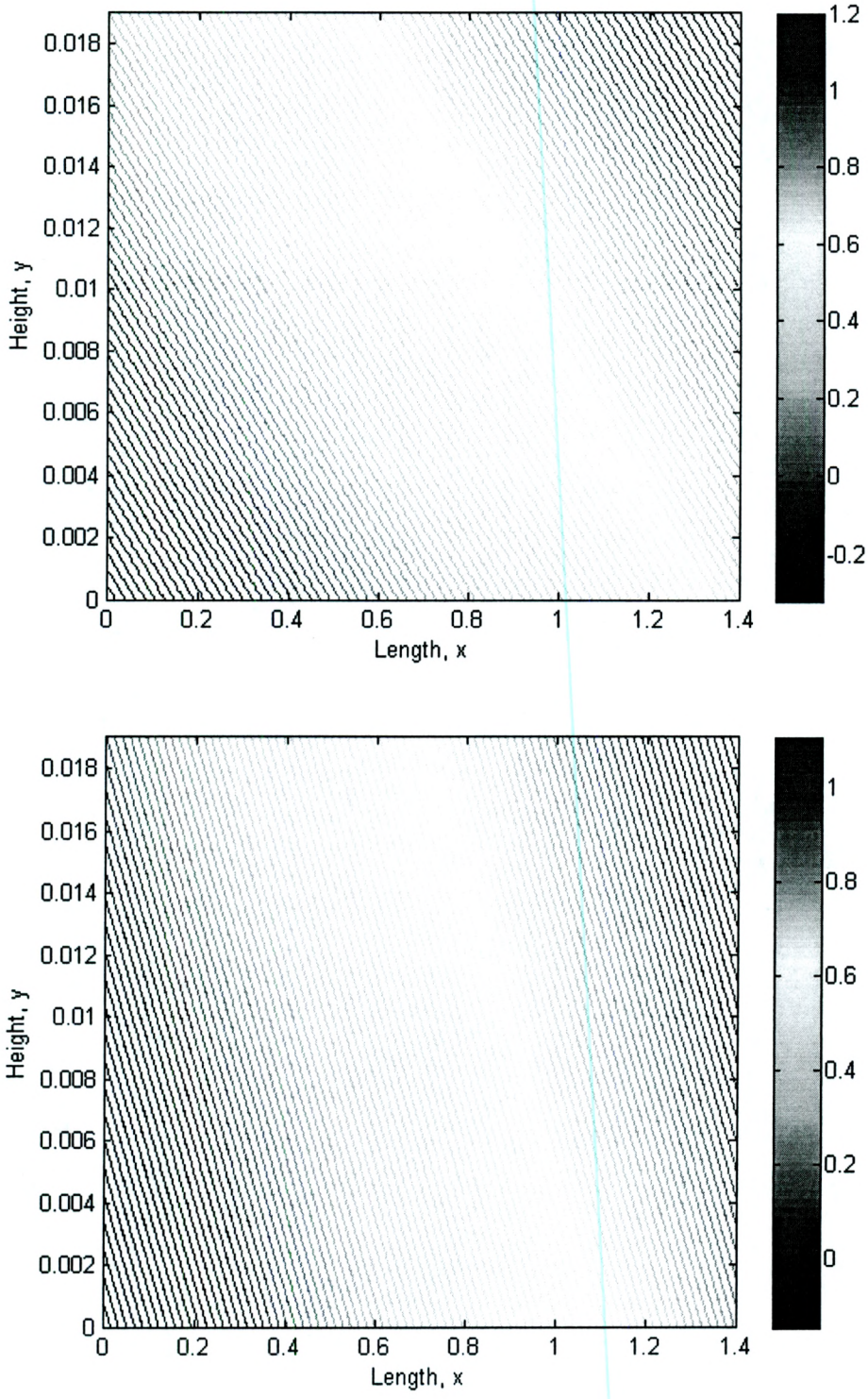

Figure 4.13: Contour plots for pressure with $n = 2.2$, $\phi_0 = 0.02$ and (a) $\Delta\pi = \frac{\Delta\pi_c}{4}$, (b) $\Delta\pi = \frac{\Delta\pi_c}{2}$.

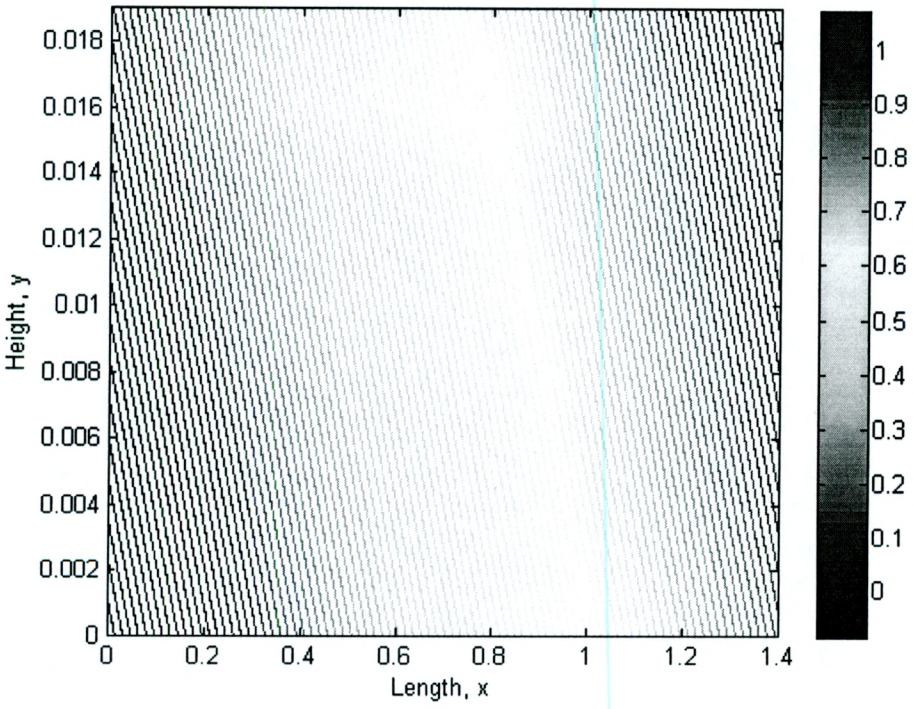

Figure 4.14: Contour plot for pressure with $n = 2.2$, $\phi_0 = 0.02$ and $\Delta\pi = \frac{3\Delta\pi_c}{4}$.

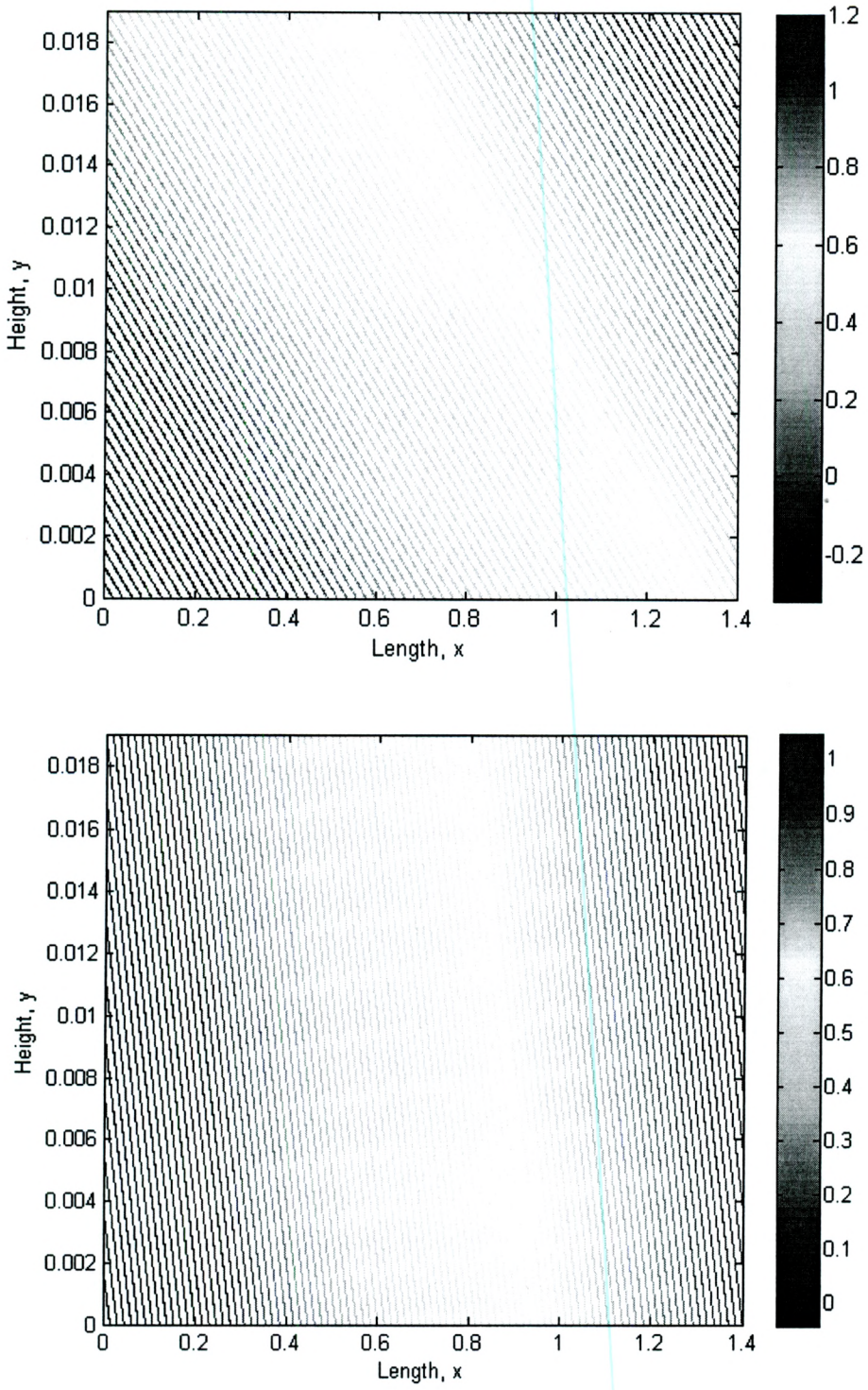

Figure 4.15: Contour plots for pressure with $\Delta\pi = \frac{\Delta\pi_c}{4}$, $\phi_0 = 0.02$ and (a) $n = 1.8$, (b) $n = 2.0$.

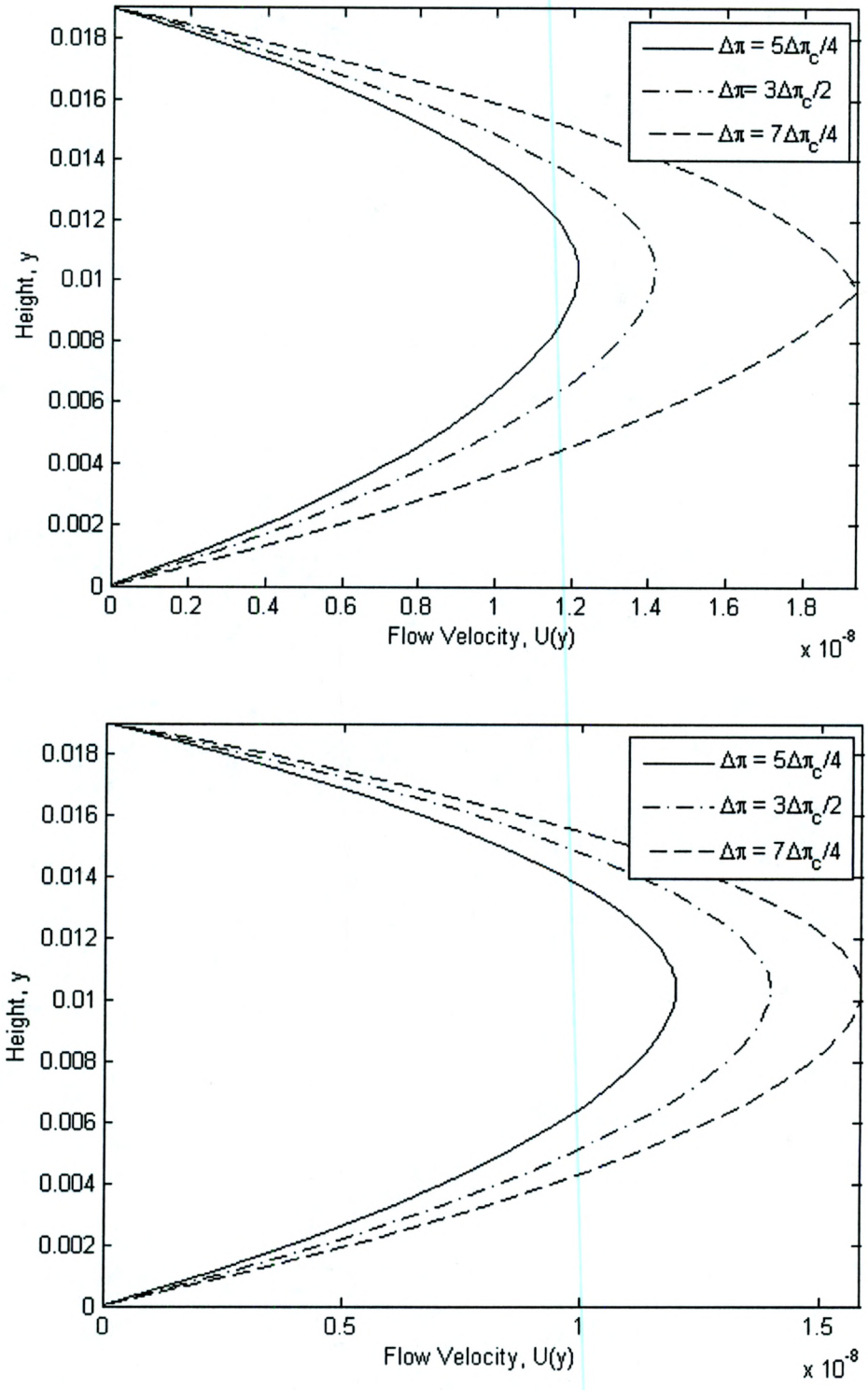

Figure 4.16: Velocity profiles for $n = 2.2$ and (a) $\phi_0 = 0.01$, (b) $\phi_0 = 0.02$.

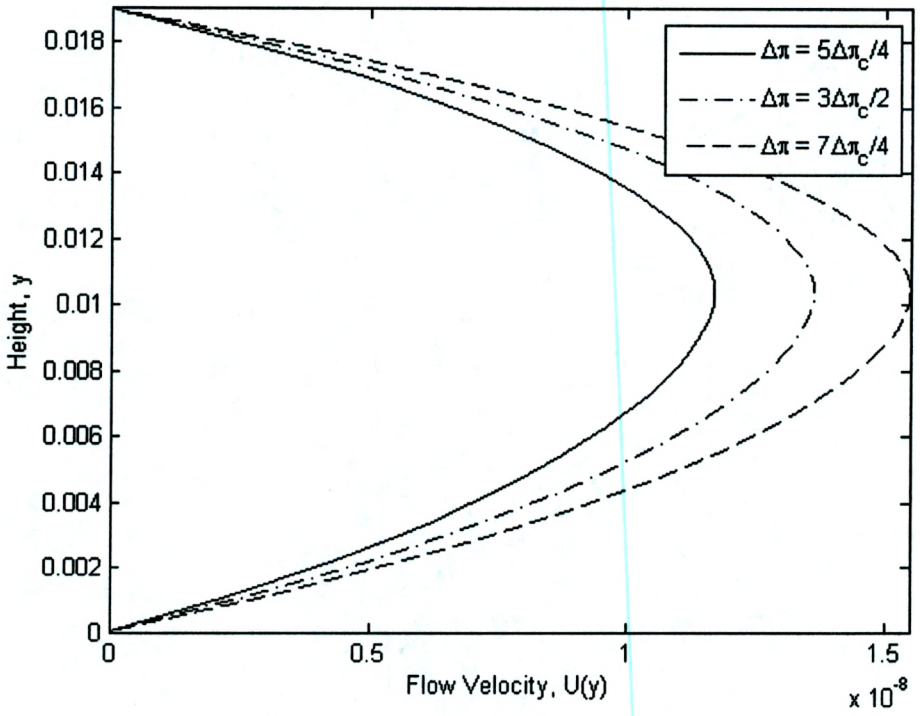

Figure 4.17: Velocity profile for $n = 2.2$ and $\phi_0 = 0.04$.

Parameter	Value	Unit
U_0	$\sqrt{-\Delta\pi/\rho_e}$	m/s
μ_0	1	$Pa \cdot s$
h	0.0190	m
L	1.4	m
ρ_e	$1000(1-\phi_0)+940\phi_0$	kg/m^3
g	9.8	$kg \cdot m/s^2$
α	0.0133	$(Pa)^{-1}$
$\Delta\pi_c$	-1350	Pa
Δy	0.002	-
$RelTol$	10^{-9}	-

Table 4.1: Summary of parameter values for the numerical study in this chapter. The values for U_0 and ρ_e vary depending on the values for $\Delta\pi$ and ϕ_0 which are swept. The parameters which are swept are not listed here.

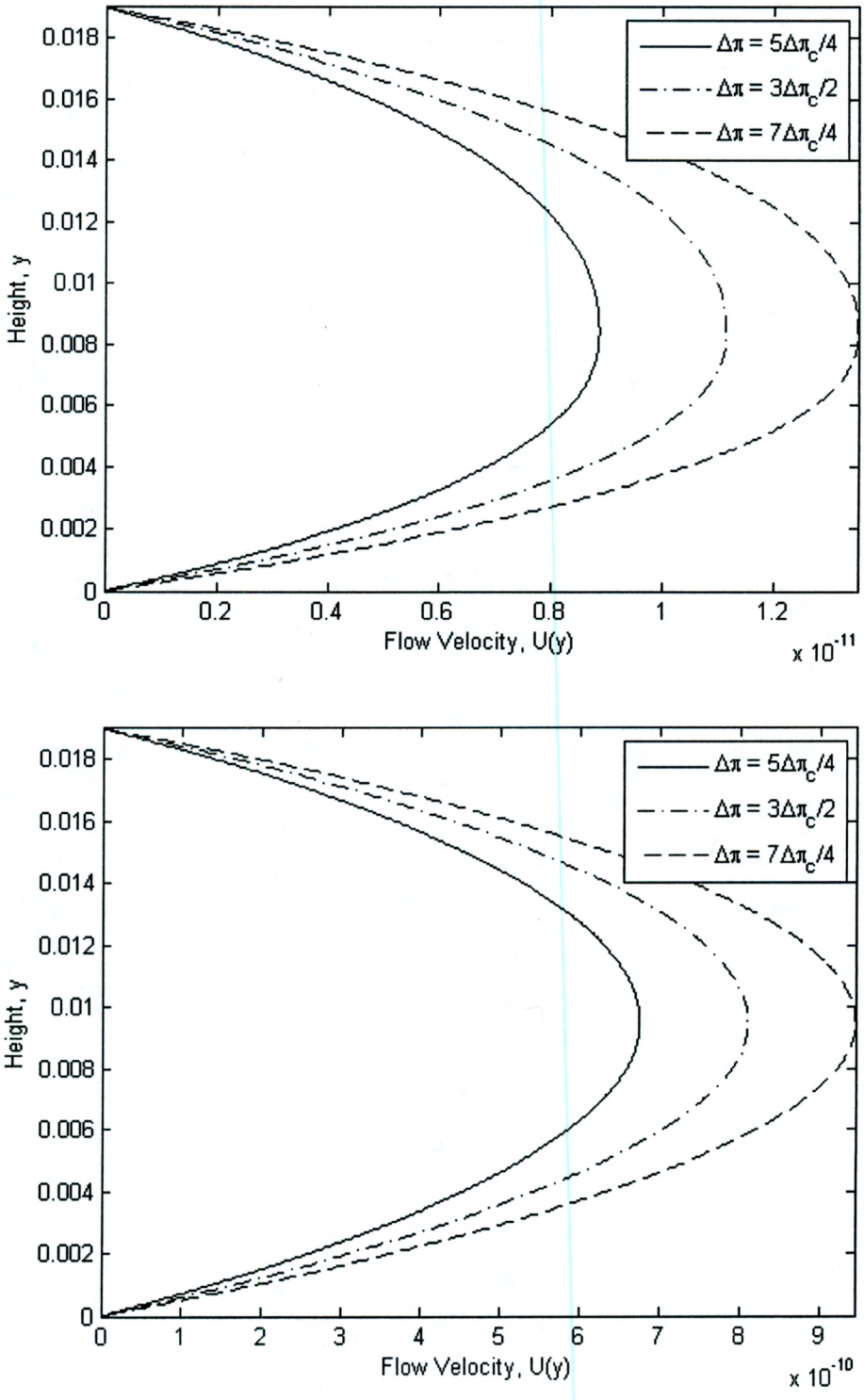

Figure 4.18: Velocity profiles for $\phi_0 = 0.02$ and (a) $n = 1.8$, (b) $n = 2.0$.

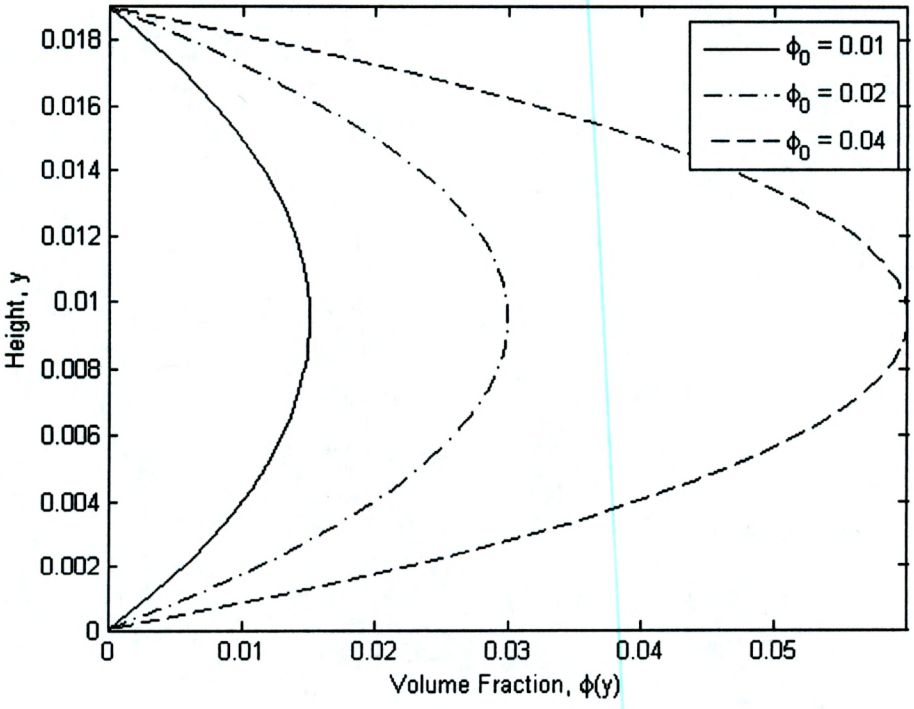

Figure 4.19: Concentration profiles for $n = 2.2$ and ϕ_0 varying.

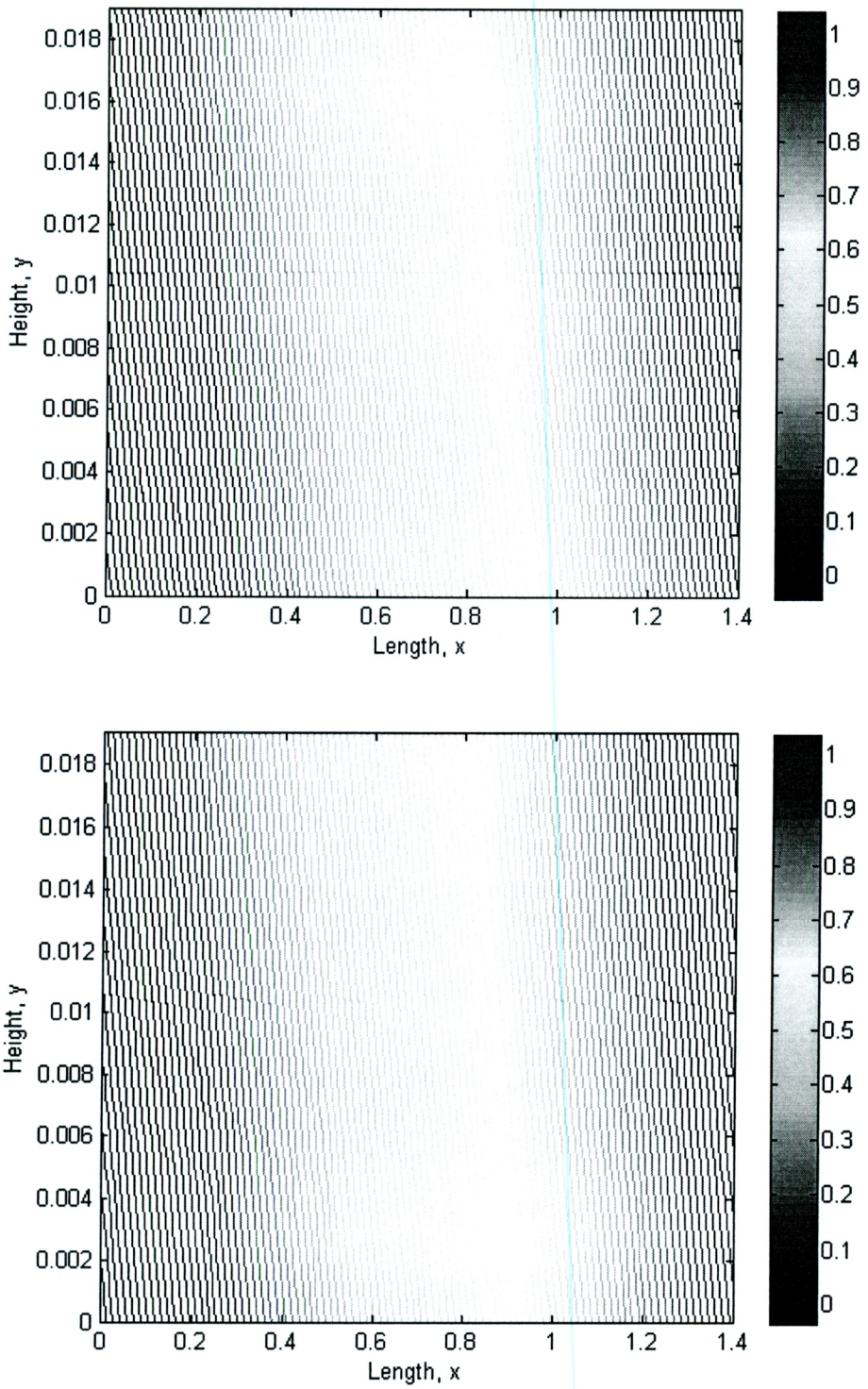

Figure 4.20: Contour plots for pressure with $n = 2.2$, $\phi_0 = 0.02$ and (a) $\Delta\pi = \frac{5\Delta\pi_c}{4}$, (b) $\Delta\pi = \frac{3\Delta\pi_c}{2}$.

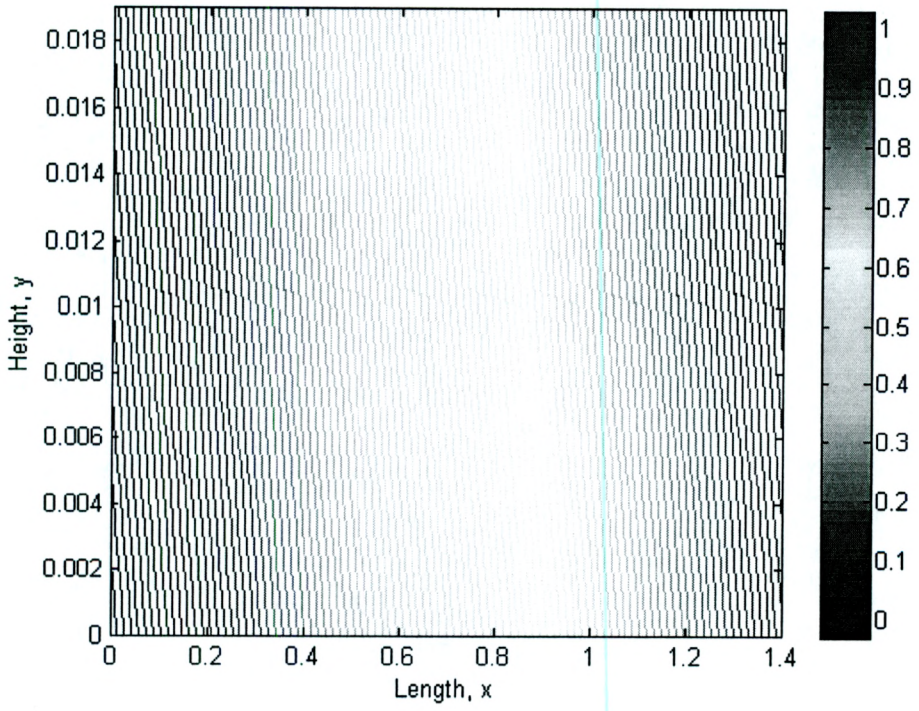

Figure 4.21: Contour plot for pressure with $n = 2.2$, $\phi_0 = 0.02$ and $\Delta\pi = \frac{7\Delta\pi_c}{4}$.

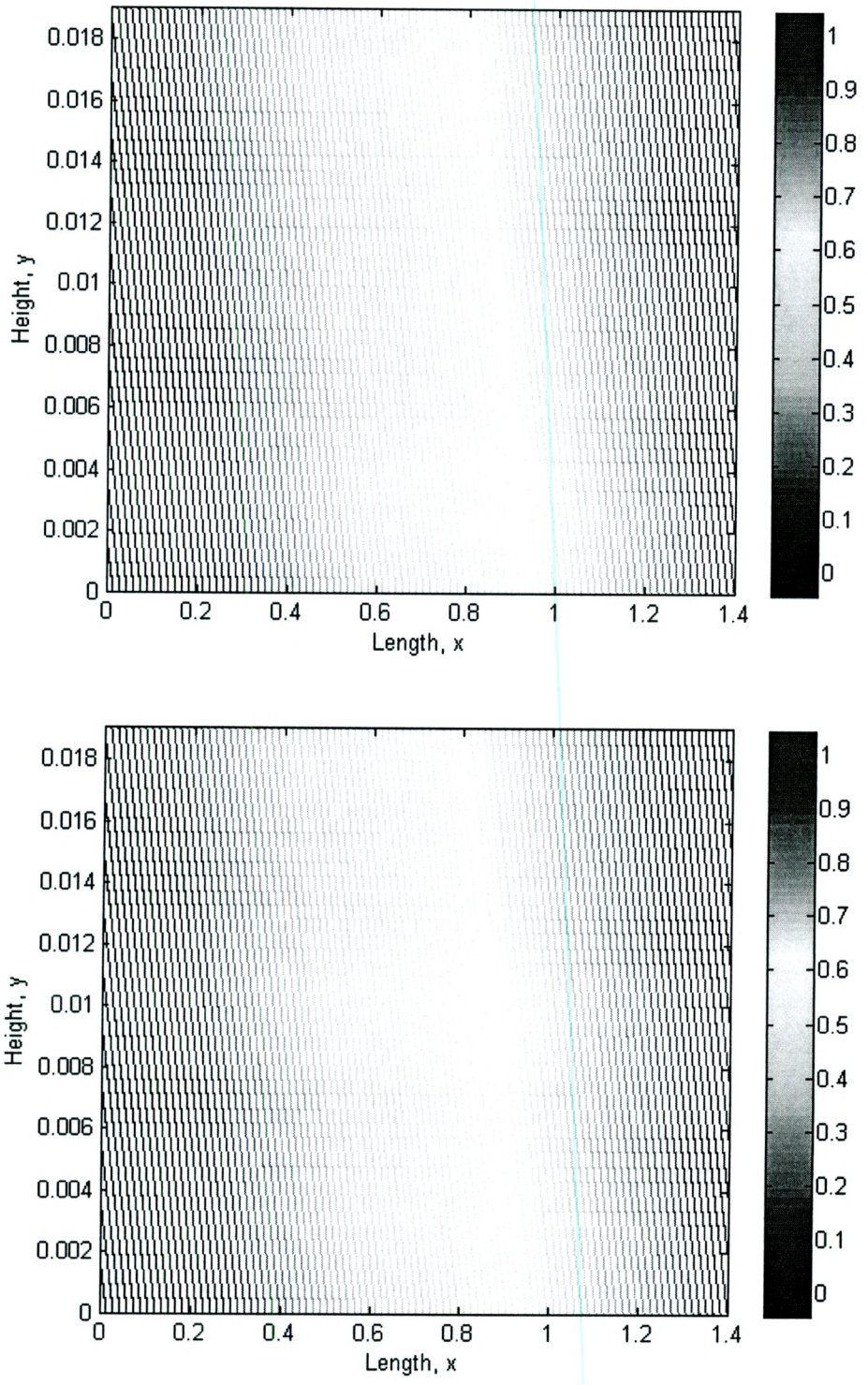

Figure 4.22: Contour plots for pressure with $\Delta\pi = \frac{\Delta\pi_c}{4}$, $\phi_0 = 0.02$ and (a) $n = 1.8$, (b) $n = 2.0$.

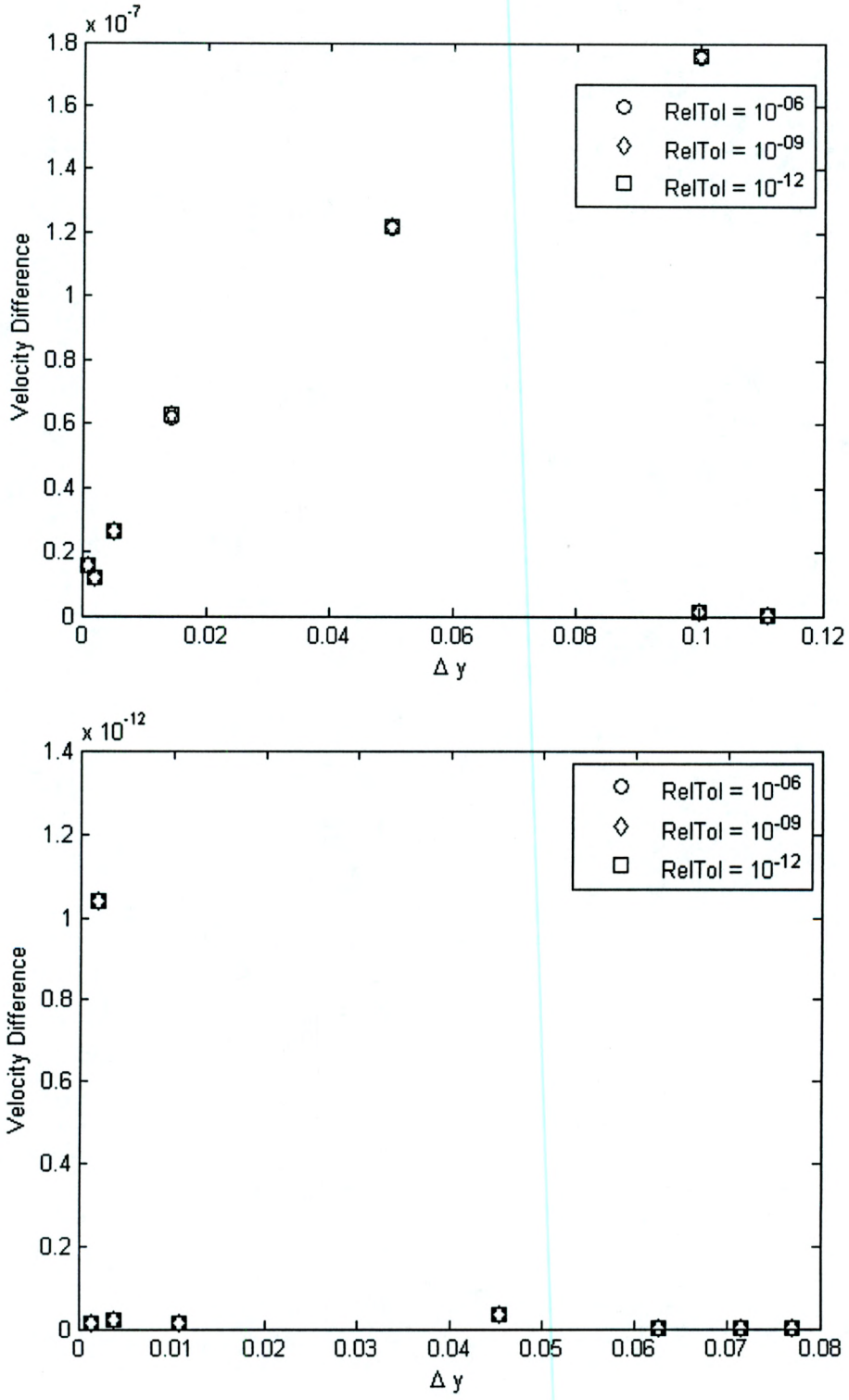

Figure 4.23: Successive differences in half-pipe velocity plotted versus step-size for $n = 1.8$ and varying relative tolerances for pressure gradient (a) dependent regime and (b) independent regime.

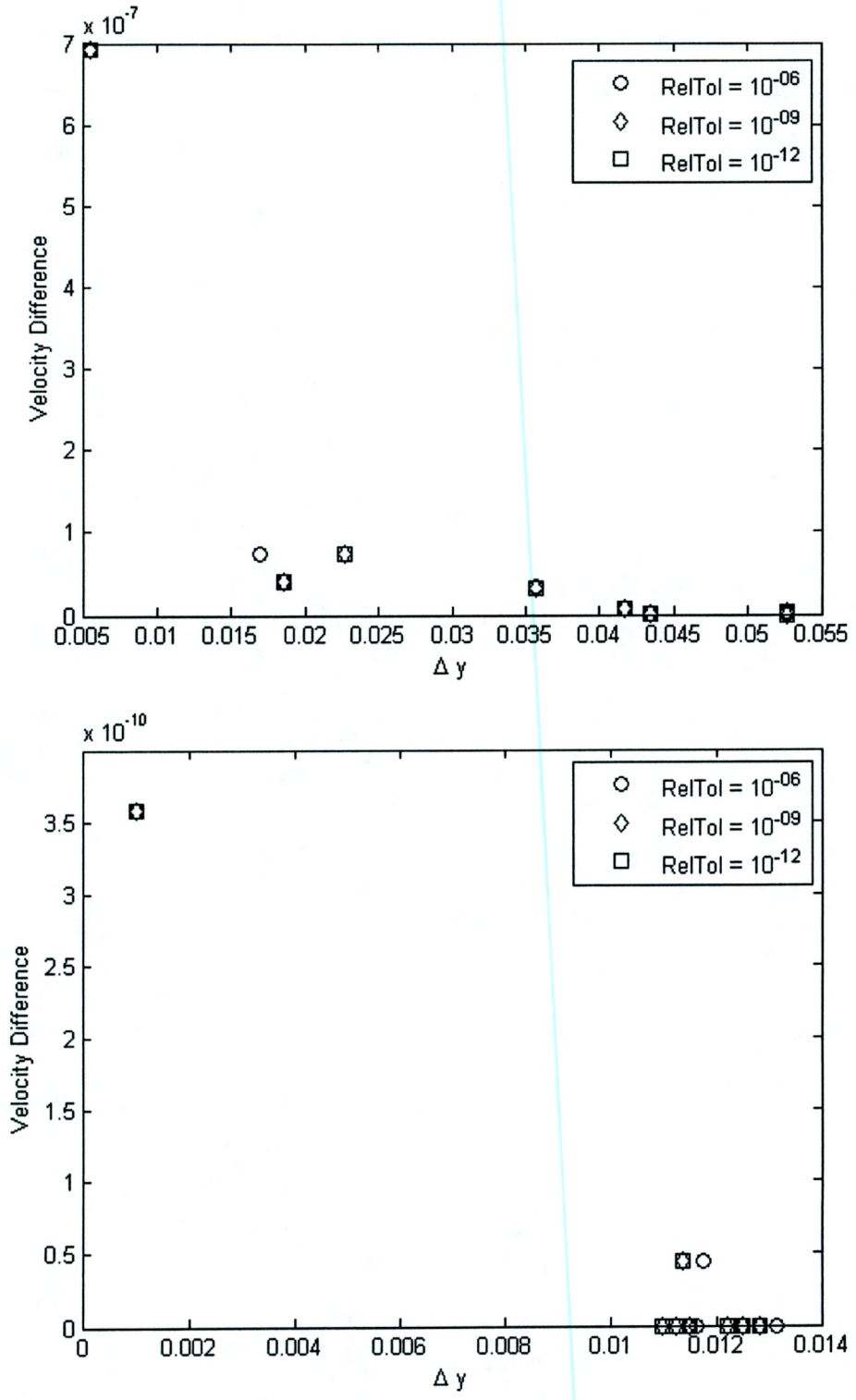

Figure 4.24: Successive differences in half-pipe velocity plotted versus step-size for $n = 2.2$ and varying relative tolerances for pressure gradient (a) dependent regime and (b) independent regime.

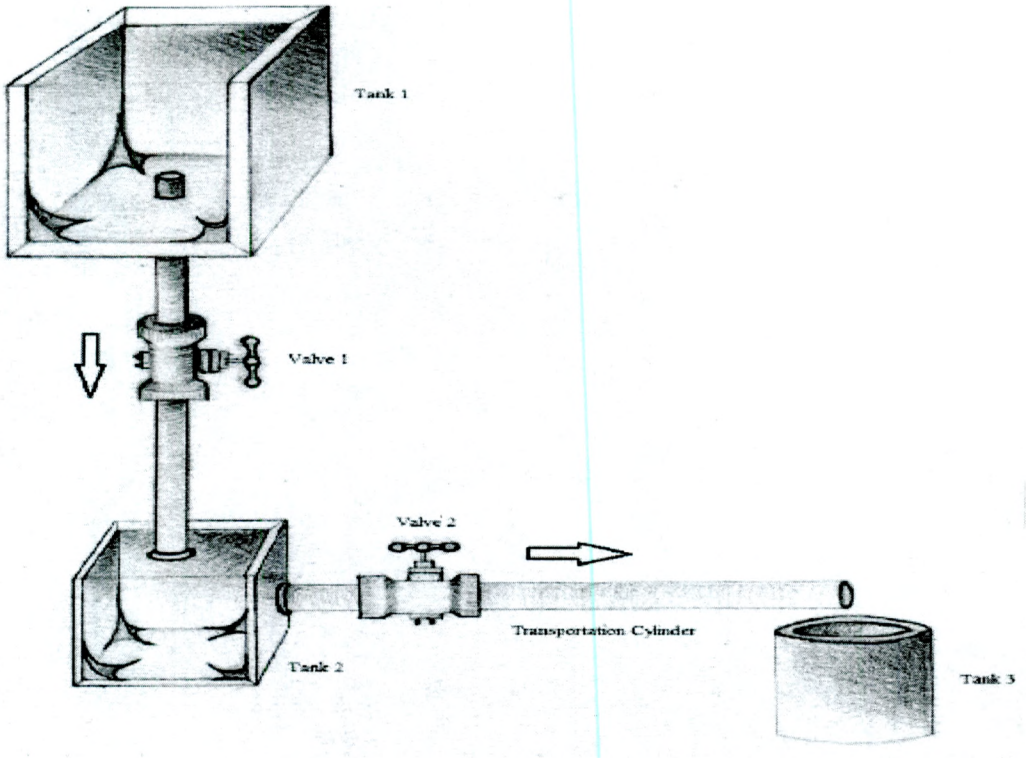

Figure 4.25: The figure illustrates the experimental configuration used in [8].

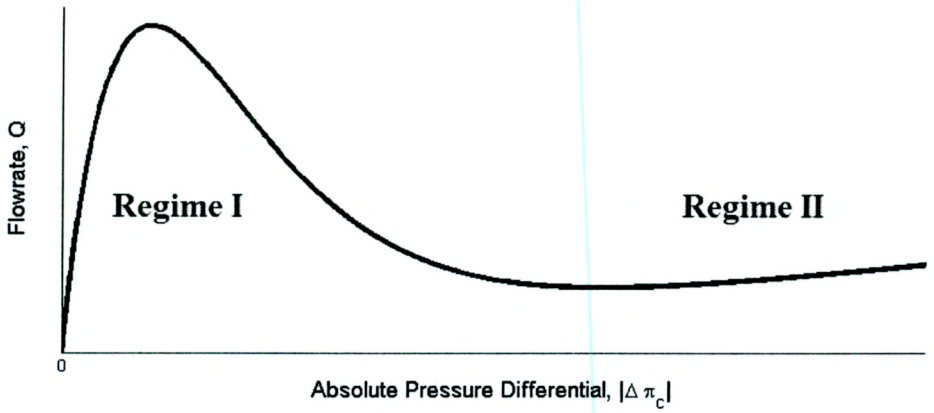

Figure 4.26: The figure illustrates the initial pressure gradient dependent regime (Regime I) and the subsequent pressure gradient independent regime (Regime II). Regime I can be considered to have two sub-regimes; an initial linear sub-regime which is then followed by an exponential decaying sub-regime.

Chapter 5

Conclusion

The flow of a non-homogeneous suspension is considered. The solid-liquid mixture is treated as an incompressible fluid where the inhomogeneity is treated through the viscosity. Two methods of attack were chosen, motivated by two different problems.

The first approach is a single regime analysis. This analysis is motivated by the bulk transport of solid material by a carrier fluid to a combustion chamber and/or processing facility; that is, biomass transport through pipeline. The viscosity is taken to be a function of products of position and temperature. Furthermore, the thermal conductivity of the fluid is taken to be a function of position, related to the viscosity function position dependence. The complete modified Navier-Stokes system of equations is considered. It is found that as we increase the amount of biomass in the suspension, fixing all other parameters, the flow rate diminishes exponentially. The velocity profiles contracts while the position of the maximum shifts downwards. No effect on temperature profile is found here.

Furthermore, as the strength of the intrinsic temperature dependence of the suspension becomes more powerful, fixing all other parameters, the flow rate and velocity profiles increase in magnitude. However, there is no effect on the temperature profile within the channel. Also, as the thermal conductivity of the biomass decreases, fixing all other parameters, the temperature distribution in the channel varies nonlinearly. This effect is extremely powerful and may be used in the context of simultaneous pipeline transport and corn saccharification as stated in Chapter 3.4. There is almost no effect on the velocity or flow rate here.

The effect of the pressure gradient, which is proportional to the parameter c, is to increase the velocity and flow rate of the biomass suspension. There is no effect on the temperature profile. Lastly, when thermal conduction and viscous dissipation are comparable, a 'hotspot' appears within the channel. This is a startling result; we would expect that the temperature within the channel should be greater than the temperature at the bottom boundary and lower than that of the upper boundary, where the latter is hotter than the former. This nonsensical result is worth confirming experimentally.

The second approach is a two regime analysis. This analysis is motivated by experiments performed at the Complex Fluids Laboratory at Montclair State University. It is found that for an inhomogeneous mixture of water and biomass (coffee, mulch, and etc.), the flow rate undergoes an initial approximate linear trend relative to the pressure gradient which is then followed by exponential decay. Furthermore, the percentage of solid material transferred increases with the pressure gradient. This leads to the consideration of a viscosity function dependent on a product of functions of pressure gradient, volume fraction, and shear rate. Furthermore, the suspension becomes independent of the pressure gradient as we approach a critical pressure, where all the biomass in the suspension has entered the fluid flow. The complete modified Navier-Stokes system of equations is solved.

The flow rate is computed and compared to the pressure gradient. It is found that the same relationship between the flow rate and pressure gradient that is seen in experiment is found in our theoretical investigation. In other words, the flow rate initially behaves approximately linearly followed by an exponential decay with increasing pressure gradient. Furthermore, the percentage of volume fraction in the fluid flow is found to increase with increasing pressure gradient. The amount of volume fraction at the top of the channel is found to decrease as a consequence. The consistence of the theoretical results with experiment is striking.

Future work can take myriad directions. In the first approach, different functional relationships can be investigated. Furthermore, the thermal conductivity could be taken to be temperature dependent as well. Also, the geometry of problem can be changed; for instance, one can consider an incline plane or snaked paths. In the second approach, temperature effects can be included, which would complicate matters dramatically. Additionally, compressibility of the fluid can be considered; that is, the density would be a function of position, temperature, volume fraction, and etc. This treatment can be performed in the first approach as well.

Bibliography

[1] Ekmann, J. M., J. C. Winslow, S. M. Smouse, and M. Ramezan. International survey of firing coal with biomass and other wastes. Fuels Process. Tech., **54**, 171-188, 1998.

[2] Easterly, J., and M. Burnham. Overview of biomass and waste fuel resources for power production. Biomass Energy, **10**, 77-92, 1996.

[3] Tsai, C. Y., Novack, M., and Roffe, G. Rheological and heat transfer characteristics of flowing coal-water mixtures, DOE Report, DOE/MC/23255-2763, December 1988.

[4] Gupta, G., and M. Massoudi. Flow of a generalized second grade fluid between heated plates. Acta Mechanica, **99**, 21-33, 1993.

[5] Massoudi, M. An anisotropic constitutive relation for the stress tensor of a rod-like (fibrous type) granular material. Math. Prob. Eng., **6**, 679-702, 2005.

[6] Kwiatkowski, K., K. Bajer, and K. Wedoowski. Turbulent combustion of biomass syngas. Archives of Mechanics, **64**, 511 - 52, 2012.

[7] Kumar, A., Cameron, J.B. and Flynn, P.C., Pipeline Transport of Biomass, Appl. Biochem. and Biotech. **113**, 27-36, 2004.

[8] Massoudi, M., G. Sanchez, S. Soltau, A. Vaidya, J. Varner, On the pressure driven flow of inhomogeneous suspensions: experiments and theory, Submitted for publishing, 2013.

[9] Anderson, J. Computational Fluid Dynamics. McGraw-Hill. New York, 1995.

[10] Kundu, P., I. M. Cohen. Fluid Mechanics. Academic Press. Massachusetts, 2008.

[11] Tritton, D. J. Physical Fluid Dynamics. Second Edition. Oxford University Press. New York, 1988.

[12] Slattery, J. C. Advanced transport phenomena. Cambridge University Press. New York, 1999.

[13] Liu, I. S. Continuum Mechanics, Springer-Verlag. Berlin, 2002.

[14] Mller, I., 1967, On the entropy inequality, Arch. Rat. Mech. and Anal., **26**, 118-141, 1967.

[15] Ziegler, H., 1983, An Introduction to Thermomechanics. Second Revised Edition. North-Holland Publishing Company. Amsterdam.

[16] Truesdell, C., and Noll, W. The Non-Linear Field Theories of Mechanics. Second edition. New York: Springer 1992.

[17] Massoudi, M., A. Vaidya, On some generalizations of the second grade fluid model, Nonlinear Analysis: Real World Applications, **9**, 1169-1183, 2008.

[18] Franta, M., J. Malek, K. R. Rajagopal, On steady flows of fluids with pressure- and shear-dependent viscosities, Proceedings of the Royal Society, **461**, 651-670, 2005.

[19] Pabst, W., E. Gregorova, G. Ticha, Effective properties of suspensions, composites and porous materials, Journal of the European Ceramic Society, **27**, Issues 2-3, 479-482, 2007.

[20] Pabst, W., Funademntal considerations on suspension rheology, Ceramics - Silikaty, **48**, Issue 1, 6-13, 2004.

[21] Derakhshandeh, B., R. J. Kerekes, S. G. Hatzikiriakos, C. P. J. Bennington, Rheology of pulp fibre suspensions: A critical review, Chemical Engineering Science, **66**, 3460-3470, 2011.

[22] J. E. Dunn and R. L. Fosdick. Thermodynamics, stability, and boundedness of fluids of complexity 2 and fluids of second grade, Arch. Rational Mech. Anal., **56**, 191-252, 1974.

[23] Anand, M., and Rajagopal., K.R., A note on the flows of inhomogeneous fluids with shear-dependent viscosities. Arch. Mech., **57**, 417-428, 2005.

[24] Massoudi, M., G. Sanchez, A. Vaidya, An engineering approach to pipeline transport of biomass, Bulletin of New Jersey Academy of Sciences, **57**, Issue 1, 9-11.

[25] Mahbubul, M., R. Saidur, M.A. Amalina, Latest developments on the viscosity of nanofluids, International Journal of Heat and Mass Transfer, **55**, Issue 4, 874-885, 2012.

[26] Arrhenius, S., Z. Physik. Chem., **1**, 285, 1887.

[27] Mooney, M., Journal of Colloid Science, **6**, 162, 1951.

[28] Stokes, G., On the theories of the internal friction of fluids in motion, and of the equilibrium and motion of elastic solids, Cambridge Philosophical Society Transactions, **8**, 287-305, 1845.

[29] Bridgman, P., The physics of high pressure, Macmillan, 1931.

[30] Griest, E., W. Webb, R. Schiessler, Effect of pressure on viscosity of higher hydrocarbons and their mixtures, Journal of Chemical Physics, **29**, 711-720, 1958.

[31] Johnson, K., R. Cameron, Shear behaviour of elastohydrodynamic oil films at high rolling contact pressures, Institution of Mechanical Engineers, **182**, 307-319, 1967.

[32] Johnson, K., J. Tevaarwerk, Shear behaviour of elastohydrodynamic oil films, Proceedings of the Royal Society A, **356**, 215-236, 1977.

[33] Antman, S., Material constraints in continuum mechanics, Atti Accad. Naz. Lincei Cl. Sci. Fis. Mat. Natur. Rend. Lincei, **70**, 256-264, 1982.

[34] Antman, S., R. Marlow, Material constraints, Lagrange multipliers, and compatiblity. Applications to rod and shell theories, Arch. Ration. Mech. Analysis, **116**, 257-299.

[35] Hron, J., J. Malek, K. R. Rajagopal, Simple flows of fluids with pressure-dependent viscosities, Proceedings of the Royal Society, **457**, 1603-1622, 2001.

[36] Malek, J., J. Necas, K. R. Rajagopal, Global existence of solutions for flows of fluids with pressure and shear dependent viscosities, Applied Mathematics Letters, **15**, 961-967, 2002.

[37] Massoudi, M., T. X. Phuoc, Unsteady shear flow of fluids with pressure-dependent viscosity, International Journal of Engineering Science, **44**, 915-926, 2006.

[38] Kalogirou, A., S. Poyiadji, G. C. Georgiou, Incompressible Poiseuille flows of Newtonian liquids with a pressure-dependent viscosity, Journal of Non-Newtonian Fluid Mechanics, **166**, 413-419, 2011.

[39] Andrade, E., Viscosity of liquids, Nature, **125**, 309-310, 1930.

[40] Bird, B.R., R.C. Armstrong, O. Hassager, Dynamics of Polymeric liquids. Volume 1. New York: Wiley 1977.

[41] Pinkerton H., R. Stevenson, Methods of determining the rheological properties of magmas at sub-liquidus temperatures, Journal of Volcanology and Geothermal Research, **53**, 47-66, 1992.

[42] Kulkarni D., D. Das, G. Chukwu, Temperature dependent rheological property of copper oxide nanoparticles suspension (nanofluid), Journal of Nanoscience and Nanotechnology, **6**, Issue 4, 1150-1154, 2006.

[43] Kaviany, M. Principles of Heat Transfer in Porous Media. Second Edition. Springer-Verlag, New York, 1995.

[44] W. Duangthongsuk, S. Wongwises, Measurement of temperature-dependent thermal conductivity and viscosity of TiO_2water nanofluids, Experimental Thermal and Fluid Science, **33**, Issue 4, 706714, 2009.

[45] Chandrasekar, M., S. Suresh, A. Chandra Bose, Experimental investigations and theoretical determination of thermal conductivity and viscosity of Al_2O_3/water nanofluid, Experimental Thermal and Fluid Science, **34**, Issue 2, 210-216, 2010.

[46] Maxwell, J., A treatise on electricity and magnetism, Clarendon Press, 1891.

[47] Hamilton, R., O. Crosser, Thermal conductivity of heterogeneous two-component systems, Industrial and Engineering Chemistry Fundamentals, **1**, Issue 3, 187-191, 1962.

[48] Timofeeva, E., A. Gavrilov, J. McCloskey, Y. Tolmachev, Thermal conductivity and particle agglomeration in alumina nanofluids: experiment and theory, Phys. Rev. E. Stat. Nonlin. Soft Matter Phys., **76**, 061203, 2007.

[49] Trelles, J., Formation of self-organized anode patterns in arc discharge simulations, Plasma Sources Sci. Technol., **22**, 025017, 2013.

[50] Wagner, N., J. Brady, Shear thickening in colloidal suspensions, Physics Today, **62**, Issue 10, 27-32, 2009.

[51] Howard, J. R., Fluidized Bed Technology: Principles and Applications, Adam Hilger Publication, Bristol, 1989.

[52] Kumar, A., J. Cameron, P. Flynn, Pipeline transport and simultaneous saccharification of corn stover, Bioresour Technol., **96**, Issue 7, 819-829, 2005.

[53] Poletto, M., D. Joseph, The effective density and viscosity of a suspension, Journal of Rheology, **39**, Issue 2, 323-343, 1995.

[54] Webster, J.G., The Measurement, Instrumentation, and Sensors Handbook, CRC Press LLC, Boca Raton, 1999.

Appendices

Appendix A

Measurement of the viscosity and thermal conductivity

There are numerous ways to measure the viscosity and thermal conductivity of a fluid. Devices which measure the viscosity of a fluid are called viscometers and are used primarily for Newtonian fluids, where flow conditions do not effect the viscosity. Rheometers are used when the fluid viscosity varies under different different flow conditions and are used primarily for non-Newtonian fluids. In such devices, the fluid is constrained to some specialized geometry (or system) in which, under physically reasonable assumptions, a closed form relationship between the shearing stress and corresponding shear strain rate can be established. The viscosity can thereby be determined, as the proportionality constant relating the two previous quantities. Three popular methods include concentric cylinders, cone-and-plate, and falling sphere; for a detailed discussion of these methods and more see [54].

As in the case of viscosity, there are a number of techniques to measure thermal conductivity for both fluids and solids. However, the transient hot-wire method is used often for suspensions due to accuracy and speed, among other factors. Measurement is performed by suspending a thin wire into a fluid, in which a constant current is supplied briefly. The thermal conductivity of the fluid is found to be related to the temperature field around the heated wire. A more detailed discussion can be found elsewhere, see [44], for instance.